ASSESSMENT OF THE IMPACT OF LAND USE AND LAND COVER CHANGE ON LAND SURFACE TEMPERATURE: A CASE STUDY OF CHIRO TOWN AND ITS SURROUNDING, ETHIOPIA

Seifegebriel Kerga Bereka

A Thesis Submitted to

Department of Geomatics Engineering,

School of Civil Engineering and Architecture

Presented in Partial Fulfillment of the Requirement for the Degree of Master's in Geoinformatics

Office of Graduate Studies

Adama Science and Technology University

September, 2022

Adama, Ethiopia

ASSESSMENT OF THE IMPACT OF LAND USE AND LAND COVER CHANGE ON LAND SURFACE TEMPERATURE: A CASE STUDY OF CHIRO TOWN AND ITS SURROUNDING, ETHIOPIA

Seifegebriel Kerga Bereka

Advisor: Tilahun Erduno Hankebo (PhD)

A Thesis Submitted to

The department of Geomatics Engineering

School of Civil Engineering and Architecture

Presented in Partial Fulfillment of the Requirement for the Degree of Master's in Geoinformatics

Office of Graduate Studies

Adama Science and Technology University

September, 2022

Adama, Ethiopia

DECLARATION

I hereby declare that this Master Thesis entitled "Assessment of the Impact of Land Use and Land Cover Change on Land Surface Temperature: A Case Study of Chiro Town and Its Surrounding, Ethiopia" is my original work. That is, it has not been submitted for the award of any academic degree, diploma or certificate in any other university. All sources of materials that are used for this thesis have been duly acknowledged through citation.

______________________________	_______________	______________
Name of student	Signature	Date

RECOMMENDATION

I, the advisor of this thesis, hereby certify that I have read the revised version of the thesis entitled “Assessment of the Impact of Land Use and Land Cover Change on Land Surface Temperature: A Case Study of Chiro Town and Its Surrounding, Ethiopia” prepared under my guidance by Seifegebriel Kerga submitted in partial fulfillment of the requirements for the degree of Mater’s of Science in Geoinformatics.

Therefore, I recommend the submission of revised version of the thesis to the department following the applicable procedures.

______________________________ ______________ ______________

Major advisor/supervisor Signature Date

APPROVAL SHEET

I, the advisors of the thesis entitled "Assessment of the Impact of Land Use and Land Cover Change on Land Surface Temperature: A Case Study of Chiro Town and Its Surrounding, Ethiopia" and developed by Seifegebriel kerga, hereby certify that the recommendation and suggestions made by the board of examiners are appropriately incorporated into the final version of the thesis.

________________	________________	________________
Major Advisor	Signature	Date

We, the undersigned, members of the Board of Examiners of the thesis by Seifegebriel Kerga have read and evaluated the thesis entitled "Assessment of the Impact of Land Use and Land Cover Change on Land Surface Temperature: A Case Study of Chiro Town and Its Surrounding, Ethiopia" and examined the candidate during open defense. This is, therefore, to certify that the thesis is accepted for partial fulfillment of the requirement of the degree of Master of Science in Geoinformatics.

________________	________________	________________
Chairperson	Signature	Date
________________	________________	________________
Internal Examiner	Signature	Date
________________	________________	________________
External Examiner	Signature	Date

Final approval and acceptance of the thesis is contingent upon submission of its final copy to the Office of Postgraduate Studies (OPGS) through the Department Graduate Council (DGC) and School Graduate Committee (SGC).

________________	________________	________________
Department Head	Signature	Date
________________	________________	________________
School Dean	Signature	Date
________________	________________	________________
Office of Postgraduate Studies, Dean	Signature	Date

ACKNOWLEDGMENT

First and foremost, I would like to thank the Almighty God who gives me strength, patience, and trust to complete my study fruitfully. Then, I wish to explicit my deepest and genuine gratitude to my advisor Dr. Tilahun Erduno, who helped me from the starting of the research to its completion and for sharing his constructive comments, scientific guidance, and invaluable input throughout this study.

I would like to extend my deepest gratitude to Mr. Dejene Mulu instructor of Madda Walabu University and Mr.Tamrat Muleta instructor of Oda Bultum University for their constructive advice, professional comments, and support. I appreciate their constructive comments and provided input in this study.

I wish to explicit my genuine thanks to Oda Bultum University for sponsoring me for this study.

Lastly but not the list, I would like to extend my thankfulness to my family for their continuous support. And I want to recognize all of those people who were my teachers, friends, and others, who helped me, to begin this long journey. Their names are too plentiful to list, but many of them encouraged me to learn and upgrade.

TABLE OF CONTENT

Content **page**

LIST OF TABLES

Table Number and Title **page**

LIST OF FIGURES

Figure Number and Title **page**

LIST OF ACRONYMS

AVHRR	Advanced Very High-Resolution Radiometer
CSA	Central Statistics Agency
DN	Digital number
ERDAS	Earth Resources Data Analysis System
ETM+	Enhanced Thematic Mapper plus
FAO	Food and Agriculture Organization
GIS	Geographical information system
GPS	Global position system
LP DAAC	Land Processes Distributed Active Archive Center
LSE	Land Surface Emissivity
LST	Landsat Surface Temperature
LULC	Land use and Land cover
MLC	Maximum Likelihood Classification
MODIS	Moderate Resolution Imaging Spectroradiometer
MS	Multi scanner
NASA	National Aeronautical and Space Administration
NDBI	Normalized Difference Built-up Index
NDVI	Normalized Difference Vegetation Index
NOAA	National Oceanic and Atmospheric Administration
OLI	Operational Landsat Imagery
RS	Remote sensing
SWA	Split Window Algorithm
SWIR:	Short-wave Infrared Band
TB	Brightness Temperature
TIRS	Thermal Infrared Sensor
TM	Thematic Mapper
UN	United Nation
UNEPA	United Nation Environmental Protection Agency
USGS	United States Geology Survey

ABSTRACT

Land use land cover change is the main cause of global climate change and currently, it is a rising trend globally in general and in Ethiopia. It has a significant influence on land use by substituting areas of natural resources and vegetation with impervious surfaces like built-up asphalt road and parking lots; this in turn increases the land surface temperature. chiro town and its surrounding high temperature season get increasingly warmer over time. Changing areas of natural resources in to different impervious surfaces in chiro town and its surrounding case Changes in land surface temperature. The objective of the study was to assess the impact of land use land cover change on LST in and around Chiro town. Supervised classification with maximum likelihood algorithm was used to assess the LULC changes and the split-window algorithm was used to extract LST from Landsat imageries which were acquired from 1990, 2000, 2010 and 2020 of the same seasons and MODIS land surface temperature was used to validate LST that was derived from Landsat thermal bands. Pearson correlation was used to analyze the relationship between land surface temperature and LULC indices (NDVI and NDBI). The results show that there is a significant change in LULC especially the built-up area of the study which becomes more than triple over the study period from 4.4% - 15%. However, Vegetation areas are decreased from 13.4% to 12.4 % from 1990 to 2020. Agricultural and bare land areas are also decreased from 65.07% to 60.3% and 17.16% to 12.3% respectively through the study period. This study shows that the land surface temperature of study area ranges from 7 ℃ to 41 ℃ from 1990-2020. Land surface temperature has a positive relationship with NDBI and a negative association between NDVI. Vegetated land has low LST. However, most of the agricultural land, bare land, and built up of study area have high LST. There was a LULC change in study area and it causes an increase in LST from 1990-2020. The output of the study provides useful information for land use planners and decision makers to make better decisions in improving future land use policies and formulating management strategies within the framework of sustainable land use planning for environmental protection.

Keywords: *LULC Change, split-window algorithm, Land Surface Temperature.*

CHAPTER I INTRODUCTION

1.1 Background of the study

For thousands of years, the life-form actions of humans changed our planet Earth and its atmosphere. Large population density, migration, and socioeconomic activity aggravate these environmental changes (Mahmood R; Pielke Sr RA; Hubbark KG; Niogi D, et al., 2010). Changes have been observed at different spatial scales, extending from regional to worldwide. Agriculture and settlement growth are two large-scale human activities that are gradually reducing the vegetation cover of the earth's surface (Lilly Rose A; Devadas MD 2009). According to the United Nations (2014), urbanization is a process through which people move from rural to urban areas and from town to town, allowing cities and towns to expand. It can also be defined as the rapid growth in the number of societies that live in cities and towns. The world's most dynamic places are urban areas. With acting as the social and economic centers of our modern lifestyles, there is always a rapid shift in both demographic and spatial dimensions (Galeon, 2009). The population of African cities will more than double in the next twenty years, and their spatial expanse could more than triple (Lamson-hall et al., 2015).

As a result of such rapid human population growth in urban areas, LULC variations in quantity and spatial extent has been increasing globally from time to time. (Hansen et al., 2013; Defries et al., 2004; Lambin et al., 2001). As the world's population grows, the demand for resources grows in lockstep, putting pressure on natural resources and causing damage. Furthermore, due to anthropogenic forces, the land has been continuously and drastically reduced (Brink et al., 2014; Niamir-Fuller et al., 2012). It has a significant impact on land usage by replacing natural resources and vegetation-rich areas with residential and commercial areas, as well as the infrastructure that supports them (Bekele, 2005).

The growth in both human and livestock populations has resulted in LULC changes in most Eastern African countries (Pomeroy et al., 2003). Land degradation occurs as a result of the overuse of land for agricultural activities such as crops and grazing. As a result, natural vegetation-covered land is turned into town areas, built-up lands, farmlands, and grazing fields. Soil erosion, deforestation, land degradation, and biodiversity loss result, as well as climate change, which leads to global warming (Maitima et al., 2009).Ethiopia is also another East African country where the problem of LULC change is severe and has been growing over time. This is due primarily to population growth (Hurni et al., 2005) and local people's not understanding of sustainable land management (Belay et al., 2014). The problem is particularly acute in Oromia National Regional State, where the land use and land cover is become changed. Forest, shrubland, bushland, and grasslands have all been severely damaged as a result of the need for more land for development, farming, and grazing. As a result of this land degradation and LST has increasing (Bekele, 2005).

Due to the conversion of vegetated surfaces into built-up, bare land, and agricultural land, an increase in LST is causing serious environmental problems in both rural and urban areas. LST is an important variable in environmental studies, and it is evaluated using thermal bands from several sensors such as MODIS, Landsat-5 thematic mapper, Landsat-7 enhanced thematic mapper plus, and Landsat-8 Thermal infrared sensor (Gebrekidan, 2016) and LULC classification to extract information and doing analysis LST. LST is defined as the surface radiometric temperatures emitted by land surfaces and measured by a sensor at specific viewing angles in remote sensing terminology (Prata et al., 1995). It's also known as the temperature of the earth's surface phenomena, as well as the sensation of how hot the earth's surface is generated from direct measurements or remotely sensed data (Kayet et al., 2016).

Therefore, LST assessment by thermal bands of Landsat imageries to examine the relationship between thermal patterns and LULC change is an important application of remote sensing in temperature studies. As result, this study goal is to assess the land use land cover change impacts on LST. Therefore, it is useful input to predict future land warming and to provide practical information for urban planners, natural resources managers, and environmental experts to manage natural land resource to be sustainable and healthy.

1.2 Statement of the problem

Global climate appears to be changing at an alarming rate (Naissan and Lily, 2016). Both urban and rural areas are experiencing warm temperature condition and it is increasing from time to time. The earth’s environment is a dynamic system, including many interacting components (physical, chemical, biological and human) that are continuously varying (Emilio, 2008). Due to the increase of population, industrialization and other natural and human activities, its land-use/land-cover patterns are changing. One of the main factors that responsible for the increment of LST is land-use land-cover change. In the recent time, global warming and environmental problems are a headache for both within developing and developed countries. Practices such as overgrazing, deforestation, unplanned land-use for settlement and other activities lead our environment to warm temperature. The urban growth rate of Ethiopia from 2010-to 2015 was 2.3% (UN, 2014). It has a serious influence on LULC by replacing areas of natural resources and vegetation with residential and commercial areas and their related infrastructure (Bekele, 2005). In west hararge zone, in and around chiro town LST has been increasing from season to season. According to Aires et al. (2001) LST is a main parameter in land surface processes, not only acting as an index of climate change, but also to control the upward terrestrial radiation, and consequently, the control of the surface sensible and latent heat flux exchange with the atmosphere. Since Chiro town and its surrounding, the pattern of LULC has been changing from time to time and increase in the number of people living in the town. Increased built-up and impervious surfaces such as asphalt and parking lots caused the depletion of other land covers such as vegetation and agricultural land in the surrounding areas, which increases solar radiation absorption and thermal conductivity. According to Voogt and Oke, (2003) the increased radiation on the biophysical surface layer causes the town to get increasingly warmer over time. These are the main cause of LST change, which is very essential to the study of town climates.

Such an increment in LST in the study area increases the unsuitable air conditioning and increases warm, as well as changing rainfall patterns that affect biotic communities (Abel, 2018). The comfort of city people may be harmed by excessive heat, which can lead to increased health risks (Rinner and Hussain, 2011). LST also modifies the air temperature of the atmospheric border layer and is a key component in the surface energy balance of the study area. Changes in LST have their effects on local weather and climate of Chiro town and its surrounding. These changes also have negative impacts on landscape aesthetics, energy efficiency, human health, and quality of living in a town environment (Yue et al., 2007).

In order to study LST, monitor and determine climate change for sustainable environmental resource management, it is critical to evaluate land use practices and land cover types, as well as their consequences. Because LULC is the most significant variable in global changes that affect ecological systems, this is the case. As a result, the characteristics of LULC and its patterns have critical implications for land surface temperature, biogeochemistry, hydrology, terrestrial species diversity and abundance, and people's livelihoods (Eckert et al., 2017).

Therefore, asses LULC change and LST using remotely sensed data is very essential to alleviate these problems and forward better solutions. This is because remote sensing is very capable to retrieve LST, land surface emissivity, NDBI, and NDVI using different algorithms and analyze the association between these parameters as well as the impacts of LULC change on the earth's LST. As a result of this study, it is feasible to demonstrate the extent to which the environment and temperature of Chiro town and its surrounding have altered.

1.3 Objectives

1.3.1 General objective

The General objective of this study is to:

Assess the impact of land use land cover change on land surface temperature through geospatial techniques in Chiro town and its surrounding.

1.3.2 Specific objective

The Specific objectives of the study include:

i. quantifying the magnitude of land use land cover change from 1990 to2020 at 10 year interval,
ii. show the relationships between land surface temperature, land use land cover indices and land use land cover types,
iii. reveal spatio-temporal variations of each LULC on land surface temperature,
iv. identify the hot spot area of LST.

1.4 Research questions

1. What are the spatiotemporal patterns of land use land cover changes from 1990 to 2020 in the study area?
2. What is the relation between land cover indices and LST in the study area?
3. What is the variation of each land use land cover types on LST change in the study area?
4. Which part of the study area is high LST?

1.5 Scope of the study

The Geographical scope of this study was in and around Chiro town Oromia Nation Regional State, Ethiopia, which cover 65,479.5 ha. Conceptually, this research focus mainly on LULC change analysis from 1990-2020 and this research was carried out to determine and calculate the trend of LULC change, the relationship between LST and LULC, and the impact of LULC change on LST change. The LST values measured and LULC classification should be validated by field verification for each LULC class. Increasing LST has negative consequences for the environment, including as climate change and seasonal fluctuations. The environment can be harmed if land for development, barren land, and farmland is not adequately maintained. To address this issue as well as defining different LULC classes and adjustments by using Geo spatial technologies and giving clue about the importance of developing land use land cover change map for validation and LST related with land use land cover change and finally conclusion and recommendations were raised based on the findings.

1.6 Limitation and assumption of the study

The high spatial resolution of remote sensing data interpretation is required to obtain better simulation results (Chaudhuri & Clarke, 2013). In this study, 30 meter Landsat satellite images obtained from USGS earth explorer website (https://earthexplorer.usgs.gov/) has been used. Generating accurate land use the land cover map was a challenge from such images due to a coarse resolution. It was difficult to make a clear distinction between different land use features classes. using High Spatial resolution Satellite image such as Quick bird, IKONOS, Geo Eye, World view, and SPOT will provides better and detail information with good quality to map Land use land cover classes and overall accuracy may greater than the value obtained.

1.7 Significance of the study

The study's goal is to examine land use land cover changes impact on LST, which have become common in recent years. The final output of this study provides information for Policymakers, city and urban planners, land administration, and environmental protection office: To form and implement more coherent and sustainable environmental planning strategies regarding existing and future land use to Planning, management and monitoring of natural resources. To serve as input parameter in many fields as geology and environmental studies. Further researcher will be interested in the findings of this analysis because it will add to the current realistic and theoretical knowledge base on the past and future LULC change. Fill in the awareness gap by running simulations and proposing adaptable LULC change impact on surface temperature.

1.8 Organization of the research

The whole thesis is divided into five chapters. To begin with chapter lays the background of the study providing general introduction about the research work including the problem statement, questions and research objectives, the scope and limitations of the study were also highlighted. The second chapter deals with literature survey in which the related works as have been performed by various other researchers were presented. In the third chapter, information about the chosen study area is given and how the several data layer maps are generated, also outlining the methodology of carrying out the task and the data sources utilized. Furthermore Chapter four presents the findings of this research work and a detailed discussion on the results obtained. In conclusion is drawn based on the results obtained along with future research possible and recommendations.

CHAPTER II LITERATURE REVIEW

In this chapter, similar studies that have been undertaken in different places, the concepts and inter-relationships among LU/LCC, LST, and NDVI, NDBI, and the applications of RS and GIS in LST research are covered in this chapter. Likewise, it aims to investigate the findings of relevant studies that have been conducted in the past in various areas, as well as the identification of gaps in the current study area.

2.1 The concept of land use land cover

Every piece of land on the earth's surface was dissimilar from its cover. Life form processes such as deforestation, agricultural activity, and urbanization have significantly changed the earth's surface in past times. The Land is the ultimate resource of biodiversity. Various studies have combined the definitions of land use and land cover. These two terms, however, refer to two distinct issues and have different meanings. The observed biophysical cover on the earth's surface, comprising water bodies, plant**s**, soil, and hard surfaces, is referred to as land cover (FAO, 2000). Human activities such as urbanization, agriculture, forestry, and pasture influence land surface processes such as biogeochemistry, hydrology, and biodiversity (Di Gregorio and Jansen, 2000). In this context, variation in the surface component of the landscape is only regarded to exist if the surface appears differently on at least two occasions (Lemlem, 2007).

2.2 The Driving factors of Land use and Land cover Change

Changes in land use and land cover are driven by a variety of factors such as human population expansion, economic development, and technological advancements. Conversion of land cover from one category to another, as well as changes to the conditions within a category, are examples of land cover changes. Land-use change, on the other hand, occurs when land experts believe that a transition to a different land-use category is desirable (Meyer and Turner, 1992). The following are the general causes of LULC alterations, according to the USEPA (2004): Natural processes such as climate and atmospheric variations, wildfire, and pest infestation. A direct effect of human activity such as road and illegal house construction, as well as deforestation. An indirect effect of human activity such as water diversion, which causes the water table to drop and groundwater to become contaminated.

Even if natural processes have a role, human-induced (Anthropogenic) influences are the primary drivers of land use and land cover change (Niamir-Fuller et al., 2012). Human-caused LULC alterations are becoming increasingly problematic nowadays (Agarwal et al., 2002). Anthropogenic concerns can cause LULC alterations in a variety of ways. One cause causing LULC change is urban expansion due to high population growth, which results in a major shift in landscape patterns and kinds. These changes have altered the availability of many biophysical resources, resulting in a reduction in the availability of various products and services for humans and livestock, as well as environmental damage. As a result, urban growth in and around cities has significant environmental consequences. It, for instance, results in it causes a rise in the temperature of urban areas (Qijiao and Zhixiang, 2015).

Furthermore, population increase reduces forest area because people utilize them for fuel wood and lumber, as well as grasslands for cattle grazing. People are the most essential natural resources, and their long-term growth is connected and interdependent. Therefore, the importance of land as a basic and limited resource for most human activities such as forestry, agriculture, industry, energy production, recreation, settlement, and water catchment and storage is reflected in Land Use. The area of earth cultivated land has increased by more than 45 percent over the last three centuries, from 2.65 million km^2 to 15 million km^2, whereas other natural resources such as forests have decreased due to agricultural land expansion and urbanization (Santa, 2011). The percentage of deforestation is high in many developing countries associated with population growth and poverty (Mather and Needle, 2000).

Another consequence of unsustainable land use and land cover change is degradation. Carbon dioxide (CO_2) levels in the atmosphere rise as a result. As a result, forest fires caused by LULC degradation result in increased emissions of hazardous gases such as carbon monoxide (CO) and nitric oxide, which impact the chemistry of the atmosphere, creating air pollution, disrupting energy balance, and contributing to global warming (Peter, 1994). Hydrology is affected by changes in land use and land cover. It affects the quality of water and the flow of water, resulting in surface water contamination and groundwater aquifer depletion. Due to ongoing and severe deforestation, changes in land use and land cover also increase the frequency and severity of flooding (Meyer and Turner, 1992).

Land use and land cover variations, in general, have become major global issues, and they are a primary driving force behind global environmental changes (FAO, 1999). Transitions in global systems and processes are being forced by such large-scale land-use class changes as a result of increased agricultural land in rural areas, deforestation, urbanization, and other natural occurrences and human activities. However, historically, the most significant change in land usage has been the worldwide expansion of agricultural land (Houghton, 1994). Climate Changes refer to a long-term or permanent change in a region's temperature. Droughts occurring more frequently, global temperature raises, tropical cyclones, floods, and lower yearly rainfall are all signs of climate change, as is a drop in glacier cover over a mountain and increasing sea levels (Mengistu, 2008). Dynamic processes are affecting human and ecological systems at all geographic scales as a result of urban transformation, particularly the large global rise in urban population and urbanized areas (Brockerhoff, 2000). Local communities and policymakers place a high value on the ability to monitor urban LULC trends. Because of increased availability and improved quality of multi spatial-temporal data, as well as new analytical tools, it is now possible to monitor urban LULC changes and urban sprawl in a timely and cost-effective manner (Yang et al., 2003). As a result, for regional planning and urban ecology, the utilization of remotely sensed data is required.

2.3 Land-use and land-cover change in Ethiopia

Natural resource availability varies greatly in Ethiopia, and management practices vary greatly as well. Because of differences in biogeography and topography weather, there is variability. Human activities are speeding up land-use/land-cover changes, but they are also result in a change that harms humans (Agarwal et al., 2002). Water, plants, soil, animal feed, and other biophysical resources are all affected by the dynamics of LU/LC (Ali, 2009). Previous studies have found that due to land scarcity, there has been significant LU/LCC in Ethiopia, with the growth of cultivated land at the expense of woodland and forest land, stretching into sloppy areas. Agricultural methods and human settlement have a long history in Ethiopia's highlands, and there has lately been a highland population strain, which includes depletion of natural resources and unsustainable activities (Miheretu et al., 2017).

Many researchers agree that human impacts are the primary source of land use and land cover change in Ethiopia, despite the fact that natural processes may also play a role (Agarwal et al., 2002; Ali, 2009; Birhan and Assefa, 2017). Changes in land use and land cover reflect human histories and, possibly, the future of humankind. A multitude of causes such as human population expansion, economic development, technological advancements, and environmental changes impact such changes (Houghton, 1994). One of the major factors of land use and land cover change is population expansion. People are the most essential natural resources, and their long-term growth is connected and interdependent (Santa, 2011).

2.4 Land Surface Temperature and its Algorithm

According to Prata et al., (1995) and Schmugge et al., (1998), LST is the surface radiometric temperature corresponding to the sensor's direct field of view. It's also known as the surface temperature, which is measured in kelvin (Kayet et al., 2016). LST is also the temperature measured at the Earth's surface, which is referred to as the planet's skin temperature (Dash et al., 2002). LST is a key element in a number of environmental models, including energy and water exchange between the atmosphere and the surface (Yuan and Bauer, 2007), numerical weather prediction, global ocean circulation, and climatic variability (Yuan and Bauer, 2007); (Voogt and Oke ,2003) define LST as the Collective result of all energy exchange processes between the atmosphere and the land surface. Hence, in surface energy and water budget modeling on various scales, LST is a basic prerequisite for validation or model limiting (Kalma et al., 2008; Kustas and Anderson, 2009). It is used in hydrologic modeling and environmental monitoring as a meter for soil moisture and vegetation intensities (Kustas and Anderson, 2009).

LST has also been employed in the identification of thermal errors and high-temperature occurrences (Sobrino et al., 2009). Land surface temperature can also be used to forecast energy and water interactions between the land surface and the atmosphere, which are important in human-environment interactions (Qijiao and Zhixiang, 2015). LST is also commonly employed in urban climate studies to determine the surface of the urban heat island and explore its link with urban LULC and air temperature fluctuation, as well as to investigate surface-atmosphere interaction mechanisms in urban areas (Voogt and Oke, 2003; Weng, 2009). As a result, LST can be easily calculated using satellite data (Lazzarini et al., 2013; Li et al., 2013), such as Landsat, NOAA-AVHRR, and MODIS (Lazzarini et al., 2013; Li et al., 2013). LST is determined by the distribution of temperature and emissivity inside a pixel, as well as the spectral channel of measurement, for a specific sensor viewing direction (Becker and Li, 1995). To obtain LST from satellite images, atmospheric, angular, and emissivity corrections must be made. Absorption, upward atmospheric emission, and downward atmospheric irradiance reflected from the surface are the principal impacts of the atmosphere. On the basis of sensor properties, many atmospheric correction methods have been developed. In Landsat 8, however, the split-window method is routinely utilized to retrieve LST.

2.4.1 Split-window algorithm concept

Becker and Li, (1990), and Price, (1984) describe a split-window algorithm is used for the sensor which has more than one channels, in which radiance differences are detected by each atmospheric window of the respective thermal infrared channel. This technique uses differential absorption between two channels within one atmospheric window to avoid the atmospheric influence and determines the temperature at the sensor using a linear combination of two brightness temperatures (Dash et al., 2002). For instance in Landsat-8 (Du et al., 2014; Rozenstein et al., 2014) and NOAA-AVHRR (Qin et al., 2001). The algorithm uses the LSE values in both thermal infrared channels for calculation of LST (Jin et al., 2015).

2.5 Normalized Difference Vegetation Index concept

As determined by reflectance measurements in the near infrared (NIR) and red portions of the spectrum, the normalized difference vegetation index (NDVI) is the difference between near infrared and visible red reflectance values adjusted over reflectance. By taking the red band out of the near infrared spectrum and dividing the result by the near infrared plus red band, the Normalized Difference Vegetation Index may be calculated. The value ranges from -1 to 1. The negative values represent non-reflective surfaces like water, snow, clouds, and other non-vegetated areas, while the positive values represent reflective surfaces like vegetated areas (Burgan and Hartford 1993). The relationship between vegetation and the earth's surface's thermal, moisture, and radiation characteristics, which define LST, is direct (Weng, 2004). By examining the correlations between land surface temperature and NDVI, Normalized Difference Moisture Index (NDMI), in addition to NDVI, is also utilized as an alternate indication of surface urban heat island effects in Landsat imagery. The index, NDMI= (NIR-IR)/(NIR+IR), measures the various humidity contents of landscape components, particularly in soils, rocks, and vegetation, and is a great indication of dryness. Light colors are used to signify values more than 0.1, which indicate high humidity, while dark colors are used to represent values closer to -1, which indicate low humidity (Mihai, 2012).

The normalized difference vegetation index is based on the ground surface feature's spectral reflectance. Each feature has a unique reflectance that varies depending on the wavelength. The near-infrared and red bands of satellite data can be used to calculate NDVI, which has a value range of negative one to positive one. A larger NDVI value, around 1, indicates the existence of healthy vegetation cover, whereas a lower value (-1) indicates the lack of vegetation. As a result, the NDVI is critical for assessing vegetation health, the greenness of the earth's surface, crop monitoring and output forecasts, and land - cover assessment, as well as deforestation and desertification. For assessing and mapping LULC, NDVI is critical (Friedl et al., 2002). Moreover, because it reveals the degree of dryness and warmth of the area, NDVI is critical for studying the urban green environment and urban climate.

2.6 Remote sensing

The world's land is degrading, and the pattern and types of land cover are changing. As a result, understanding how LULC change occurs at different times and places is critical for long-term land management and economic growth. Moreover, evaluating and visualizing the effects of LULC change, as well as potential solutions, is critical. Monitoring variations in LULC over time is also critical for environmental management. Remote sensing has played a critical role in this area, enabling satellite imageries to assess natural resources and monitor environmental changes. The ability to gather information without coming into direct contact with it is known as remote sensing (Lillesand and Kiefer, 2000). The modern meaning of the phrase "remote sensing" refers to technology methods of gathering data from the air and space. Although the majority of the invention and improvement has occurred in the last century, earth observation from airborne platforms has a 150-year history (Zubair, 2006). The first earth observation balloons, which were launched in the 1860s, were considered a watershed moment in the history of remote sensing (Lillesand and Kiefer, 2000). Instruments at the natural level, such as our naked eyes or cameras, collect data (radiometric which measure radiation).

Satellite-based remote sensing provides useful information for assessing different aspects of the atmosphere, including climatology, meteorology, ecology, agronomy, and environmental protection (Kern, 2011). The measurement and recording of electromagnetic radiation emitted or reflected from the earth's surface are at the heart of remote sensing (Hardegree, 2006). This method allows us to analyze and determine the trend of LU/LC change over time. Furthermore, utilizing satellite data, LST and NDVI can be easily estimated, and thermal remotely sensed data is critical for monitoring and measuring the urban thermal environment (Sun et al., 2012). It also serves as a tool for assessing thermal variations in physical, environmental, and socioeconomic elements in urban settings (Small, 2004). The relationship between LULC change and LST, NDBI, and NDVI can also be studied using remote sensing data. The term "resolution" is frequently used to characterize remotely sensed imagery. There are four distinct resolution types. Spatial, spectral, radiometric, and temporal are the four types. The functionality of both remote sensing sensors and remotely sensed data can be described using these resolution qualities (ERDAS Field Guide, 2002).

The smallest object that the sensor can resolve, or the smallest region on the ground depicted by each pixel, is known as spatial resolution. It indicates the level of detail captured by the sensor on the earth's surface. In remote sensing, finer spatial resolution refers to imagery in which each pixel represents a small area on the ground and the detail recorded by the recorder. Small scale imaging is defined as imagery where each pixel represents a vast region on the ground. The spectral resolution of an EM spectrum sensor refers to the exact wave length intervals that it can record. Coarse spectral resolution refers to wide intervals in the electromagnetic spectrum, while fine spectral resolution refers to short intervals. The dynamic range, or the number of possible data files values in each band, is referred to as radiometric resolution. The number of bits into which the recorded energy is divided is referred to as this. The overall intensity of the energy the sensor monitors, from 0 to the highest amount, is broken down into 256 brightness values for 8-bit data, for example. For each pixel, the data file values vary from 0 to 255, with 0 representing no energy return and 255 representing maximum return. Temporal resolution refers to how frequently a sensor system acquires imagery of a certain area, how often an area may be revisited, or how frequently satellite data about an earth's surface feature is recorded. In change detection investigations, temporal resolution is an essential issue to consider.

2.7 Geographic Information System (GIS)

A Geographic Information System (GIS) is a computer-based system for capturing, storing, manipulating, analyzing, managing, and displaying spatial or geographic data (Coppin and Bauer, 1996). In GIS, data types are divided into two categories: geographical and non-spatial data. Non-spatial data are data that describe spatial data in the form of a table, while spatial data are data that have a location value. Data in a GIS, according to Burrough (1990), has three dimensions: spatial (geographic), time, and attribute. Some individuals consider a geographic information system to be a hardware and software system that aids in the analysis of applications or the processing of data (Maguire, 1991). A geographic information system (GIS) is not only a digital repository of spatial objectives (areas, points, and lines), but it can also do spatial analysis based on the relationships between them, such as the r/ship between objects determined by their location and geometry.

According to Foresman (1998), in the 1960s, the combination of computer technology with cartography paved the way for the use of superimposing and overlaying map techniques in domains other than cartography. The power amplification that occurs as a result of the integration of climate, environment, topography, agronomic, economic, social, and institutional management data makes new and powerful modeling available to managers and scientists alike.

2.8 Role of Remote Sensing and GIS in Land-use and Land-cover change

For the study of historical variations in LU/LC and LST analyses, remote sensing and geographic information system techniques have been widely applied around the world. Vegetation cover, air pollution, LST, and other surface features have all been identified using remote sensing (Zha, 2012; Weng, 2004). Understanding the relationship between LST and LU/LC is also crucial for land management. With the use of numerous airborne and space borne sensors, it delivers a vast variety and amount of data about the earth's surface for deep analysis and change detection. Remote sensing technology is poised to make an even greater influence on monitoring land-cover change, thanks to the availability of historical remote sensing data, lower data costs, and increased resolution from satellite platforms. Image classification techniques can be used to examine land-use/land-cover changes over time using Landsat sensors such as Landsat Multi Scanner (MSS) data and Landsat Thematic Mapper (TM) data (Gumindoga, 2010). Since 1972, Landsat satellites have given global covering of high-resolution multispectral imageries in a repeatable, synoptic manner. Their long history and dependability have made them a popular source for documenting changes in LU/LC through time (Turner et al., 2003) and their evolution has been underlined by the United States' launch of Landsat7 (Enhanced Thematic Mapper Plus sensors) in 1999. There are four LU/LCs change detection (aspects of change detection) that are significant when monitoring natural resources, according to Macleod and Congation (1998): Distinguishing the nature of the change, Detection/finding of the changes that have occurred, Measuring the area extent of the change, Assessing and investigating spatial pattern of the change.

2.9 LULCC Response to Land Surface Temperature in world

The impact of land-use/land-cover change on land surface temperature is one of the major factors that are responsible for the increase of LST is LU/LCC, and different researchers agree with that land-use change and unplanned use of land resources lead to increasing LST. According to Oluseyi et al., (2011) have studied that spatially there are correlations with changes as reflected in the characteristics of individual land-use classes or categories. The influence of LU/LCCs on LST is different at different latitude, for example in South Asia and East Asia tropical temperate regions (Shukla, 1990). The relationship between land-use changes, biodiversity and land degradation across East Africa shows that the original land-covers were transformed to grazing land, farmland and settlement area (Matimal et al., 2009). According to Yue et al. (2007), the relationship between NDVI and LST with integrated remote sensing application to quantify Shanghai Landsat7 ETM+ data was used. The result shows that different LU/LC classes have significantly different impacts on LST, and the NDVI was calculated using the Enhanced Thematic Mapper Plus sensor in the Shanghai urban environment. The populations of African cities will more than double in the next twenty years, and their spatial expanse could more than triple (Lamson-hall et al., 2015).

Land use and land cover is continuously changing in urban areas, which directly impact natural resource for sustaining life and environment. To find out how land use and land cover change, such analysis and mapping of land use and land cover are important aspects in monitoring studies, resource management and planning activities (Aspinalls and Hill, 2008; Foody and Atkinson, 2002). Land cover patterns on the Earth are constantly being changed by different human activities, thereby influencing biophysical processes (Li and Shao, 2014).

Thus, a detailed land use and land-cover mapping is an important research topic nowadays. Climate change will modify temperature and precipitation patterns (Thapa, 2019). It has resulted in an increase in temperature, erratic and extreme rainfall patterns, and the increased frequency of floods, landslides, and droughts that annually result in the massive loss of lives and properties (FAO, 2014; Karki et al., 2011; NAPA, 2010; Dixit et al., 2008). Climate and land-use changes are two major global ecological changes predicted for the future. Heretofore, causes and consequences of human-induced climate change and land-use activities have largely been examined independently (Turner et al. 1993). However, land use, land cover, and climate change impact each other.

2.10 LULCC Response to Land Surface Temperature in Ethiopia

Natural resource availability varies greatly in Ethiopia, and management practices vary greatly as well. Because of differences in biogeography and topography weather, there is variability. Human activities are speeding up land-use/land-cover changes, but they are also result in a change that harms humans (Agarwal et al., 2002). Water, plants, soil, animal feed, and other biophysical resources are all affected by the dynamics of LU/LC (Ali, 2009). Previous studies have found that due to land scarcity, there has been significant LU/LCC in Ethiopia, with the growth of cultivated land at the expense of woodland and forest land, stretching into sloppy areas. Agricultural methods and human settlement have a long history in Ethiopia's highlands, and there has lately been a highland population strain, which includes depletion of natural resources and unsustainable activities (Miheretu et al., 2017).

Despite the possibility that natural processes may also contribute to changes in land use and land cover in Ethiopia, many scholars concur that these changes are primarily the result of human activities (Agarwal et al., 2002; Ali, 2009; Birhan and Assefa, 2017). Changes in land use and cover provide insight into human histories and, maybe, human futures. Such changes are influenced by a wide range of factors, including human population growth, economic development, technology improvements, and environmental changes (Houghton, 1994). Population growth is one of the main causes of change in land use and land cover. The most important natural resource is people, and their long-term development is tied to and dependent upon one another (Santa, 2011).

A study of land use and land cover changes in Ethiopia and their effects is necessary to develop management and monitoring policies because 85% of the country's population lives in rural areas and 85% of its economy depends on agriculture, with traditional farming (plough) as the primary method of production. As a result, migration from rural areas to urban areas for better living conditions has increased. Depending on the availability of data and analytical techniques, studies on the changing land use and land cover in Ethiopia span a variety of geographical areas and academic fields. The majority of research, however, has been on deforestation, the expansion of farmed land to land degradation, river catchments and watersheds, natural ecosystems, and forests, as well as the resulting effects. Amsalu et al. (2007); Bewket and Abebe (2013); Tekle and Hedlund (2000); and Zeleke and Hurni (2001) were discovered among them. There were few research on urban development and modeling in cities of poor nations like Ethiopia. However, only a small number of investigations, including those by Haregeweyn et al. (2012); Dorosh and Schmidt (2010) ; Zeleke and Hurni (2001); Amsalu et al. (2007); Bekalo, have been reported (2009).

Zeleke and Hurni (2001) reported an expansion of cultivated land at the expense of natural forest cover between 1957 and 1982 in Dembecha area, north-western Ethiopia. The study also looked into a number of trends that have led to land degradation as a result of the spread of farmed land on steep slopes at the expense of natural forests. According to Amsalu et al. (2007), Ethiopia's central highlands experienced a considerable reduction in natural vegetation cover between 1957 and 2000, however there was an increase in plantation in the Beressa watershed. Despite an increase in eucalyptus tree plantations after the 1980s, Yeshaneh et al. (2013) also demonstrated a considerable decline in the wild woody vegetation of the Koga watershed since 1950 as a result of deforestation. In the Gish Abay watershed in north-western Ethiopia, Bewket and Abebe (2013) noted a decline in natural vegetation cover but an increase in open grassland, cultivated land, and villages.

Numerous studies have documented the effects of changes in land use and land cover on the watershed's hydrological flow regime. A change in the equilibrium between precipitation and evaporation and the runoff response has an influence. Due to long-term changes in land use and land cover, Muluneh and Arnalds (2011) found an increase in yearly direct runoff in the Gum-Selassa and Maileba catchments from 1964 to 2006. According to a related study, these long-term effects caused Lake Chelelека to dry up and Lake Haramaya to vanish. Geremew (2013) also noted that changes in land use and land cover have an impact on the stream flow in Ethiopia's Gilgel Abbay watershed. As a result of the conversion of farmed land from 1986 to 2001, his study found that stream flow increased by 16.26 m 3 /s during the rainy months and dropped by 5.41 m 3 /s.

According to various research, there have been changes in land use and land cover in reaction to urban growth. Bekalo (2009) found that urban areas in Addis Abeba, Ethiopia, increased dramatically from 34% in 1986 to 51% in 2000, displacing agricultural land and vegetated areas as a result of population growth. Dorosh and Schmidt (2010) noted that the urban population has grown significantly over the past three decades as a result of the expansion of the Ethiopian highlands' population. degradation was a result of population increase that was unsustainable, according to Muluneh and Arnalds (2011), referenced Haile (2004). According to Zeleke and Hurni (2001) and Amsalu et al., the majority of these research make it clear that population pressure is one of the main factors influencing changes in land use and land cover through the clearing of forest and vegetation for agricultural and urban expansion (2007). According to a research by Zeleke and Hurni (2001), population increase combined with rural-to-urban migration causes urban areas to continue to grow at the expense of vegetative cover. This is a frequent practice in Ethiopia's western highlands.

CHAPTER III MATERIAL AND METHOD

The geographical location, population and topography of Chiro town and its surrounding were described. The category of data that were used for this study and their sources, the methods of data processing such as layer stack, sub-setting, digital image processing. Multispectral radiometric correction, image classification, accuracy assessment, change detection analysis, and the method used to calculate NDVI, NDBI, and LST were included in this chapter. Additionally, the methods of analysis (zonal statistics and Pearson correlation coefficient) used in this study also a part of this chapter. From these zonal statistics used to determine the value for each LULC class and the Pearson correlation coefficient was used to analyze the association between LST with LULC indices (NDVI and NDBI).

3.1 Description of Study Area

3.1.1 Location and area

Chiro is a town Located in the West Hararge Zone in Oromia Regional State, Ethiopia Ahmar Mountains, it has a latitude and longitude of 9°05′N 40°52′E and an altitude of 1826 meters above sea level. It is the administrative center of the West Hararge Zone in Oromia Regional State. The total area coverage of the study area is 65,479.5ha. It is situated at about 326 kilo meters far from Addis Ababa. The district has 39 rural kebeles and the total population 198,020 Based on the 2007 census conducted by the Central Statistical Agency of Ethiopia this town has total population of 33,670 out of this 18,118are men and 15,552women are living in the town (CSA, 2007).

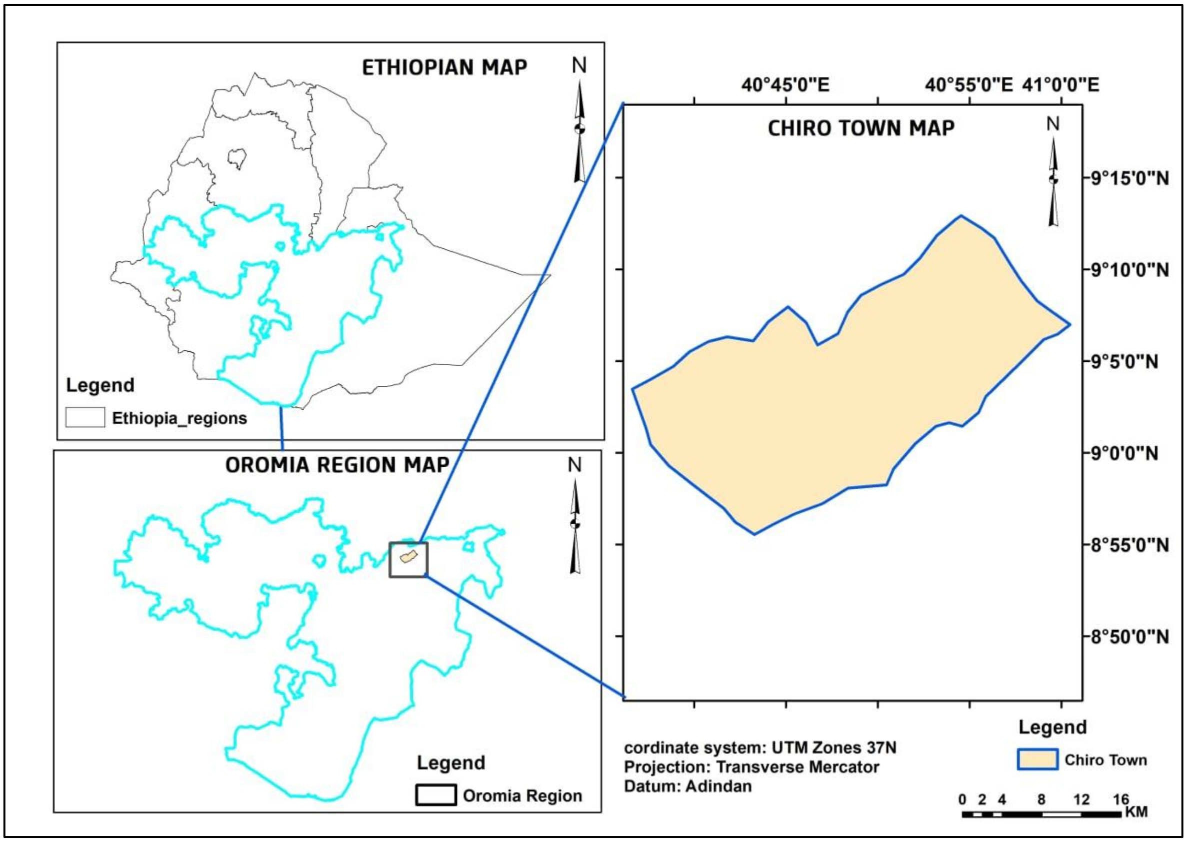

Figure 3.1: Location map of the study area

3.1.2 The topography of the study area

Topography describes the shape and feature of the earth‘s surface and other related phenomena or it is an integral part of the land surface. Landforms, elevation, latitude, longitude, and topographic maps are included in topography. The topography of Chiro town and its surrounding is uneven surface. The elevation of the target varies from 3036m to 1423m and slope range from 68.6617m to 0m.

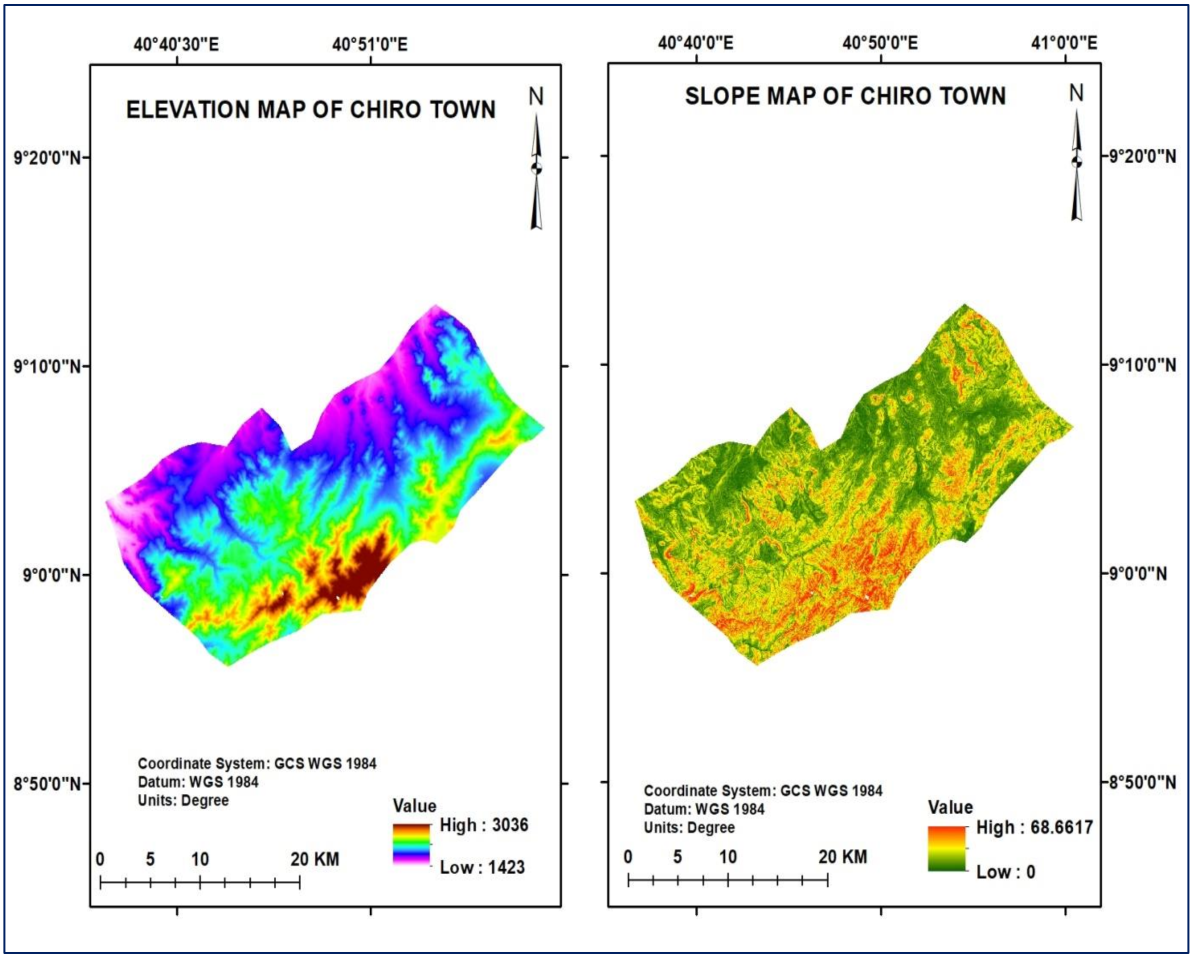

Figure 3.2: The elevation and slope map of the study area (m)

3.1.3 Population

Based on the 2007 G. C. national census conducted by the Central Statistical Agency of Ethiopia, ChiroWoreda has a total population of 207,553out of this, 106,277 are men and 101,276 were women and a total households of 35747out of this 30384 were men and 5363 were women. (Chiroworeda RLAUO 2011). According to national census, (2007) report the total population of town was 33670 peoples from whom 18118 where men and 15552 where women. The majority of the inhabitants were Muslim, which accounts 49.88% of the population, while 43.34% of the population practiced Ethiopian orthodox Christianity and 5.33% of the pupation were protestant. The 1994 national census reported that the town had a total population 18678 of whom 9218 were males and 9460 were females. It is the largest town in Chiro Woreda (CSA, 2007). In 1984 CSA reported that the town had a total population 11344 and in 2015 the town had a total population 49500

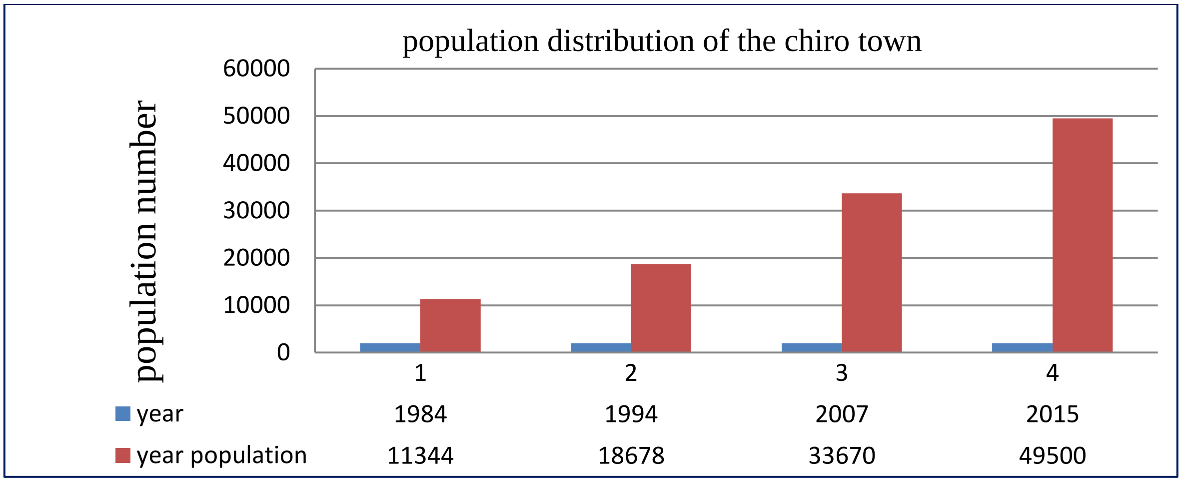

Figure 3.3: The population distribution of chiro town

3.2 Data sets and Sources

3.2.1 Remotely Sensed Data

The Landsat image acquired by Landsat 5 TM, Landsat 7 TM, Landsat 8 OLI/TIRS, and MODIS were used to conduct this research. Landsat 5, 7 and 8 were downloaded from the USGS website from (https://earthdata.nasa.gov/about/daacs/daac-lpdaac) website accessed in which is free of charge by using path 167 and row 054 of land sat satellite series.

The study period covered from the year 1990 to 2020. Thus, the years 1990, 2000, 2010, and 2020 were selected for analysis with 10 years interval. Imageries that were acquired by selecting criteria to avoid, cloud and haze-free imageries can easily be obtained during dry seasons where there is no cloud cover and rain and avoid the effects. The detailed description of Landsat data, which was used to access LULC change, NDVI NDBI, and LST distribution of the study provided in tables below.

Table 3.1: Remote sensing datasets were used for the study and their descriptions

path/row	Acquisition date	Satellite	Sensor	Resolution PAN/MS/TIRS	Source
167-054	12/26/1990	Landsat	TM	15/30/120	USGS
	12/15/2000		TM	15/30/60	
	12/13/2010		TM	15/30/60	
	12/13/2020		OLI	15/30/100	
	01/13/2020	Terra	MODIS	1Km	LP DAAC

A) Landsat Thematic Mapper (TM)

Landsat Thematic Mapper (TM) sensor was carried on Landsat 4 and Landsat 5 starts from July 1982. It has seven spectral bands; from these bands, three in the visible, three in infrared, and one in the thermal region of the spectrum. TM image has a spatial resolution of 30m for MS (band 1 to 5 and 7) and 120 m for thermal (band 6). Therefore, TM Band 6 is specifically sensitive to thermal infrared radiation to measure the LST of the earth‘s surface. Additionally, TM has a temporal resolution or repeat the cycle of 16 days. The scene size of TM images is approximately 170 km north-south and 183 km east-west. Detail about thematic mapper sensor bands and other descriptions are provided in Table 3.2.

Table 3.2: Landsat 5 TM sensor description

	Band	Description	Wave Length(µm)	Temporal Resolution(day)	Spatial Resolution(m)
Land Sat 5-	1	Blue	0.45 - 0.52	16	30
	2	Green	0.52- 0.60	16	30
	3	Red	0.63.- 0.69	16	30
	4	NIR	0.76 – 90	16	30
	5	SWIR-1	1.55 - 1.75	16	30
	6	Thermal	10.40 - 12.50	16	120
	7	SWIR-2	2.08 – 2.35	16	30

NB: NIR-near infrared, SWIR-short wave infrared

B) Landsat 7 Enhanced Thematic Mapper plus (ETM+)

Landsat 7 Enhanced Thematic Mapper Plus (ETM+) images consist of eight spectral bands with a spatial resolution of 30m for Bands 1to7. The resolution for Band 8 (panchromatic) is 15m. All bands can collect one of two gain settings (high or low) for increased radiometric sensitivity and dynamic range, while Band 6 collects both high and low gain for all scenes. Approximate scene size is 170 km north-south by 183 km east-west (106 mi by 114 mi).

Detail about enhanced thematic mapper sensor bands and other descriptions are provided in Table 3.3.

Table 3.3: Landsat 7 ETM+ sensor description

	Band	Description	Wave Length(μm)	Temporal Resolution(day)	Spatial Resolution(m)
Land Sat -7	1	Blue	0.45 - 0.52	16	30
	2	Green	0.52- 0.60	16	30
	3	Red	0.63.- 0.69	16	30
	4	NIR	0.77 – 90	16	30
	5	SWIR-1	1.55 - 1.75	16	30
	6	Thermal	10.40 - 12.50	16	60
	7	SWIR-2	2.08 - 2.35	16	30
	8	Panchromatic (PAN)	0.52 - 0.90	16	15

NB: NIR-near infrared, SWIR-short wave infrared

C) Landsat Operational Land Imager (OLI) and Thermal Infrared Sensor (TIRS)

Landsat 8 was launched on February 11, 2013, with OLI and TIRS. It has 11 bands; from these bands, 1 to 7 and 9 is MS, and band 8 is panchromatic while band 10 and 11 are thermal, which is used to determine LST. The spatial resolution of Landsat 8 is 15m, 30m, and 100 m for PAN, MS, and TIRS respectively. Band 1 is ultra-blue useful for coastal and aerosols studies while Band 9 is useful for cirrus cloud detection. The scene size of Landsat 8 images is 170 km north-south and 183 km east-west (USGS, 2013). Detail explanation about OLI and TIRS bands are provided in Table 3.4.

Table 3.4: Landsat 8 OLI and TIRS bands description

	Band	Description	Wave Length(μm)	Temporal Resolution(day)	Spatial Resolution(m)
OLI and TIRS	1	Blue	0.43 - 0.45	16	30
	2	Green	0.45- 0.51	16	30
	3	Red	0.53.- 0.59	16	30
	4	NIR	0.64 – 67	16	30
	5	SWIR-1	0.85 - 0.88	16	30
	6	Thermal	1.57 - 1.65	16	30
	7	SWIR-2	2.11 – 2.29	16	30
	8	Panchromatic	0.50 – 0.68	16	15
	9	Cirrus	1.36 – 1.38	16	30
	10	TIRS - 1	10.60 – 11.19	16	100
	11	TIRS - 2	11.50 – 12.11	16	100

3.2.2 Ground Truth Data and Google Earth Data

Ground truth data were collected from the field using GPS after stratified sample points generated from the image of Landsat and their coordinates from Google Earth. Field data were used for validating the LULC classified image into different classes by observing the real LULC of the study area. To minimize errors in classification, pictures showing different LULC classes in the area were captured. Google Earth map was used as a visual interpretation during the image classification process. According to Jensen (2015); Lillesand et al. (2008); and Congalton and Green (2009) a minimum of 50 sample points for each mapping class should be collected for maps of < 4,000 km^2 in size and fewer than 12 classes to do accuracy assessment. The area in Chiro town and its surrounding is 65,479.5ha and four LULC classes were identified for this study. Therefore, the two hundred ten sample points were collected for this study to accuracy assessment and classification.

3.2.3 MODIS Data

Moderate Resolution Imaging Spectro radiometer data were used to validate the LST extracted from Landsat imageries. This MODIS data were downloaded from the National Aeronautics and Space Administration Land Processes Distributed Active Archive Center (NASA LP DAAC) website (https://earthdata.nasa.gov/about/daacs/daac-lpdaac) accessed in Jan 2020.

3.3 Software and tool

ERDAS IMAGINE 2015, ArcGIS 10.8, Google Earth PRO 2021, Microsoft word and excel 2016, XLSTAT and GPS was used to process satellite imageries and analyze urban LULC changes, NDVI, NDBI, LST and the association LST with LULC indices. From this, ERDASIMAGINE 2015 was used for image preprocessing and image classification. Arc GIS10.8 was used to prepare the layout map of the town, zonal statistics, and reclassification. Mapping of NDVI, NDBI, and LULC map of a study, conversion detection analysis and extract LST were also done by ArcGIS 10.8 While, and Google Earth PRO 2020 was used as a base map in visual image interpretation, and generate coordinate points for the image of 2020. XLSTAT were used to develop correlation statistics of LST with NDVI and NDBI. GPS was used to download point data from GPS for accuracy assessment and Microsoft word and excel 2016 also used to compile the whole parts of this study.

3.4 Methods of analysis

This study has four main methods. The first was the LULC analysis from Landsat 5, 7 and 8. The second one is the calculation of NDVI, NDBI and LST from Landsat imageries. Validation of LST from the MODIS data set in the third step. Finally, zonal and correlation statistics were done for NDVI and NDBI with LST.

3.4.1 Digital Image Preprocessing

Satellite imagery is affected by various factors, which decrease the image quality. Therefore, to get important information from those images, they should be processed and corrected digitally before using them for further analysis. Digital image processing involves the operation and interpretation of digital images through the help of computer application software. It is helpful to increase the quality of an image and maintain the quality image for interpretation and classification; it is possible to minimize interpretation errors since the image can easily be manageable on a computer (Abel, 2018). Therefore, preprocessing mostly comprises a series of sequential processes, including atmospheric correction or normalization, image registration, and geometric correction. Digital image pre-processing functions include those processes that are essential before using information extraction for data analysis.

3.4.2 Multispectral Radiometric Correction

Preprocessing is very essential to get an accurate image because radiation, which comes from the source, always interacts with the atmosphere (Abel, 2018). The energy, which is reflected to the sensor after its contact with the target object, is useful for remote sensing. Therefore DN should be converted into spectral radiance. Landsat 5 TM image was radiometrically corrected and spectral radiance converted to radiance in Arc GIS by using the following formula (Markham and Barker, 1986):

$$L\lambda = \frac{L\lambda max - L\lambda min}{Qcalmax - Qcalmin} \times (Qcal - QCALmin) + L\lambda min \ldots\ldots\ldots\ldots\ldots\ldots\ldots\ldots\ldots\ldots\ldots\ldots\ldots\ldots (1)$$

Where; Lλ is Spectral radiance received by the sensor (W/ (m^2 × sr × μm)), QCAL is the quantized calibrated pixel value in DN of band 6, L is the spectral radiance that is scaled to Qcalmin (W/ (m^2 × sr × μm), Lλmax is the spectral radiance that is scaled to Qcalmax (W/ (m^2 × sr × μm), Qcalmin is the minimum quantized calibrated pixel value (corresponding to L in DN which is 1) and Qcalmax is the maximum quantized calibrated pixel value (corresponding to L x in DN which is 255). Then, level pixel DN values were converted to top of atmospheric (TOA) reflectance using the equation provided below:

$$\mathrm{P\lambda} = \frac{\pi \times \mathrm{L\lambda} \times \mathrm{d}^2}{\mathrm{ESUN\lambda} \times \cos\theta} \ldots\ldots\ldots\ldots\ldots\ldots\ldots\ldots\ldots\ldots\ldots\ldots\ldots\ldots\ldots\ldots\ldots\ldots\ldots\ldots\ldots\ldots\ldots\ldots\ldots\ldots (2)$$

Where; Pλ is unit less planetary reflectance, Lλ is Spectral radiance at the sensor's aperture, d is Earth-Sun distance in astronomical, ESUNλ is mean solar exo-atmospheric irradiances and θ is solar zenith angle in degrees.

Landsat 8 OLI image is also radiometrically corrected and spectral radiance changed to radiance in ArcGIS using the formula given by (USGS, 2016):

$$\mathrm{L\lambda} = \mathrm{M\lambda} * \mathrm{Qcal} + \mathrm{AL} \ldots\ldots\ldots\ldots\ldots\ldots\ldots\ldots\ldots\ldots\ldots\ldots\ldots\ldots\ldots\ldots\ldots\ldots\ldots\ldots\ldots\ldots\ldots\ldots\ldots\ldots\ldots\ldots (3)$$

Where; Lλ = Spectral radiance (W/ (m^2 × sr ×μm)); M_λ is Radiance multiplicative scaling factor for the band (radiance_multi_band_n from the metadata); AL is Radiance additive scaling factor for the band (radiance_add_band_n from the metadata); Qcal is Level one pixel value in DN.

Then, level 1 pixel DN values were converted to top of atmosphere reflectance using the equation (USGS, 2016):

$$\rho\lambda' = Mr * Qcal * Ar \ldots\ldots\ldots\ldots\ldots\ldots\ldots\ldots\ldots\ldots\ldots\ldots\ldots\ldots\ldots\ldots\ldots\ldots\ldots\ldots\ldots\ldots\ldots (4)$$

Where; ρλ′ is Top-of-Atmosphere Planetary Spectral Reflectance, before correction for a solar angle, Mr is Reflectance multiplicative scaling factor for the band (reflectance multi band N from the metadata), Ar is the Reflectance additive scaling factor for the band (reflectance add band N from the metadata), and Qcal is Level one pixel value in DN. Once a solar elevation angle is selected, then conversion to true top of atmosphere reflectance is given by:

$$P\lambda = \frac{\rho\lambda'}{cos\theta SZ} \ldots\ldots\ldots\ldots\ldots\ldots\ldots\ldots\ldots\ldots\ldots\ldots\ldots\ldots\ldots\ldots\ldots\ldots\ldots\ldots\ldots\ldots\ldots (5)$$

Where: ρλ′ = Top-of-Atmosphere Planetary Reflectance; θ_{SZ} = Local solar zenith angle.

3.4.3 Image Classification

According to Gao (2009) and Lillesand et al. (2004), image classification is a technique of extracting information from the image based on the reflectance value of an object. The class can be grouped into a thematic layer of having similar LULC in the image. It is the most common method to extract information in digital remote sensing. A human analyst uses the components of visual interpretation to recognize homogenous groups of pixels, which represent different land, cover classes of interests to classify features of an image. The spectral information is characterized by the DN in each spectral band and assumes to classify each pixel based on spectral information.

Image classifications using remote sensing procedures have attracted the devotion of the research community because classification is the backbone of environmental, social, and economic applications (Lu and Weng, 2007). Multispectral data were used to classify the spectral pattern presented in each pixel used as the numerical basis for categorization. This concept is called Pattern Recognition. The definition of spectral pattern recognition is the family of classification procedures that utilizes this pixel-by-pixel spectral information as the basis for automated land covers classification (Ziena, 2017). To do this supervised classification with maximum Likelihood Classifier technique was used.

3.4.3.1 Supervised Classification

The supervised classification technique uses a training sample for each category, that is, a group of data points known and come from the class of interest. The classification was done by considering how close a point to be categorized is to each training sample. The Supervised classification has different techniques such as maximum likelihood, parallelepiped, and minimum distance to mean. This study uses supervised classification because it has an advantage in regards to the development of information classes, self-assessment by using training sites and training sites reusable. However, information classes may not match spectral classes, the signature homogeneity, and uniformity of information classes may vary.

3.4.3.1.1 The Maximum Likelihood Classifier Technique

The maximum Likelihood of supervised classification is used statistics (mean, variance, or covariance) to classify pixel values. The MLC technique applies the probability theory to the classification task. This method defines the class centers and the variability in raster values in each input band for each class from the training set classes. The information allows the procedure to define the probability that an assumed cell in the input image belongs to a specific training set class center and the size and shape of the class in spectral space. It calculates all of the class probabilities for every raster cell and gives the cell to the class with the highest probability value. This technique yields more accurate class assignments than the minimum distance to means technique when classes vary significantly in size and shape in spectral space (Lillesand et al., 2004).

The MLC quantitatively defines both the variance and covariance of a class spectral response patterns when classifying unidentified cells. We may compute the statistical probability of an assumed cell value being a member of a particular land class, the computer would calculate the probability of the cell value occurring in the distribution of class then the likelihood of its occurring in class. After assessing the probability in each category, the cell would be allocated to the highest probability value class. The MLC technique has its weakness and strength. The weakness of this procedure is computational ineffective compared to the other technique. The strength of this technique is advantageous for different degrees of variance in the spectral response data. Therefore, to do this study, the MLC technique was used. Because in urban areas, there are different degrees of variance in spectral response data. There is a problem of cell mixing especially in low-resolution imageries such as Landsat and this has seriously affected the LULC classification accuracy of the study. To minimize this problem in image classification, a Google Earth map and field survey data were used.

After classification accuracy was conducted, final LULC thematic layers were identified and mapped for three study periods (1990, 2000, 2010 and 2020). Therefore, Chiro town and its surrounding have the following LULC classification schemes such as built up, vegetation, agriculture, and bare land. This classification scheme was developed based on (Anderson et al., 1976) the first level of the classification scheme, and has been made to provide as much compatibility as possible with other classification systems. Currently, this is being used by the various Federal agencies involved in land use inventory and mapping such as the Ethiopian Mapping Agency, based on prior knowledge and a brief reconnaissance survey in the study area.

3.4.4 Accuracy Assessment

The accuracy assessment of image classification and simulation results is slightly different, because in the latter case the accuracy assessed by using the maps not the specific points which are indicating the real category information (Rossiter, 2004). LULC classification accuracy was assessed quantitatively using error matrix which is the commonly used method in LULC classification accuracy assessment (Bulti, D., 2019). In this regard, sample pixels were selected from each of classified images through a stratified random sampling scheme in ARCGIS software. The samples were overlaid with Google earth (for 1990, 2000, 2010 and 2020) and existing map (for 2007). These sample points per each LULC class were collected to develop the confusion/error matrix and it is used for accuracy assessment. It was calculated to assess the association of reference pixels with classified land use and land cover maps. The arrangement of at error/confusion matrix was numbered representing the number of samples allocated to each class comparative to the reference data, in records and fields. The records 31 indicate LULC maps derived from classification while fields indicate reference data collected from the field. The advantage of error/confusion matrix is to determine different statistical values like producer's accuracy (omission error), user's accuracy (commission error), overall accuracy, and kappa coefficient used to assess accuracy assessment (Congalton and Green, 2009). According to Landis, J., (1977) Strength of Agreement for Kappa Statistic < 0 poor, 0.00-0.20 slight, 0.21-0.40 fair, 0.41-0.60 moderate, 0.61-0.80 substantial and 0.81-1.00 Almost Perfect/Perfect.

Producer's accuracy is calculated by dividing the diagonal elements in each category by the sum of pixels of that category which is calculated from the reference data. This statistic shows the chance of a reference data being exactly classified and is a measure of omission error or error of exclusion. The producer‘s accuracy can be calculated based on the following equation.

$$Producer's\ accuracy\ = \frac{number\ of\ corrected\ pixels\ in\ a\ class}{total\ sample\ points\ in\ a\ class} \times 100 \ldots\ldots\ldots\ldots\ldots (6)$$

User's Accuracy is calculated by dividing the diagonal elements in a category by the sum of pixels that were classified in that category; the result is a measure of commission error or error of inclusion. It is calculated based equation provided below.

$$User's\ accuracy = \frac{number\ of\ corrected\ pixels\ in\ a\ class}{tatal\ number\ of\ classified\ points\ in\ a\ class} \times 100 \ldots\ldots\ldots\ldots.. (7)$$

Overall accuracy is calculated by the sum of exactly classified pixels divided by the sum of sample points (Congalton, 1991). It includes only the diagonal elements of the error matrix and it is hard to relate unalike overall accuracy values if an unalike number of accuracy sites were used. The value of overall accuracy was calculated based on the following equation provided below.

$$Overall\ accuracy = \frac{\text{the sum of classified pixels}}{\text{total sample points}} \times 1oo \ldots\ldots\ldots\ldots\ldots\ldots\ldots\ldots\ldots.. (8)$$

Kappa analysis is used to show the variation between actual agreements and the agreement anticipated by chance. It includes both diagonal and non-diagonal elements of the error matrix (Tempfli et al., 2009). Kappa analysis gives Khat statistics which is the measure of an agreement (Congalton,1991). This study uses khat statistics because it considers non-diagonal elements and compares two classification products statically. It is calculated by the following equation provided below:

$$K = \frac{N\sum_{i=1}^{r} Xii - \sum_{i=1}^{r}(Xi+X+i}{N^2 - \sum_{i=1}^{r}(Xi+X+i)} \ldots\ldots\ldots\ldots\ldots\ldots\ldots\ldots\ldots\ldots\ldots\ldots\ldots\ldots\ldots\ldots\ldots\ldots\ldots\ldots\ldots\ldots\ldots\ldots(9)$$

Where: N- total number of samples included in the matrix, Xii- number of observations in row i and column i, Xi+-total observations in row i, and X+i- total observations in column i. The value of K falls between 0 and 1, where the former and later indicates no better than would be expected by chance and perfect agreement respectively. This value is often multiplied by 100 to give a percentage measure of classification accuracy (Worku, 2018).

3.4.5 Urban Land use and Land cover Thematic Layer of the study area

Four LULC thematic layers were determined and mapped for 1990, 2000, 2010 and 2020 after classification accuracy was done. Therefore, Chiro town and its surrounding has the following LULC classes and is presented in table 3.5

Table 3.5: LULC thematic layer of the classified class

No	LULC	Description
1	Built-up	The area is occupied by buildings including mixed and pure Residences, factories, offices, churches, schools, mosques, hospitals, hotels, warehouses, and roads.
2	Vegetation	The area covered by shrubs, and tree.
3	Agriculture	The area covered by annual and perennial crops
4	Bare land	The area covered by dry soil, sand/rock and, dry salt flats, beaches, a non-vegetated area dominated by rock, eroded and degraded lands.

3.4.6 Change Detection Analysis

Change detection was carried out by using the post-classification method. Post classification is the most commonly used approach for change detection purposes (Xiuwan, 2002). The analysis of LULC Change maps involved technical procedures of integration using ArcGIS software techniques. The first task is to develop a table indicating the area coverage in hectare and the percentage change for each year 1990, 2000, 2010 and 2020 measured against each LULC class. Therefore, to calculate the rate of LULC Change, the following percentage equation was used (Lambin et al., 2001).

$$percentage\ area\ change = \frac{area\ i\ year\ x+1\ - Area\ i\ year\ x}{\sum_{i=1}^{r}(Area\ i\ year\ x+1)} \times 100 \ldots\ldots\ldots\ldots\ldots\ldots (10)$$

Where; Area i year x = area of cover i at the previous year, Area i year x +1 = area of cover i at the next year,

$\sum_{i=1}^{r}(Area\ i\ year\ x+1)$ is the total cover area in the next year

3.4.7 Determination of the land use land cover indices

3.4.7.1 Normalized Difference Vegetation Index

This is very essential to discriminate vegetation from no-vegetation and indicates the amount of vegetation present on the surface. In addition to this, NDVI computation is important to calculate the emissivity (ε). Since, these parameters are highly associated with the NDVI (Weng et al., 2004). Therefore, NDVI was acquired from the red bands in spectral reflectance measurements and near-infrared bands in the ArcGIS software. The NDVI was calculated by the following equation.

$$\text{NDVI} = \frac{Near-\ infrared - Red}{Near - infrared + Red} \ldots\ldots\ldots\ldots\ldots\ldots\ldots\ldots\ldots\ldots\ldots\ldots\ldots\ldots\ldots\ldots\ldots\ldots\ldots\ldots\ldots\ldots\ldots\ldots\ldots. (11)$$

Where; NDVI is Normalized Difference Vegetation Index

3.4.7.2 Normalized Difference Built-up Index

This index is very important for mapping urban or built-up areas from Landsat data. It is useful to recognize the extent and density of imperviousness surfaces like built-up, asphalt road, and parking areas and map these areas (Zha et al., 2003 and Malik et al., 2019). Urban areas have a higher reflectance value in the SWIR region than the NIR region (Alhawiti and

Mitsova, 2016). The NDBI can be calculated using short wave and near-infrared bands of the Landsat image in the following way.

$$\text{NDBI} = \frac{Short\ wave\ infrared - Near\ infrared}{Short\ wave\ infrared + Near\ infrared} \ldots\ldots\ldots\ldots\ldots\ldots\ldots\ldots\ldots..\ldots\ldots\ldots\ldots. (12)$$

Where; NDBI-Normalized difference built-up index

3.4.8 Land Surface Temperature Computation

The land surface temperature can be calculated in different ways based on the parameters (for instance, normalized difference vegetation index, emissivity, water vapor, and resources (data and software) were used.

3.4.8.1 Land Surface Emissivity

According to Becker and Li (1995), Emissivity is the ratio of the radiance which is emitted by the real surface materials at their temperature and the radiance emitted by the black body at the same temperature. Emissivity can be represented by the function of wavelength is controlled by several environmental factors such as surface water content, chemical composition, structure, and roughness. For vegetated areas, emissivity varies significantly with types of plants, areal densities, and growth rates. Land surface emissivity is closely associated with NDVI (Weng and Larson, 2005; Tran and Ha, 2010). Therefore, the emissivity value can be calculated by the following equation provided below in different NDVI values (Sobrino et al., 2001).

$$E = \begin{cases} EW & NDVI < 0 \\ ES & 0 \geq NDVI < 0.2 \\ EvPv + Es(1 - PV) + Ce & 0.2 \geq NDVI < 0.5 \\ Ev & NDVI \geq 0.5 \end{cases} \ldots\ldots\ldots\ldots\ldots\ldots\ldots\ldots\ldots\ldots (13)$$

Where; Ev- emissivity of vegetation; Es- emissivity of soil; Ce-is the surface geometrical distribution is given by (1-Es) + (1-Ev) ×F ×Ev, and F = 0.55, shape parameters factor considering different geometrical distribution and Pv proportion of vegetation which is calculated based on the equation provided below (Jin et al., 2015).

$$PV = \left(\frac{NDVI - NDVImin}{NDVImax - NDVImin}\right)^2 \ldots\ldots\ldots\ldots\ldots\ldots\ldots\ldots\ldots\ldots\ldots\ldots\ldots\ldots\ldots\ldots\ldots\ldots\ldots\ldots\ldots\ldots\ldots (14)$$

Where; PV is Proportion of Vegetation, NDVI is Normalized Difference Vegetation Index, NDVI min is the Normalized Difference Vegetation Index minimum value and NDVImax is the Normalized Difference Vegetation Index maximum value.

3.4.8.2 Land Surface Temperature Algorithms

After spectral radiance is converted to radiance, the raw digital numbers of the thermal bands are converted to Top of Atmosphere brightness temperatures, which are the effective temperature viewed by the satellite under an assumption of emissivity (Chander et al., 2009) using Planck's equation provided below:

$$TB = \frac{K2}{ln\left(\frac{K1}{L\lambda} + 1\right)} \dots \dots \dots \dots \dots \dots \dots \dots \dots \dots \dots \dots \dots \dots \dots \dots \dots \dots \dots \dots \dots \dots \dots \dots \dots \dots \dots \dots \dots \dots \dots \dots (15)$$

Where; TB is effective at-sensor brightness temperature (K), $K2$ is calibration constant 2 (K), $K1$ is calibration constant 1 (W/ (m^2 × sr ×µm)), $L\lambda$ is spectral radiance at the sensor's aperture (W/ (m^2 × sr ×µm)) and ln is natural logarithm.

Table 3.6: calibration constants for thermal bands in different Landsat series

Satellite	Band	k1	k2	$L\lambda$min	$L\lambda$max	Mλ	AL
Landsat5	6	607.76	1260.56	1.2378	15.303	-----	----
Landsat7	6	666.09	1282.71	3.200	17.040	6.7087E-02	-0.06709
Landsat8	10	774.8853	1321.0789	-----	----	0.0003342	0.1
Landsat8	11	480.8883	1201.1442	-----	----	0.0003342	0.1

For Landsat 5, Landsat 7 the LST can be determined by this equation (Xiong et al., 2012, Yue et al., 2007).

$$LST = \frac{TB}{1 + \left(\lambda \times \left(\frac{TB}{P}\right)\right) \times ln\varepsilon} \dots \dots \dots \dots \dots \dots \dots \dots \dots \dots \dots \dots \dots \dots \dots \dots \dots \dots \dots \dots \dots \dots \dots \dots \dots \dots (16)$$

Where; LST is land surface temperature in kelvin, TB is sensor brightness temperature in kelvin, λ (11.45) is the wavelength of the emitted radiance (for peak response and average limiting wavelengths), and ε is land surface emissivity.

$p = \frac{hc}{\sigma} = 1.4388 \times 10^{-2}\ MK,$

where, h is Plank's constant (6.626 $\times 10^{-34}$Js, C indicates light velocity (2.998 $\times 10^{8}$m/s) and σ is The Boltzmann constant (5.67 $\times 10^{-8}$ Wm^{-2}k-4=1.38 $\times 10^{-23}$J/k)

3.4.8.2.1 Split Window Algorithm

The split window algorithm uses different absorption between two thermal infrared channels within one atmospheric window to eliminate the atmospheric influence and calculates surface temperature as a linear combination of two brightness temperatures (Dash et al., 2002). The algorithm assumes that the LSE values in both thermal infrared channels are known (Jin et al., 2015). This algorithm is functional for sensor where there is two thermal infrared channel, for instance, OLI in Landsat-8 (TIRS band 10 and 11), which was used by (Du et al., 2014; JiménezMuñoz et al., 2014; Jin et al., 2015; Qin et al., 2001; Rozenstein et al., 2014). The general algorithm of the split window can be expressed as:

$$Ts = TB10 + D1(TB10 - TB11) + D2(TB10 - TB11)^2 + D0 + (D3 + D4W)(1 - \varepsilon) + (D5 + D6W)\Delta\varepsilon \ldots\ldots\ldots \ldots (17)$$

Where; Ts is Land Surface Temperature, D0 up to D6 =Split Window Coefficient Value,

TB10 is the brightness temperature of band 10, TB11is brightness temperature of band 11, and ε is the mean land surface emissivity of thermal infrared bands (mean of band 10 and band 11), $W$is atmospheric water vapor content and $\Delta\varepsilon$ is Difference in LSE of band 10 &11.

Table 3.7: Constant value of a split algorithm

Constant	D0	D1	D2	D3	D4	D5	D6
Value	-0.268	1.378	0.138	54.3	-2.238	-129.2	16.4

According to (Wang et al., 2015), the water vapor content of the atmosphere from the first layer to the altitude of the satellite can be determined as follows:

$$W = \frac{w0}{w1} \ldots\ldots\ldots\ldots (18)$$

Where; w is the total water vapor of the atmosphere from the first layer to the altitude of the satellite, w0 is the water vapor of the ground and w1 is the ratio of water vapor content at the first layer to the altitude of the satellite.

The value of w1differ in different atmospheres, with w1= 0.6834 for tropical atmosphere, w1 = 0.6819 and w1 = 0.6593 for subtropical summer and winter atmospheres, respectively, and w1 = 0.6834 and w1 = 0.6356 for mid-latitude summer and winter atmospheres, respectively (Qin et al., 2001). The value of w1 is 0.6834. The water vapor content of the ground also can be computed as follows:

$$W0 = \frac{H \times B \times D}{100} \dots\dots\dots\dots\dots\dots\dots\dots\dots\dots\dots\dots\dots\dots\dots\dots\dots\dots\dots\dots\dots\dots\dots\dots\dots\dots (19)$$

Where, H is air humidity (%) at the ground from meteorology station, B is the saturation mix ratio (g/kg) and D is air density (g/m3) at specific air temperature. The values of saturation mix ratio and air density at specific air temperature were provided in table 3.7.

Table 3.8: The values of saturation mix ratio and air density at specific air temperature

T (°C)	45	40	35	30	25	20	15	10	5	0	-5	-10
b (g·kg−1)	66.33	49.81	37.25	27.69	20.44	14.95	10.83	7.76	5.5	3.84	2.52	1.63
d (kg·m−3)	1.11	1.13	1.15	1.17	1.18	1.21	1.23	1.25	1.3	1.29	1.32	1.34

Finally, Land surface temperature computed from Landsat TM and OLI/TIRS was converted into degree Celsius, by subtracting 273.15. Therefore, to convert temperature in degree Kelvin to degree Celsius equation 3.17 was used.

$$℃ = K - 273.15 \dots\dots\dots\dots\dots\dots\dots\dots\dots\dots\dots\dots\dots\dots\dots\dots\dots\dots\dots\dots\dots\dots\dots\dots\dots\dots\dots\dots\dots .. (20)$$

Where: °C: LST in degree Celsius; K: LST in degree Kelvin

3.4.9 Validation of Land Surface Temperature

The results of LST extracted from the thermal band of Landsat 5 TM and Landsat 8 OLI/TIRS images of the study area for the study periods were validated using MODIS data that acquired during a similar period. The MODIS LST and emissivity product at 1km spatial resolution and 8-day temporal resolution retrieved in the Hierarchical Data Format, which is accessed from the NASA Land Process Distributed Active Archive Center (NASA LP DAAC) website (https://earthdata.nasa.gov/about/daacs/daac-lpdaac). The LST of the study area for 2020 has been derived from MOD11A2. The DN value of LST is converted to degree Celsius by using the following formula with the scale factor of 0.02 (Wan, 2013)

$$LST = (DN \times 0.02) - 273.15 \ldots \ldots \ldots \ldots \ldots \ldots \ldots \ldots \ldots \ldots \ldots \ldots \ldots \ldots \ldots \ldots \ldots \ldots \ldots \ldots \ldots \ldots \ldots \ldots \ldots \ldots (21)$$

The validation was carried out based on the ranges and pixel to pixel comparison (Pearson correlation) of the two images' of land surface temperature in this study. But, the spatial resolution of the two images is different and difficult to compare using pixel to pixel comparison. Therefore, the resolution of these two images resamples to 400 m in this study using the nearest resampling technique. Finally, convert pixel values (raster) to point (vector) and extract the values of these points in the ArcGIS environment using extract multi-value to points.

3.4.10 Zonal Statistics

A zone is all the pixels in a raster that have the same value. Zonal statistics are used to calculate statistics for each zone of a dataset based on values from another dataset, a value raster. It divides the raster data based on the zone and calculates statistics for the raster data in the same zone, the cells in the same zone was assigned the same value and output to a new raster dataset (Abel, 2018). A single output value was computed for each cell in each zone defined by the input zone dataset. To analyze NDVI, NDBI, and LST and to understand their spatial distribution in each LULC type and their variation, zonal statistics were applied in ArcGIS 10.8 software. Therefore, to analyze the spatial distribution and temporal variation of LST in each LULC and analyze the impacts of LULC change on LST data was summarized using MS Excel 2016.

3.4.11 Zonation for spatial coverage of LST

The surface temperature was classified into three temperature categories such as low, medium, and high-temperature categories by using minimum, maximum, mean, and standard deviation to see the spatial distribution of LST. Each zone was identified using a pair of temperature thresholds that were determined based on the minimum, maximum, and mean temperatures of the study area (including all LULC types) and its standard deviation. The range of the medium zone was determined by adding the standard deviation from the mean and subtracting the standard deviation to the mean. Therefore, the minimum value of the medium zone was obtained as standard deviation minus the mean, and its maximum value was determined by standard deviation plus the mean temperature of the study area for a specific year. The minimum temperature of the study area for a specific year and minimum value of the medium zone were used to determine the range of low zone, while the maximum value of the medium zone and the maximum temperature of the study area was the range of high zone (Wei et al., 2015).

3.4.12 Correlational Analysis

Pearson correlation was used to test the strength of the linear relationship of NDBI and NDVI, with LST for each pixel. It is a measure of the linear relationship between two variables X and Y, giving value range from +1 to -1, where +1 indicates a perfect positive relationship, -1 indicates a perfect negative relationship and 0 indicates no relationship exists (Guo et al., 2014). To analyzed the degree of the relationship between the LST and LULC indices (NDVI and NDBI), the value of Pearson correlation coefficient was group based on the absolute value of the correlation coefficients into a weak correlation ($0 < |r| \leq 0.3$), a low correlation ($0.3 < |r| \leq 0.5$), a moderate correlation ($0.5 < |r| \leq 0.8$), and a strong correlation ($0.8 < |r| \leq 1$) (Li et al., 2004).

The mathematical equation of the Pearson correlation coefficient is presented as follows.

$$r_{xy} = \frac{\sum_{r=1}^{n}(xi-xj)\times(yi-yj)}{\sqrt{\sum_{i=1}^{n}(xi-xj)^2}\sum_{i=1}^{n}(yi-yj)^2} \text{...} (22)$$

Where, rxy is the simple correlation coefficient of variables X and Y, xi is NDBI, and NDVI of the ith year, Yi is LST of the ith year; Xm is the average NDVI and NDBI for all years, Ym is LST for all years.

The general methodology for data processing is described in the technical scheme of the research work in figure 3.4 and 3.5.

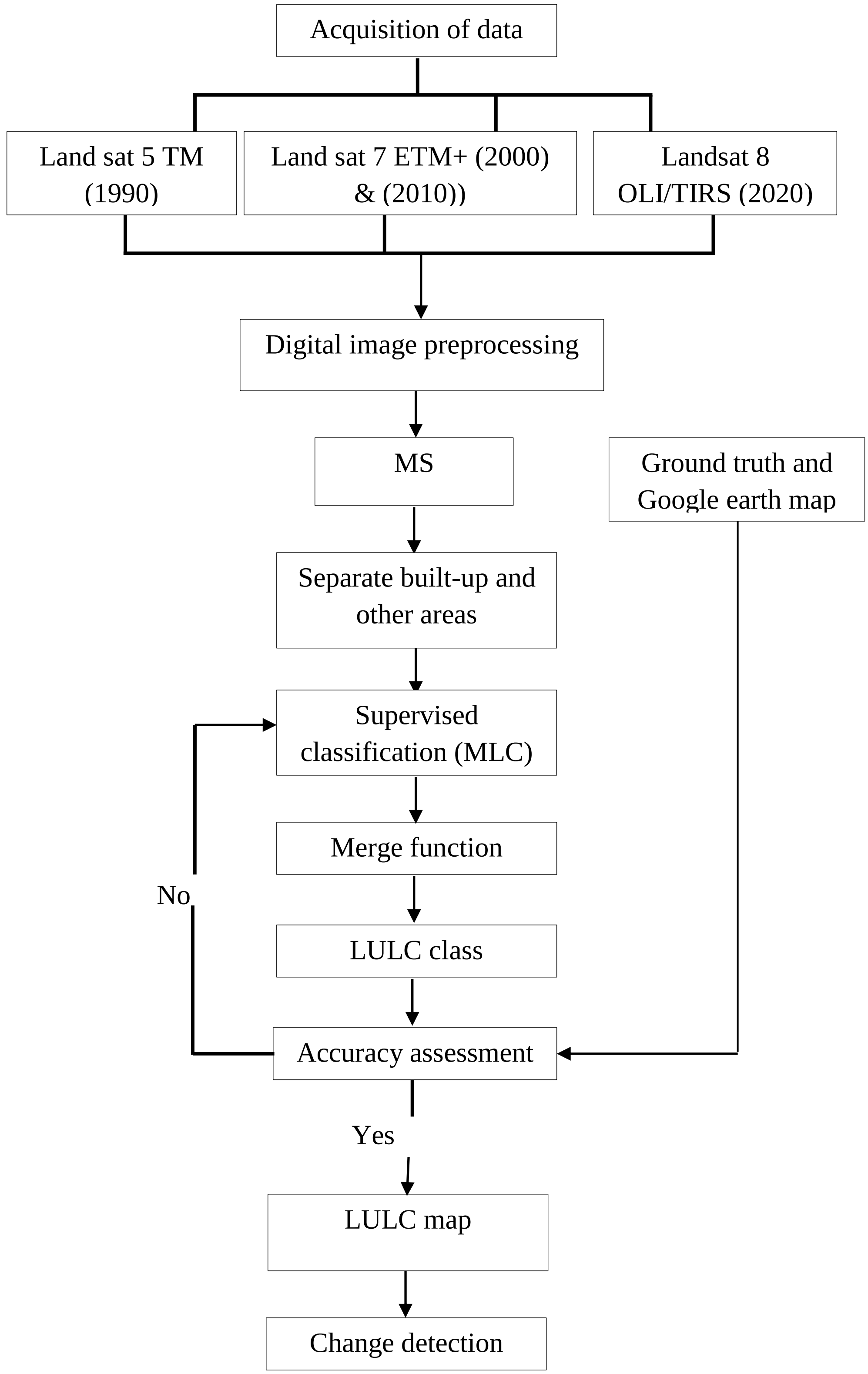

Figure 3.4: Technical scheme of image classification for research work

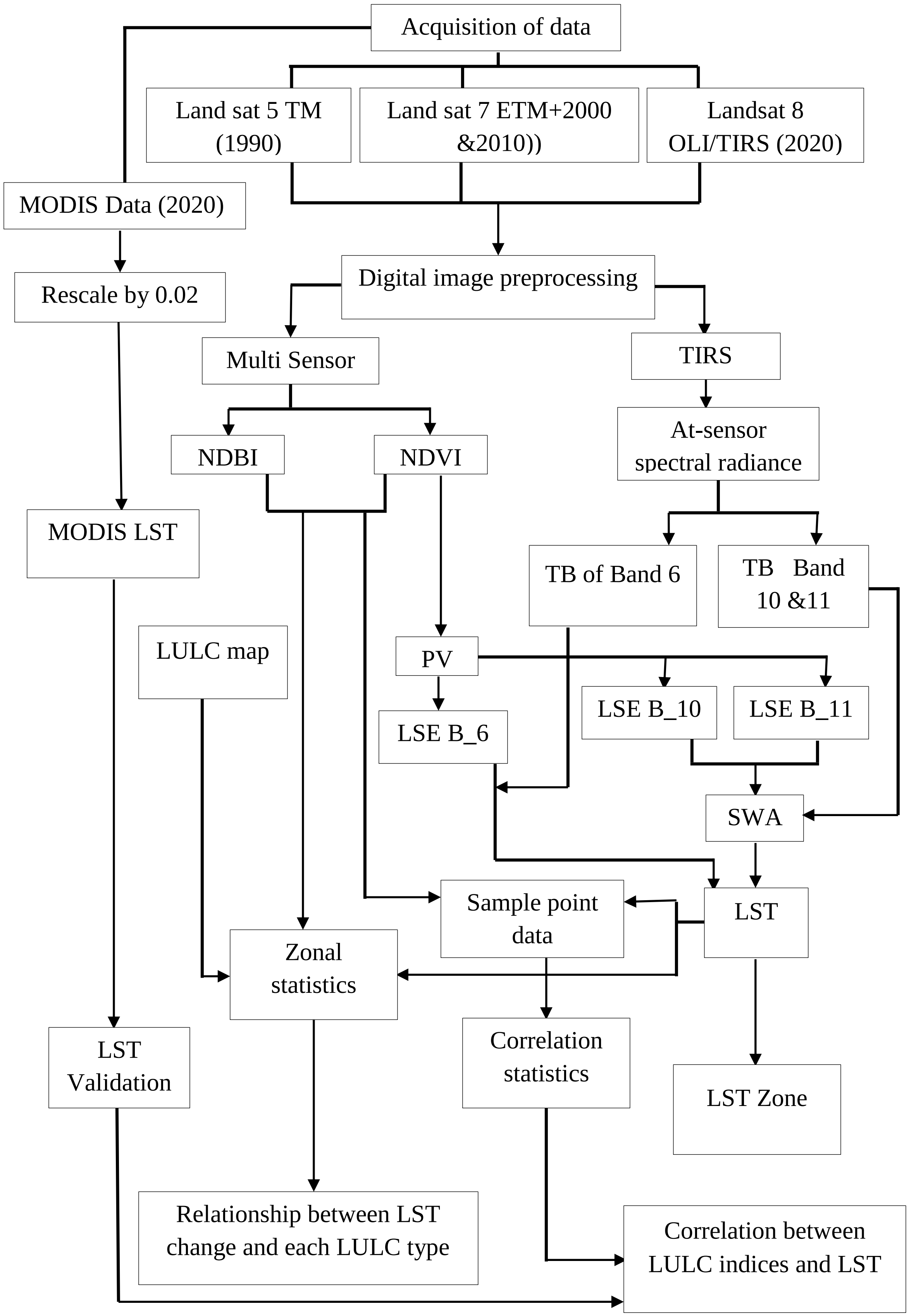

Figure 3.5: Technical scheme of LST analysis for research work

CHAPTER IV RESULT AND DISCUSSION

4.1 Accuracy Assessment for classified Land use land cover images

Based on the error matrix generated for each classified map, overall accuracy, user's accuracy and producer's accuracy were calculated, in addition to kappa variance. The accuracy details of Error matrix results were shown in table 4.2, 4.3, 4.4.and 4.5

Table 4.1: Land sat classification accuracy for 1990-2020

No.	LULC Types	1990		2000		2010		2020	
		PA(%)	UA (%)	PA (%)	UA (%)	PA (%)	UA (%)	PA (%)	UA (%)
1	Built up	86.2	89.3	88.2	90	94.1	90.6	98	96
2	Agriculture	84.3	82.7	84.5	96.1	86.8	92	98.1	98.1
3	Vegetation	91.1	82	96.1	84.5	92.2	90.4	96.2	98.2
4	Bare land	78.6	84.6	96	94.2	94.5	94.5	98.2	98.2
	OA	85.76%		90.95%		91.9%		97.62%	
	OK	0.82		0.88		0.89		0.97	

Note: PA, UA, OA and OK-producers accuracy, Users accuracy, overall accuracy and overall kappa respectively.

Landsat _5TM image (1990) was classified for four land cover classes successfully. However, agricultural lands and bare land were classified with a lower producer‘s accuracy (84.3% and 78.6%) respectively than other classes. This is due to the combination of omission and commission errors particularly mixing with built-up areas and vegetation classes. Therefore for evidence for both Systematic commission and omission errors, watching the higher overall classification accuracy of (85.76%), it was acceptable as good classification.

Likewise, Landsat ETM+ image (2000) was classified into four classes. It indicated better overall classification accuracy (90.95%). In classifying the third Landsat ETM+ image (2010), overall accuracy and kappa coefficient (91.9% and 0.89) was achieved. But in classifying fourth land sat 8 image (2020) the overall accuracy and kappa coefficient (97.62% and 0.97) was achieved. In general, there was some evidence for both systematic commission and omission errors resulting from the classifier side as incorrectly commits pixel of the class being sought to other classes as well when some class on the ground were misidentified as another class by the classifier.

Table 4.2: Landsat 5TM classification accuracy for 1990

		Reference map					
Classified 1990 LULC		Built-up area	agricultural	vegetation	Barren land	Row total	User accuracy in %
	Built-up area	50	3	0	3	56	89.3
	Agricultural	4	43	0	5	52	82.7
	Vegetation	0	5	41	4	50	82
	Barren land	4	0	4	44	52	84.6
	column total	58	51	45	56	210	
	Producer acc in %	86.2	84.3	91.1	78.6		
	Over all accuracy in % = 85.76			**Kappa coefficient(K) = 0.82**			

Table 4.3: Landsat ETM+ classification accuracy for 2000

		Reference map					
Classified map 2000 LULC		Built-up area	agricultural agricultural	vegetation vegetation	Bare land	Row total	User accuracy in %
	Built-up area	**45**	5	0	0	50	90
	Agricultural	0	49	2	0	51	96.1
	Vegetation	3	4	49	2	58	84.5
	Barren land	3	0	0	48	51	94.2
	column total	51	58	51	50	210	
	Producer acc in %	88.2	84.5	96.1	96		
	Over all accuracy in% = 90.95				**Kappa coefficient(K) = 0.88**		

Table 4.4: Landsat TM classification accuracy for 2010

	Reference map						
		Built-up area	agricultural	vegetation	Barren land	Row total	User accuracy in %
Classified 2010 LULC	Built-up area	48	2	0	3	53	90.6
	Agricultural	1	46	3	0	50	92
	Vegetation	2	3	47	0	52	90.4
	Barren land	0	2	1	52	55	94.5
	column total	51	53	51	55	210	
	Producer acc in %	94.1	86.8	92.2	94.5		
	Over all accuracy in% = 91.9			**Kappa coefficient(K) = 0.89**			

Table 4.5: Landsat 8 classification accuracy for 2020

	Reference map						
		Built-up area	agricultural	Vegetation	Barren land	Row total	User accuracy in %
Classified 2020 LULC	Built-up area	48	0	1	1	50	96.0
	Agricultural	1	53	0	0	54	98.1
	Vegetation	0	1	50	0	51	98.1
	Barren land	0	0	1	54	55	98.2
	column total	49	54	52	55	210	
	Producer acc in %	98	98.1	96.2	98.2		
	Over all accuracy in % = 97.62		**Kappa coefficient(K) = 0.97**				

This level of accuracy found almost perfect agreement because of the heterogeneity of the study area and also kappa agreement accuracy was almost perfect agreement level which means it can be used (Pontius, 2000).

4.2 The Magnitude of Land Use Land Cover in 1990, 2000, 2010 and 2020

The supervised classification maximum likelihood was applied to generate the LULC map in 1990, 2000, 2010 and 2020 figure 4.1 and 4.2, with high accuracy as seen in table 4.2, 4.3, 4.4, & 4.5.

Table 4.6: The magnitude of LULC in 1990, 2000, 2010 and 2020

Class name	1990		2000		2010		2020	
	Area in ha	Area in %	Area in ha	Area in %	Area in ha	Area in %	Area in ha	Area in %
BU	2,875.23	4.4	3,457.62	5.3	6,494.76	9.9	9,849.06	15
VE	8,752.95	13.4	7,347.78	11.2	8,330.44	12.7	8,776.98	12.4
AG	42,611.8	65.07	41,074.83	62.7	40,082.8	61.2	39,474	60.3
BL	11,239.52	17.16	10,571.41	16.1	13,599.27	20.8	7,379.37	12.3
Total (ha.)	65,479.5	100	65,479.5	100	65,479.5	100	65,479.5	100

Where: BU-built-up, VE- vegetation AG-agriculture and BL-bare land.

The dominant LULC classes of 1990 classification were Agriculture and bare land in the study area. These two classes accounted for 53,851.32 ha of total area coverage. From a total area of 65,479.5ha, bare land covered 11,239.52ha (17.16%), and Agriculture cover 42,611.8 ha (65.07%). The other LULC classes, the vegetation and built-up or urban together accounted for 11,628.18ha of the total area. The LULC result of 2000 also shown that agriculture covers the largest proportion of land in and around Chiro town with a value of 41,074.83ha (62.7%), followed by bare land, which covered 10,571.41ha (16.1%). The other LULC classes such as vegetation and built-up or urban, together cover 10,805.4 ha (16.5%) of the total area. In 2010, LULC classification results of the study area revealed that the dominant LULC categories were bare land and Agriculture together accounted for 53,682.07 (81.9%) of total area coverage. From this, bare land accounted for 13,599.27ha (20.8%) and Agriculture area accounted for 40,082.8 ha (61.2%). The remaining LULC classes were vegetation and built up or urban together accounted for 14,825.2 ha (22.6%) of the total area in 2020, LULC classification results of the study area revealed that the dominant LULC categories were Agriculture and built up or urban together accounted for 49,321.06 (75.3%) of total area coverage. From this, built up or urban accounted for 9,849.06 ha (15%) and Agriculture area accounted for 39,474ha (60.3%). The remaining LULC classes were bare land and vegetation together accounted for 16,156.35 (24.7%) of the total area.

However, the extent of bare land and agriculture within the study period decreased by 5.86%, 4.77% from 1990 to 2020 respectively. In general, Agriculture is the dominant LULC of the study area concerning area coverage in all the study periods (1990, 2000, 2010 and 2020), followed by bare land and built-up or urban area. A description of statistical data for each class and the LULC map in and around chiro town are shown in Figure 4.1 and 4.2.

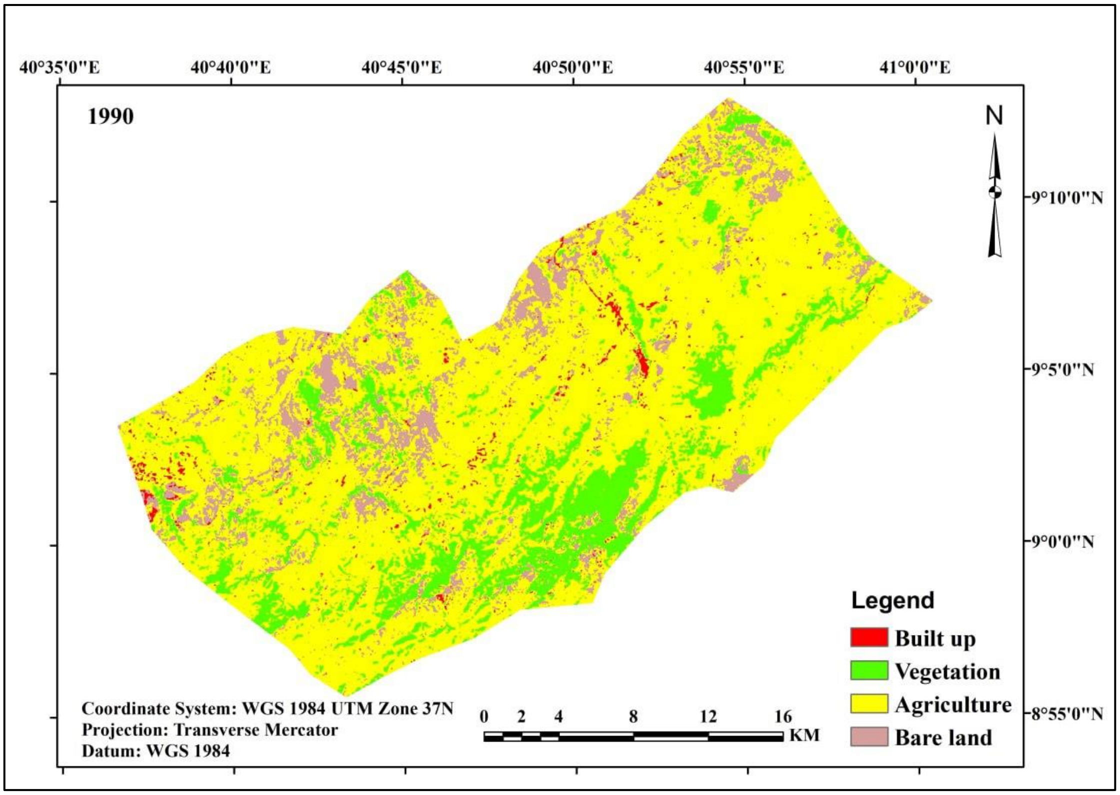

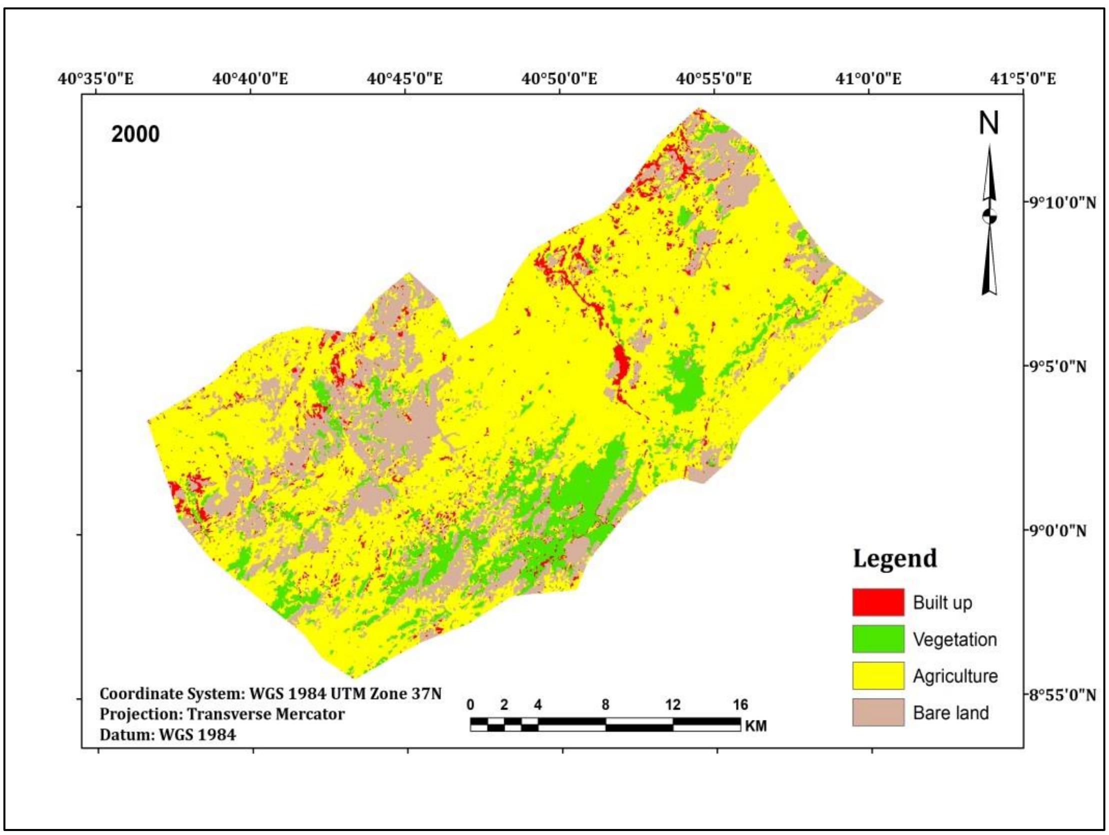

Figure 4.1: LULC maps of in and around Chiro town 1990 & 2000

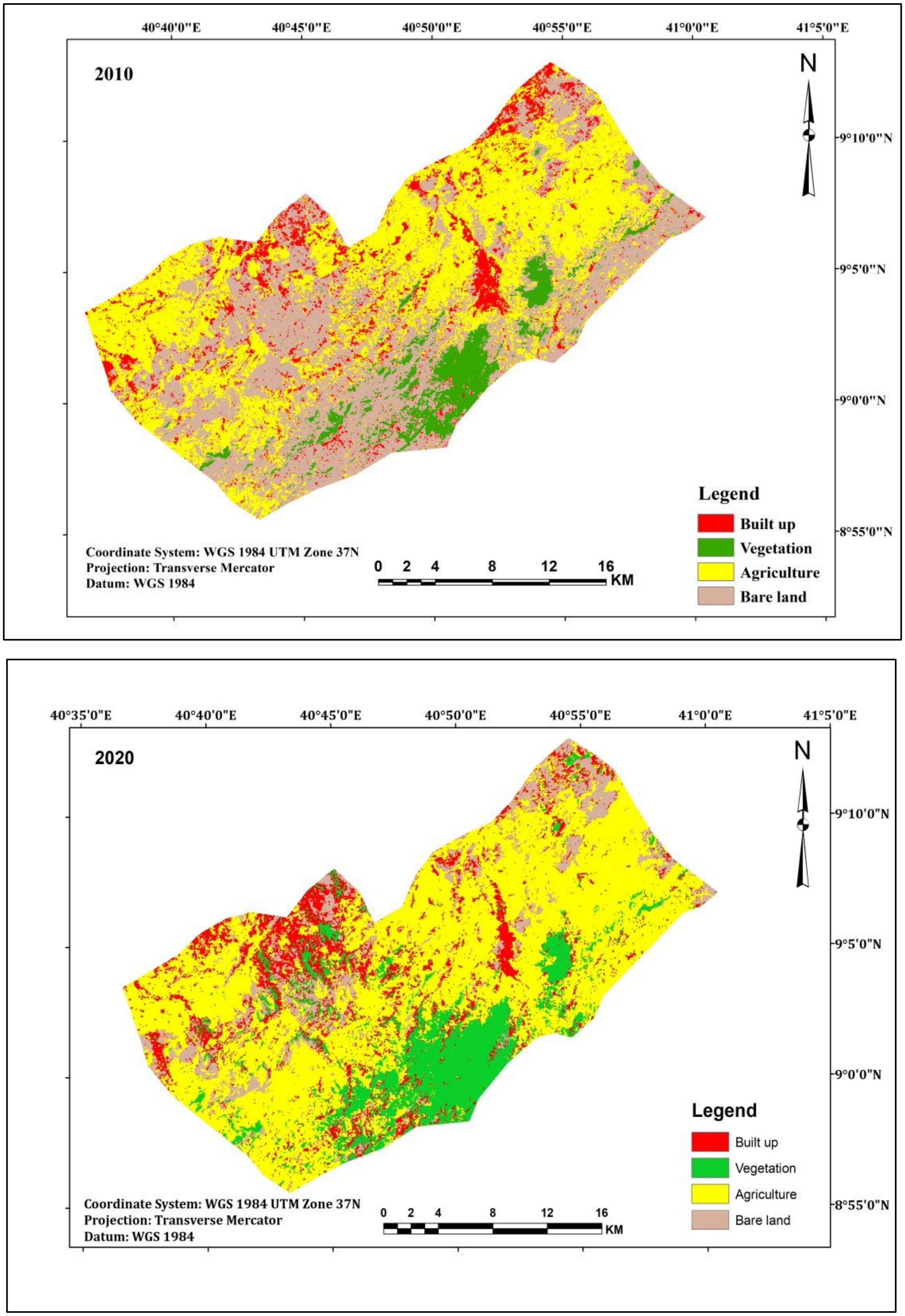

Figure 4.2: LULC maps of in and around Chiro town 2010 & 2020

4.3 Spatial and temporal changes of LULC

The LULC classification result shows that there was a change in the pattern of LULC in and around Chiro town from 1990 to 2020. From the total LULC classes, more than half of Chiro town and its surrounding was Agriculture. However, it has reduced from 42,611.8 ha (65.07%) by 1990 to 39,474 ha (60.3%) in 2020, but, it was decreased from 42,611.8 ha in1990 to 41,074.83 ha in 2000. Vegetation had also decreased from 8,752.95ha (13.4%) in 1990 to 7,347.78ha (11.2%) in 2000, increased from 7,347.78ha in 2000 to 8,330.44ha in 2010 and 8,776.96 ha (12.4%) in 2020. Similarly, the spatial extent of built up increased from 2,875.2ha (4.4%) in the initial study year 1990 to 3,457.62 ha (5.3%) in 2000, 6,494.76ha (9.9%) in the year 2010 and 9,849.06ha (15%) in 2020. However, the lands covered with built-up or urban has increased from 1990-2020. Generally, agriculture and bare land LULC classes were decreased from 1990 - 2020. Whereas, built-up or urban was increased through the study period. The description of the Spatio-temporal LULC change of Chiro town and its surrounding is provided in table 4.7.

Table 4.7: LULC changes in study area from 1990-2020

No.	Year	LULCC 1990 to 2000		LULCC 2000 to 2010		LULCC 2010 to 2020		LULCC 1990 to 2020	
	LULC types	Area (ha)	%	Area (ha)	%	Area (ha)	%	Area (ha)	%
1	Built up	582.39	0.9	3,037.14	4.6	3354.3	5.1	6973.83	10.6
2	Vegetation	-1,405.17	-2.14	982.66	1.5	446.54	0.7	24.03	0.03
3	Agriculture	-1536.97	-2.34	-992.03	-1.5	-608.8	-0.9	-3137.8	-4.8
4	Bare land	2359.75	3.6	-3027.86	-4.6	-3192.04	-4.8	-3860.15	-5.9

.

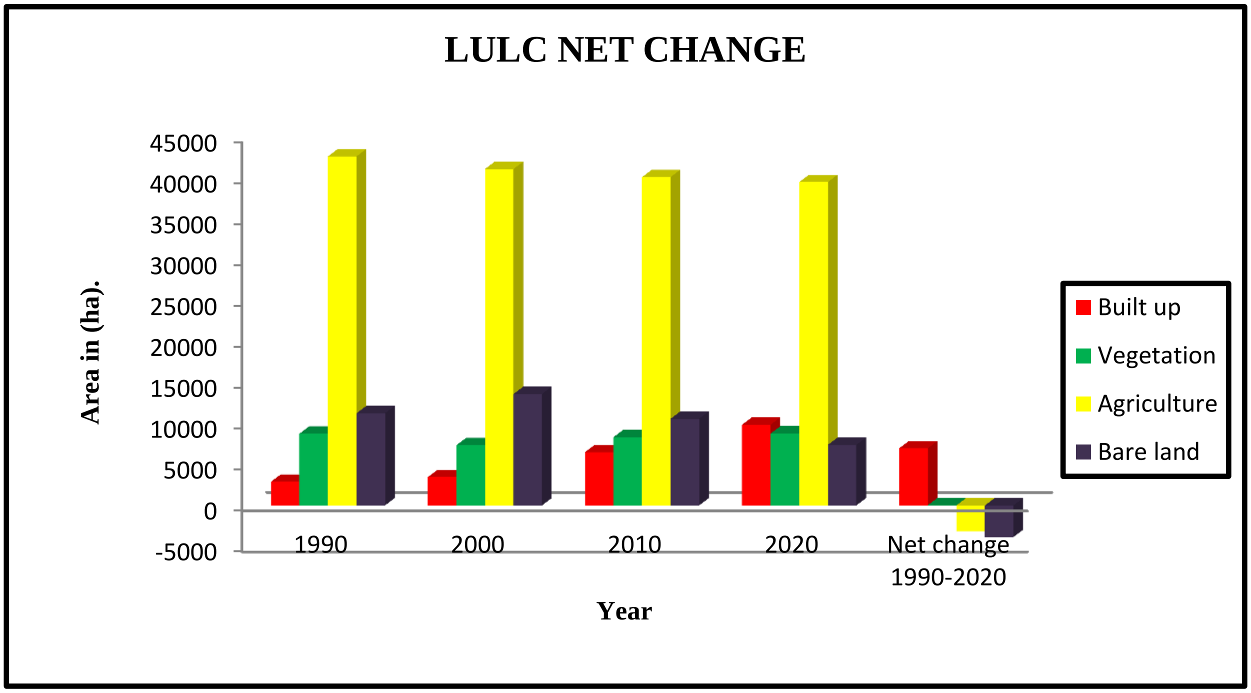

Figure 4.3: LULC changes in 1990, 2000, 2010 and 2020

The LULC transformation matrix from 1990 - 2020 provided in Table 4.9 indicates that the vegetation land in 1990 converted into agricultural land, built-up and bare land in 2020. The major agriculture transformation was made by the expansion of bare land (1322.3ha) and built-up or urban (478.5ha). In contrary to this, 301.95 ha vegetation areas were gained from bare land and agriculture in 2020. Agricultural land in 1990 also had changed to built-up (urban), vegetation, and bare land by 27702.8ha, 3661.0ha, and 239.72 ha correspondingly. In the same manner, bare land was converted to vegetation, agricultural land, and built-up or urban by 623.7ha, 6271.1ha, and 151.90 ha in 2020, respectively. Besides, the built-up or urban areas also received 146.68ha, 151.90ha, and 562.85ha from vegetation, bare land, and agricultural land respectively. The details of the LULC transformation matrix from 1990-2000 are presents in table 4.8.

Table 4.8: LULC transformation matrix of study area from 1990-2020 in ha

				2020		
	LULC	Agriculture	Bare land	Built up	Vegetation	Total
	Agriculture	**4290.8**	1322.3	478.5	13.7	6105.4
	Bare land	20262.4	**22313.3**	4584.3	623.7	47783.7
	Built up	1685.3	126.9	**1016.1**	0.2	2828.5
	Vegetation	926.7	3940.2	192.1	**3661.0**	8720.0
1990	Total	27165.2	27702.8	6271.1	4298.6	65437.7

4.4 The temporal Distribution of NDVI

Based on NDVI results, extracted from near-infrared and red bands within the study periods show that LULC classes have different NDVI values. The value varies from area to area based on vegetation intensity and condition. Vegetation cover has the highest NDVI value than other classes. The spatial extent of vegetation cover in 1990 was greater than in 2000 and 2010 in and around Chiro town . Since the NDVI value was higher than 2000 and 2010 . This shows that there was high vegetation cover in 1990 than in 2000, 2010 and less coverage than 2020 (table4.9).

Table 4.9: The NDVI values for 1990, 2000, 2010 and 2020

Year	Maximum	Mean	Minimum	Standard devetion
1990	0.714	0.21	-0.088	0.08
2000	0.546	0.03	-0.378	0.12
2010	0.588	0.24	-0.171	0.05
2020	0.741	0.18	-0.666	0.10

Figure 4.6 & 4.7 shows the place that has the highest NDVI value corresponds to vegetation cover mostly south, and south east parts of the study area, whereas the area covered by built-up, agriculture, and bare land has low NDVI values.

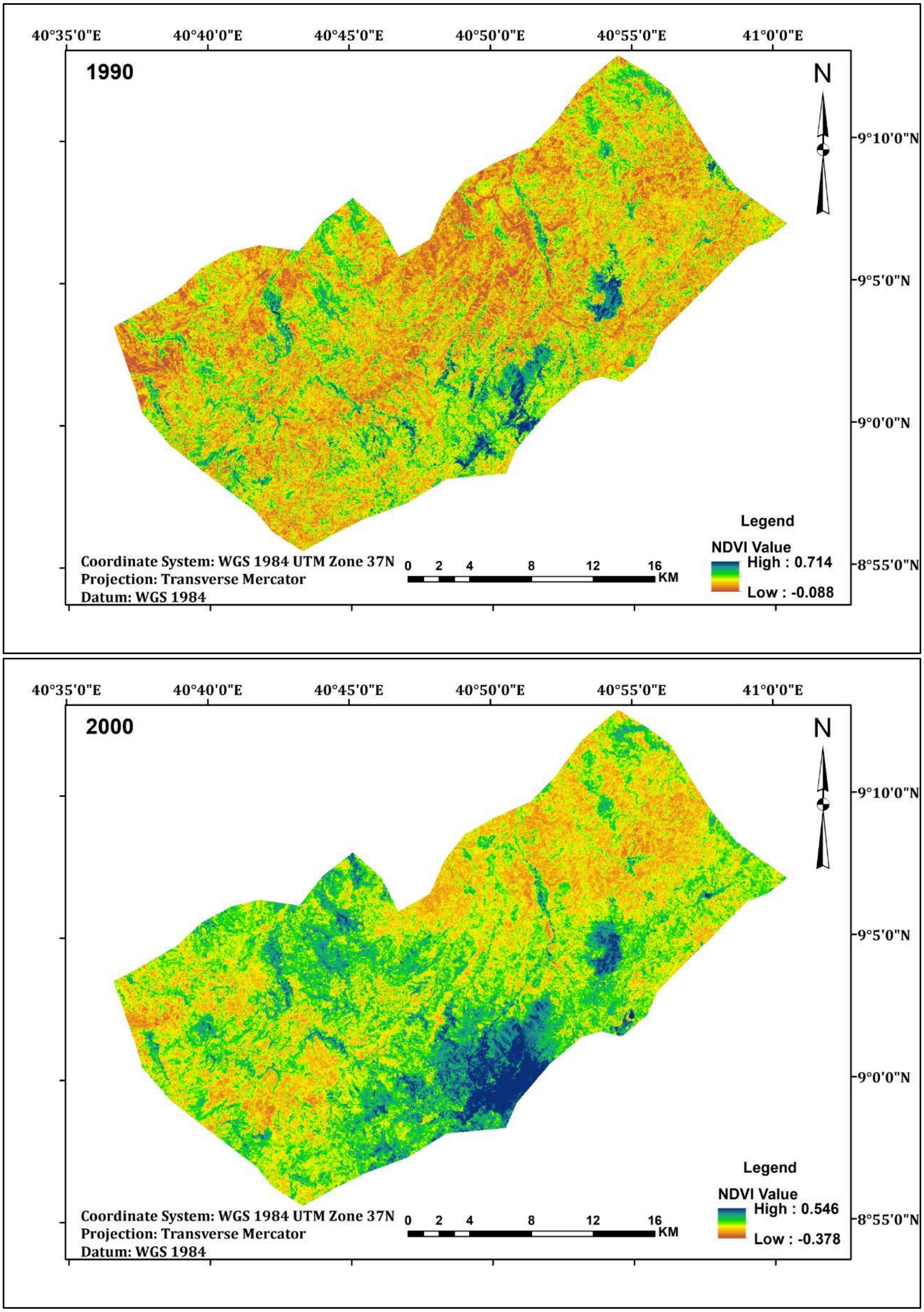

Figure 4.4: NDVI map of in and around study area for the year 1990 and 2000

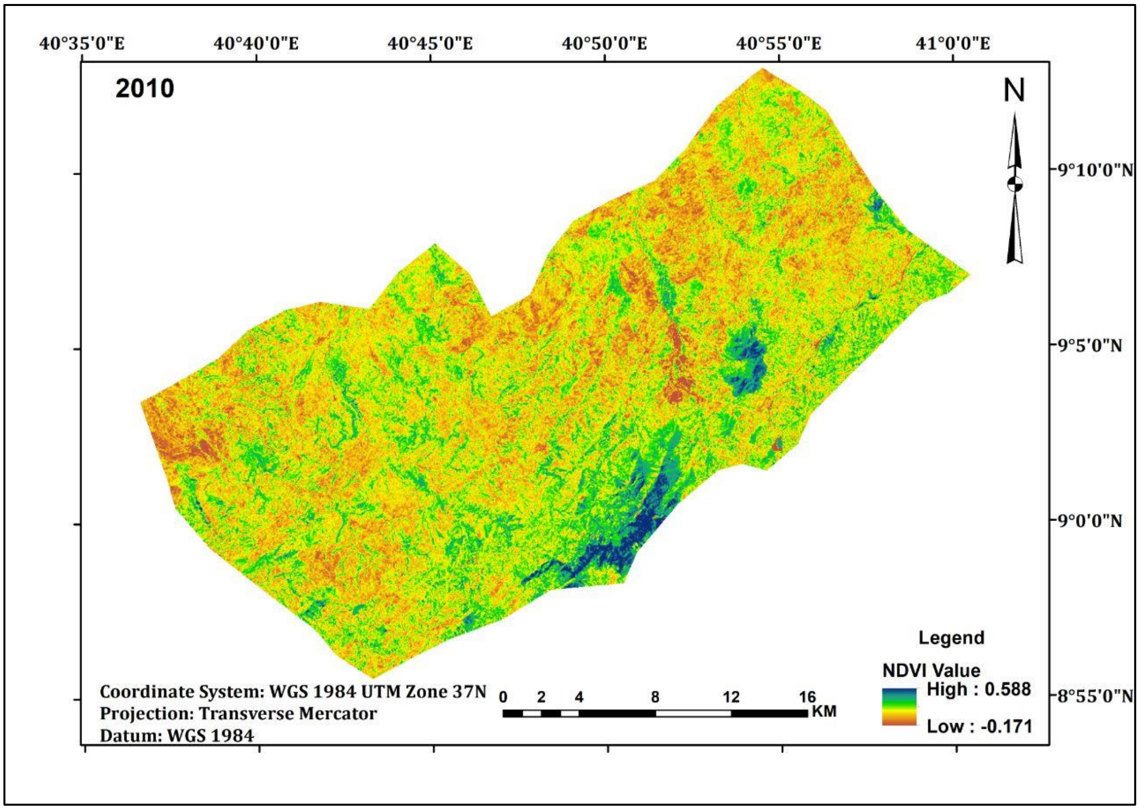

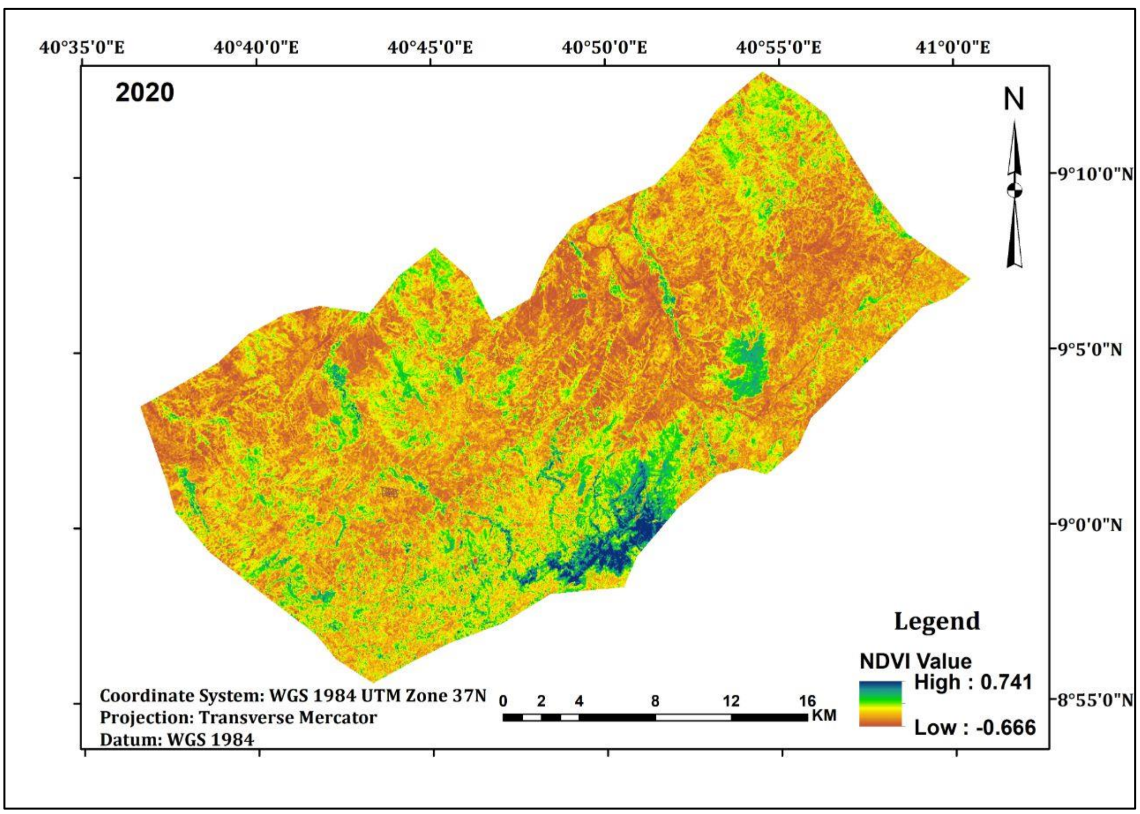

Figure 4.5: NDVI map of in and around study area for the year 2010 and 2020

4.5 The temporal Distribution of NDBI

The distribution of NDBI value in figure 4.8 shows an opposite design to the NDVI maps in the sense that vegetation covers high NDVI values and received low NDBI values. Likewise, an urban or built-up area is characterized by low NDVI and high NDBI values. The lowest NDBI was computed from agriculture land. In general, the built-up or urban areas have higher reflectance to the short wave Infrared band and it was expected to have higher NDBI (Malik et 48 al., 2019). It is observed that higher NDBI values correspond to urban (built-up), bare land, and agriculture areas in the central, east, and west parts of a study area, while lower values were observed in vegetation areas. The NDBI values of the study area ranged from-0.372 to 0.179 in 1990, -0.36 to 0.362 in 2000, -0.358 to 0.446 in 2010 and -0.387 to 0.524 in 2020. Figure 4.8, 4.9 & 4. 10 shows the place that has the highest lowest NDBI value

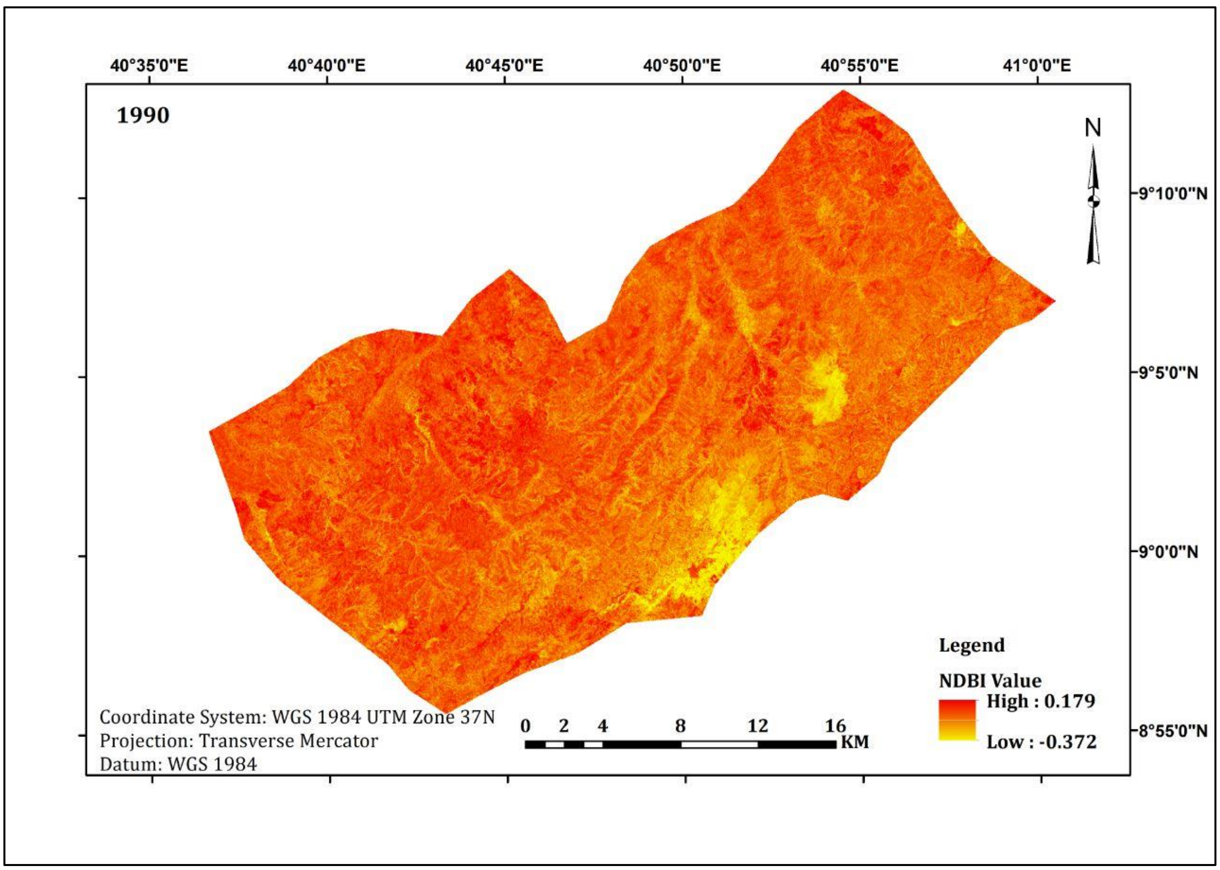

Figure 4.6: NDBI map of in and around study area for the year 1990

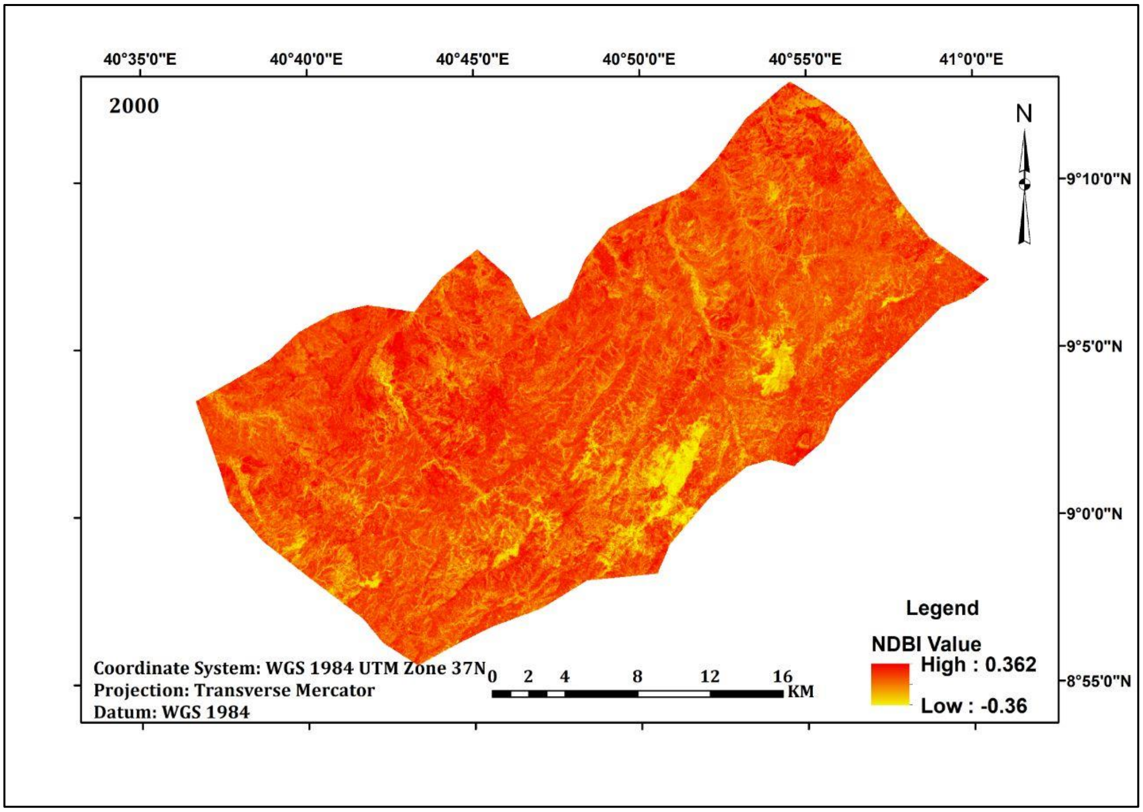

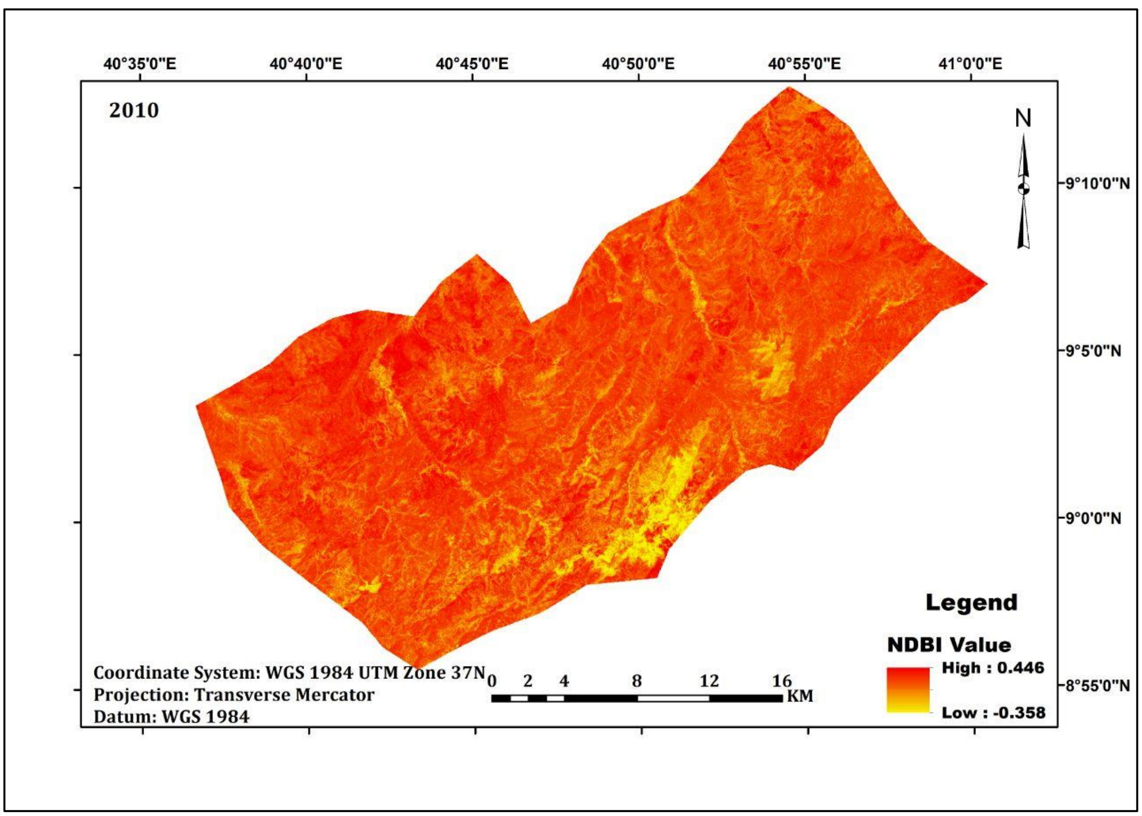

Figure 4.7: NDBI map of in and around study area for the year 2000 and2010

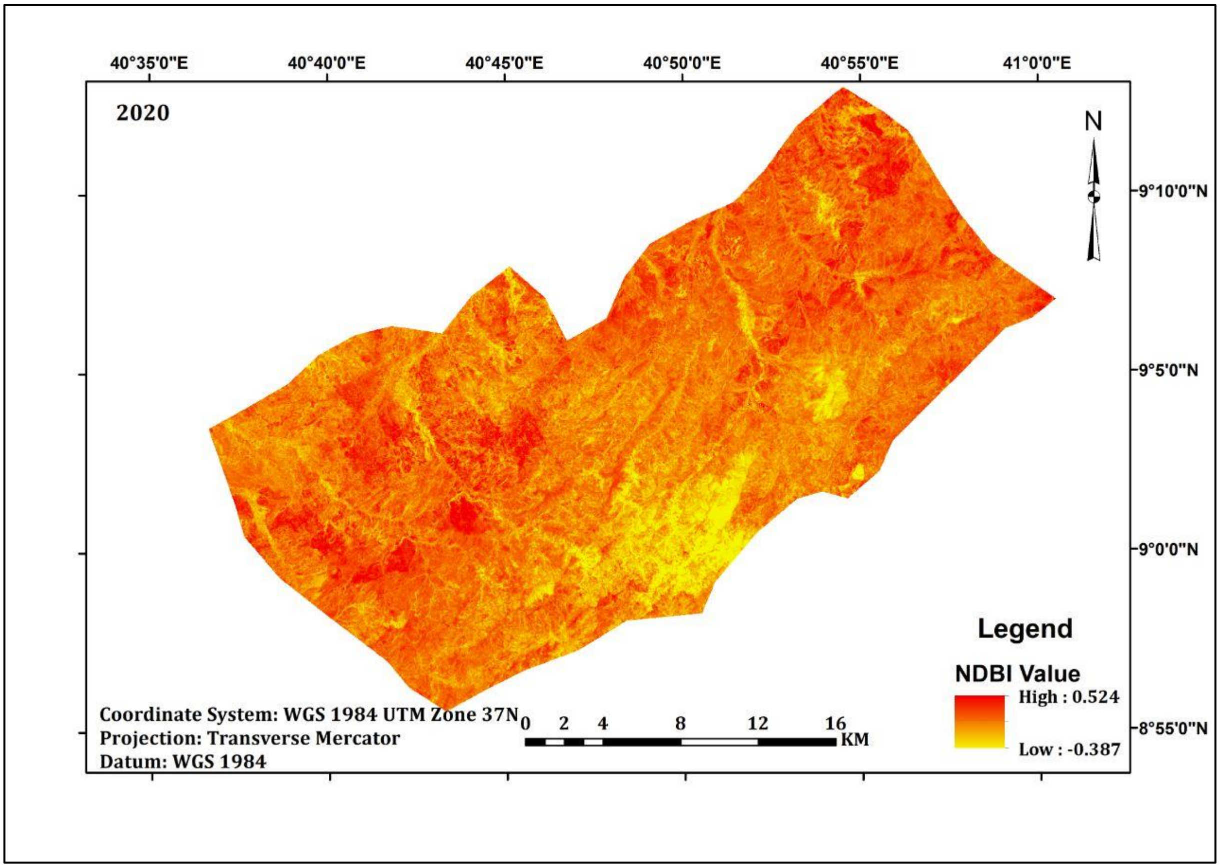

Figure 4.8: NDBI map of in and around study area for the year 2010 and 2020

4.6 The temporal Distribution of LST from 1990-2020

According to the results produced by the researcher, the calculated values of the LST for the year 1990 ranged from 7 ^{0}C - 37 ^{0}C, with the mean values of, 26.45 ^{0}C. For the year 2000, it ranged from 10 ^{0}C - 38^{0}C, with the mean value of 27.76 ^{0}C, for the year 2010, its ranged from 11 ^{0}C - 39 ^{0}C , with the mean value of 28.46 ^{0}C while in 2020 it ranged from 7 ^{0}C -41, with the mean value of 29.04 ^{0}C. The mean temperature increased by 1.3 ^{0}C from 1990 to 2000, 0.70 ^{0}C from 2000 to 2010 and 0.58 ^{0}C. The mean LST was increased sharply by 2.59 ^{0}C from 1990 to 2020. Areas denoted by an oval shape and the like had a high temperature. Most of those areas were covered by bare land, agriculture, and built up which was exposed directly to incoming radiation. The areas denoted by a rectangle and the like had a low temperature, which is covered with vegetation. The distribution of LST of Chiro town and its surrounding for 1990 to 2020 is presented in figure 4.9 and 4.10.

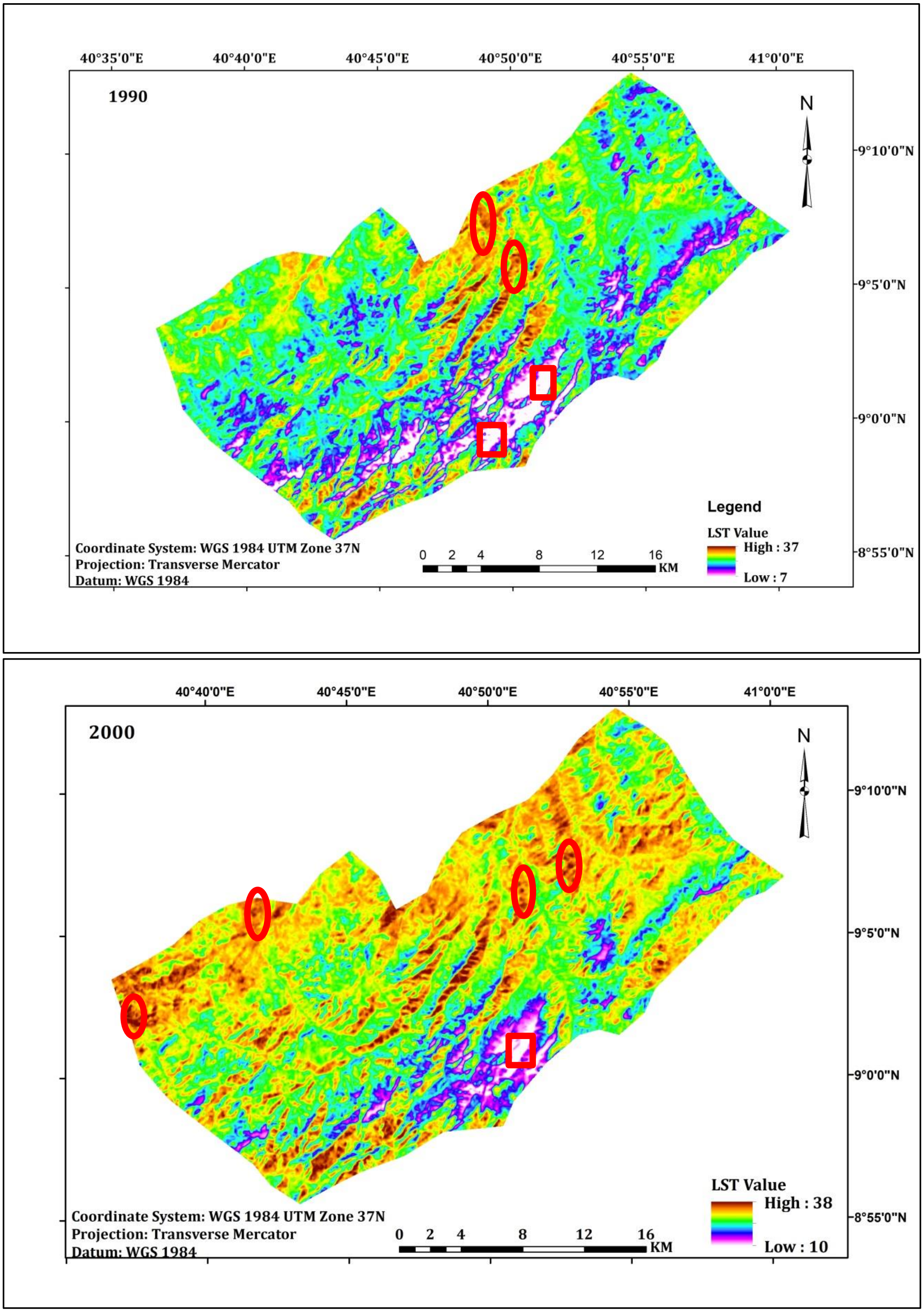

Figure 4.9: LST map of in and around study area for the year 1990 and 2000

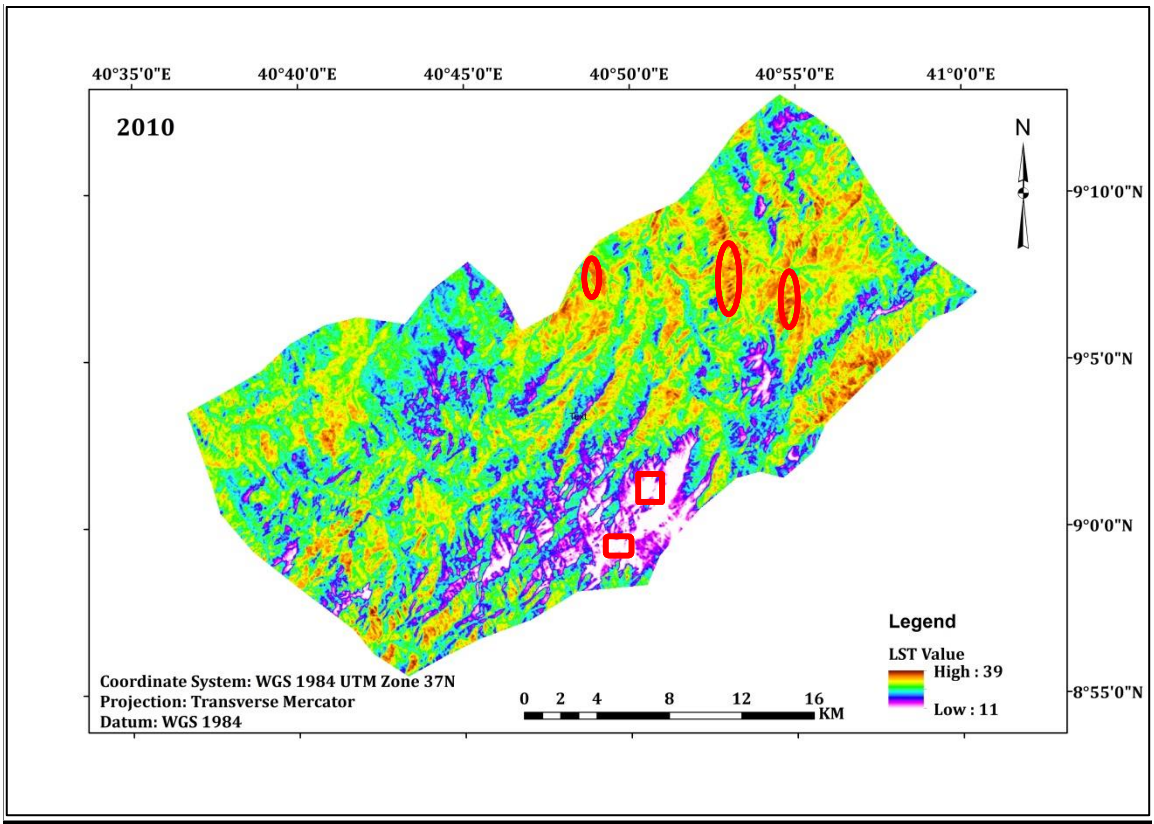

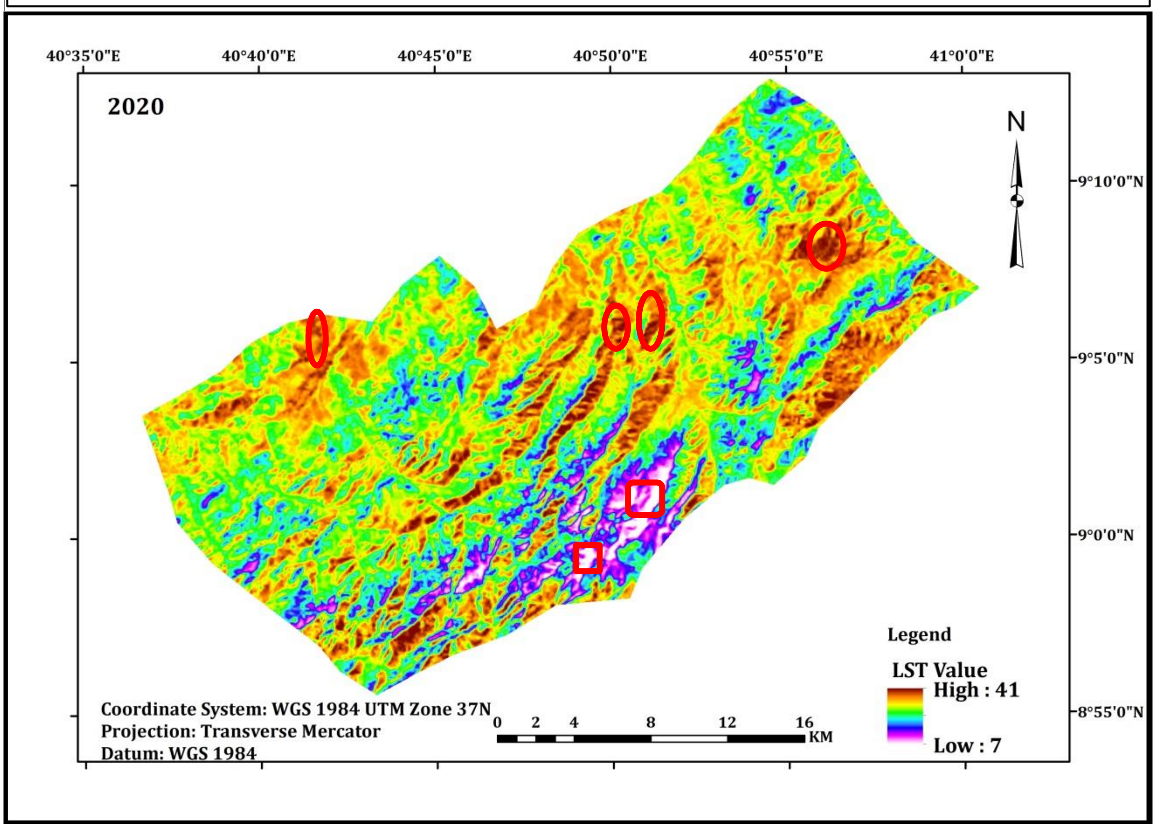

Figure 4.10: LST map of in and around study area for the year 2010and 2020

4.7 Validation of LST Derived from Landsat Thermal Band

In this study, MODIS data were used to validate the Landsat eight LST of study area in 2020 that were acquired during a similar period, even if, MODIS has a coarser resolution. The LST result derived from MODIS and Ladsat8 ranges from 9℃ to 41.67℃ and 7℃ to 41 ℃ respectively. Central, southern and western part of the study area in most places has a high temperature in both sensors. Whereas, the southeast part of the study area has a low temperature in both sensors. Therefore, the ranges of LST extracted from both sensors in and around Chiro town were close to each other. Figure 4.11 shows MODIS LST.

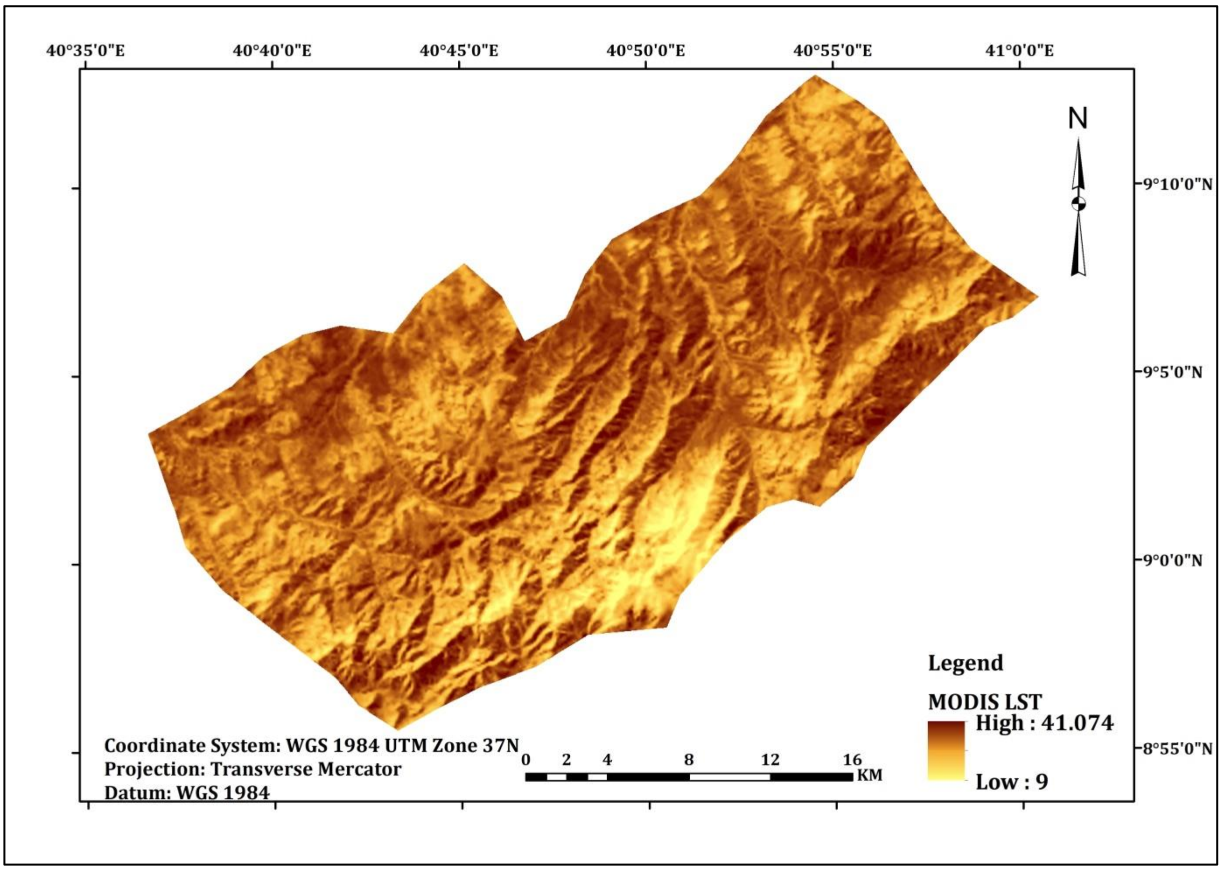

Figure 4.11: MODIS LST data used to validate LST extracted from Landsat

The scatter diagram of Landsat and MODIS LST also shows a moderate positive relationship with a coefficient of determination (R^2) and Pearson correlation coefficient (r) are 0.4 and 0.63 respectively. This indicates the value of LST of Landsat increases the values of MODIS LST also increases.

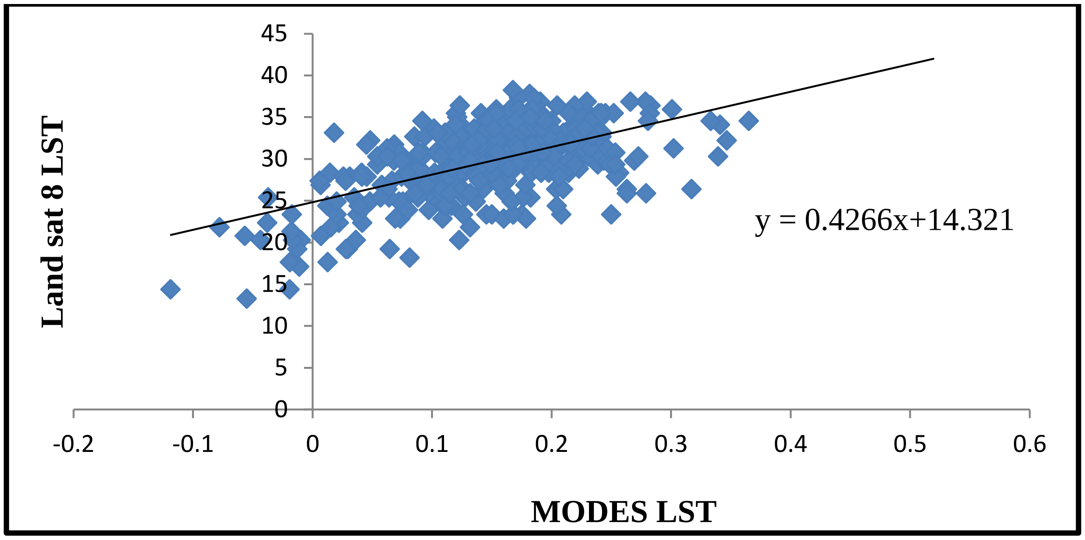

Figure 4.12: Scatter plot of the MODIS and Landsat8 LST

4.8 The spatial coverage of LST and Distribution in 1990, 2000, 2010 and 2020 Results

In this study show that LST was progressively changed from 1990 -2020. The range of LST of study area is 13.44 ºC - 41.07ºC. This LST was categorized into three zones such as High, Medium, and Low presented in table 4.10. In 1990, most of the areas of study area had a medium temperature range from 11.40 ºC - 30.42 ºC that spatially covered about 36,474.02ha. In this year, the low-temperature zone that ranges from 7.00 ºC - 11.40 ºC with spatial coverage of 10,205.80 ha, and the high-temperature zone was covered 18,799.14ha with the range 30.42 ºC - 37.2 ºC. This temperature was changed to 39.11℃ in the year 2000. Therefore, the spatial coverage of high, medium and low zones was 27,052.05ha, 28,942.26ha, and 9,484.67ha respectively. In 2010 the result implies that the temperature was changed to 38.00℃. And, the spatial coverage of high, medium and low zones was 28,942.26ha, 27,698.18ha, and 17,009.7ha respectively. Moreover, larger parts of study area were covered by a high temperature zone in 2020 because the maximum LST of the town changed to 41.1 ^{0}C. The LST zone and their aerial coverage are tabulated as follows in Table 4.10.

Table 4.10: LST zones and their aerial coverage in 1990, 2000, 2010 and 2020

Year	Zone	Range in ^{0}C	Area coverage in ha	Total area in ha
1990	High	30.42 - 37.2	18,799.14	65,479.5
	Medium	11.40 - 30.42	36,474.02	
	Low	7.00 - 11.40	10,205.80	
2000	High	36.38 - 39.11	27,052.05	65,479.5
	Medium	21.29 - 36.38	28,942.26	
	Low	11.02 - 21.29	9,484.67	
2010	High	32.73 - 38.00	29,275.96	65,479.5
	Medium	13.68 - 32.73	27,698.18	
	Low	10.17 - 13.68	17,009.7	
2020	High	35.60 - 41.07	31,499.88	65,479.5
	Medium	23.25 - 35.60	26,454.08	
	Low	7.00 - 23.25	7,525.03	

4.9 The Association of Land Surface Temperature with LULC Indices

4.9.1 The Association of land surface temperature with NDVI

NDVI is an index that indicates the status of vegetation, and the greenness of the earth's surface. So, it is used to assess the urban environment and urban heat island since it shows the level of dryness and warmness of the town. The association between LST and NDVI is inverse in 1990, 2000, 2010 and 2020 (table 4.12 and figure 4.14 and 15).

This means Low LST has high NDVI and high LST has low NDVI. This indicates that higher temperature is one reason for the increase of evaporation, and consequently, a lower plant production. The results in this study have similar suggestions with the study done by Lakshmi Kumar et al., (2013) on the relationship between temperature and vegetation changes. The higher NDVI has lower LST, the lower NDVI has a higher LST except for the water body. Since the reflectance of a water body in the infrared region is lower than the red spectrum, it emits radiation in the thermal region; the result of this analysis LST and NDVI have a negative relationship similar researcher Abel, (2018).

The value of coefficient determination of NDVI and LST is 0.72, 0.76, 0.89 and 0.97 in 2020, 2010, 2000 and 1990 respectively. Therefore, 72%, 76%, 89% and 97% distribution of LST was influenced by NDVI in in 2020, 2010, 2000 and 1990 correspondingly without ignoring other factors like topography and elevation. Hence, the results in this study indicate that there was a strong negative association LST with NDVI having a value of Pearson correlation coefficients (R) -0.85, -0.87, -0.94 and -0.98 for 2020, 2010, 2000 and 1990 respectively. Studies like Sobrino et al. (2001); Sun et al. (2012); Worku, (2018), and Yue et al. (2007) also agreed with a negative association between LST and NDVI.

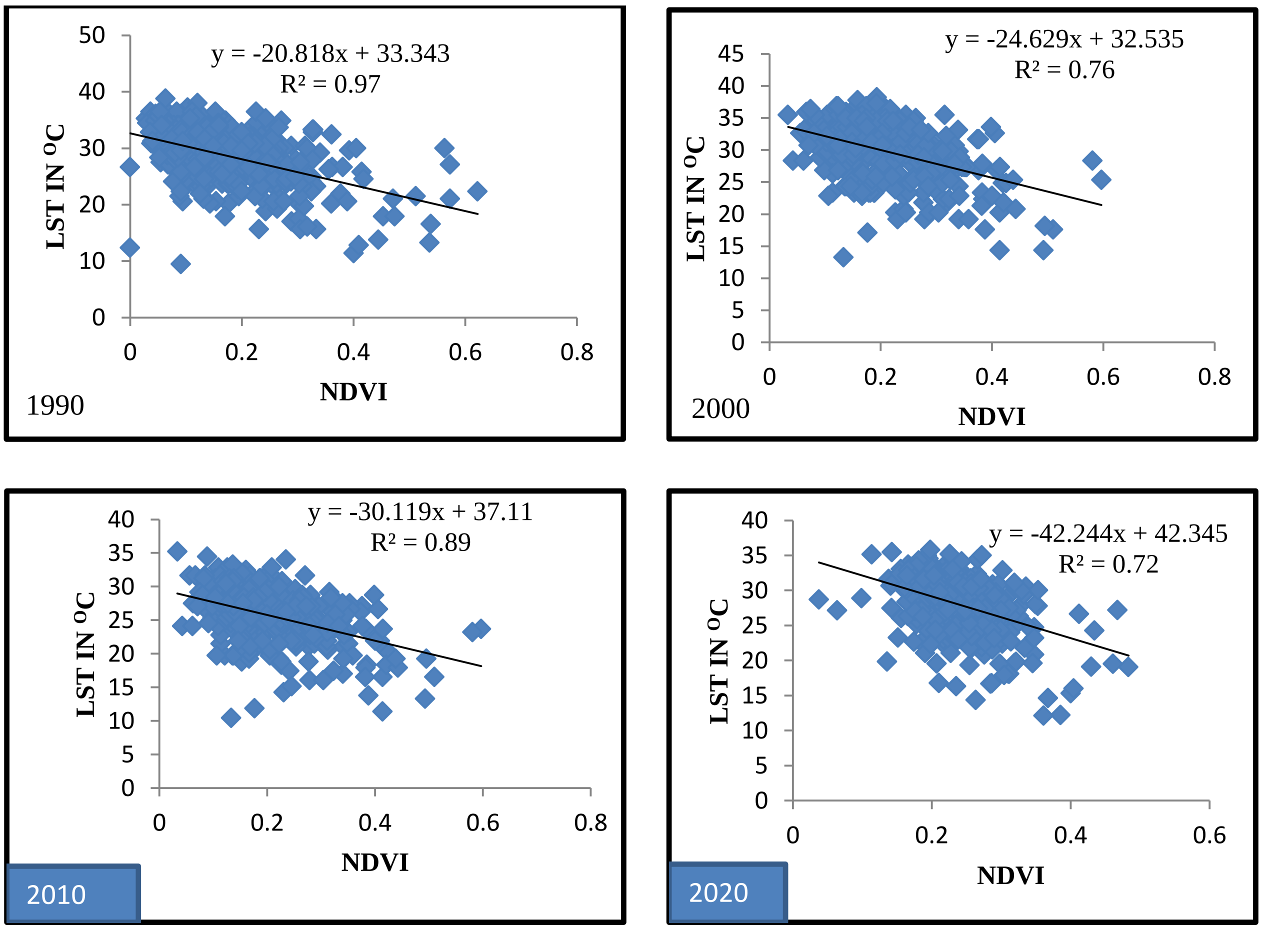

Figure 4.13: Correlation of LST with NDVI for the year1990, 2000, 2010 and 2020

Table 4.11: Pearson Correlations of LST with NDVI in 1990, 2000, 2010 and 2020

LST	Year	R^2	R	Linear equation
	1990	0.97	-0.98	y = -20.818NDVI + 33.343
	2000	0.89	-0.94	y = -24.629NDVI+ 32.535
	2010	0.76	-0.87	y = -30.119NDVI + 37.11
	2020	0.72	-0.85	y = -42.244NDVI + 42.345

4.9.2 The Association of Land Surface Temperature with NDBI

The result shows that increasing impervious surfaces like asphalt, built-up and parking lots modified thermal behavior and was important to increased NDBI. This arrangement can be seen in Tables 4.13, showing the association of NDBI with Land surface temperature. Therefore, the sign of the coefficient shows whether the correlation is positive or negative. The amount of the correlation indicates the weakness or strength of the correlation. It is possible to describe in words the degree of the association based on the guide that Li et al. (2004) mentioned in chapter three. The results indicate that the association between LST and NDBI is moderately positive in 1990. However, the correlation of LST with NDBI was strongly positive in 2000, 2010 and 2020. This indicates low NDBI has low LST and high NDBI has high LST. Generally, the relation of LST and NDBI in this study is positive in all study periods. The results in this study have similar suggestions with the study done by Malik et al. (2019) on the relationship between LST with NDBI, and NDVI. The value of the correlation of LST with NDBI was 0.97, 0.98, 0.96 and 0.97 in 2020, 2010, 2000 and 1990 respectively. It indicates that built-up or urban areas, agriculture, and bare land aggravate the LST in Chiro town and it’s surrounding because of this land-use classes have high NDBI values figure 4.14 and table 4.13 shown below.

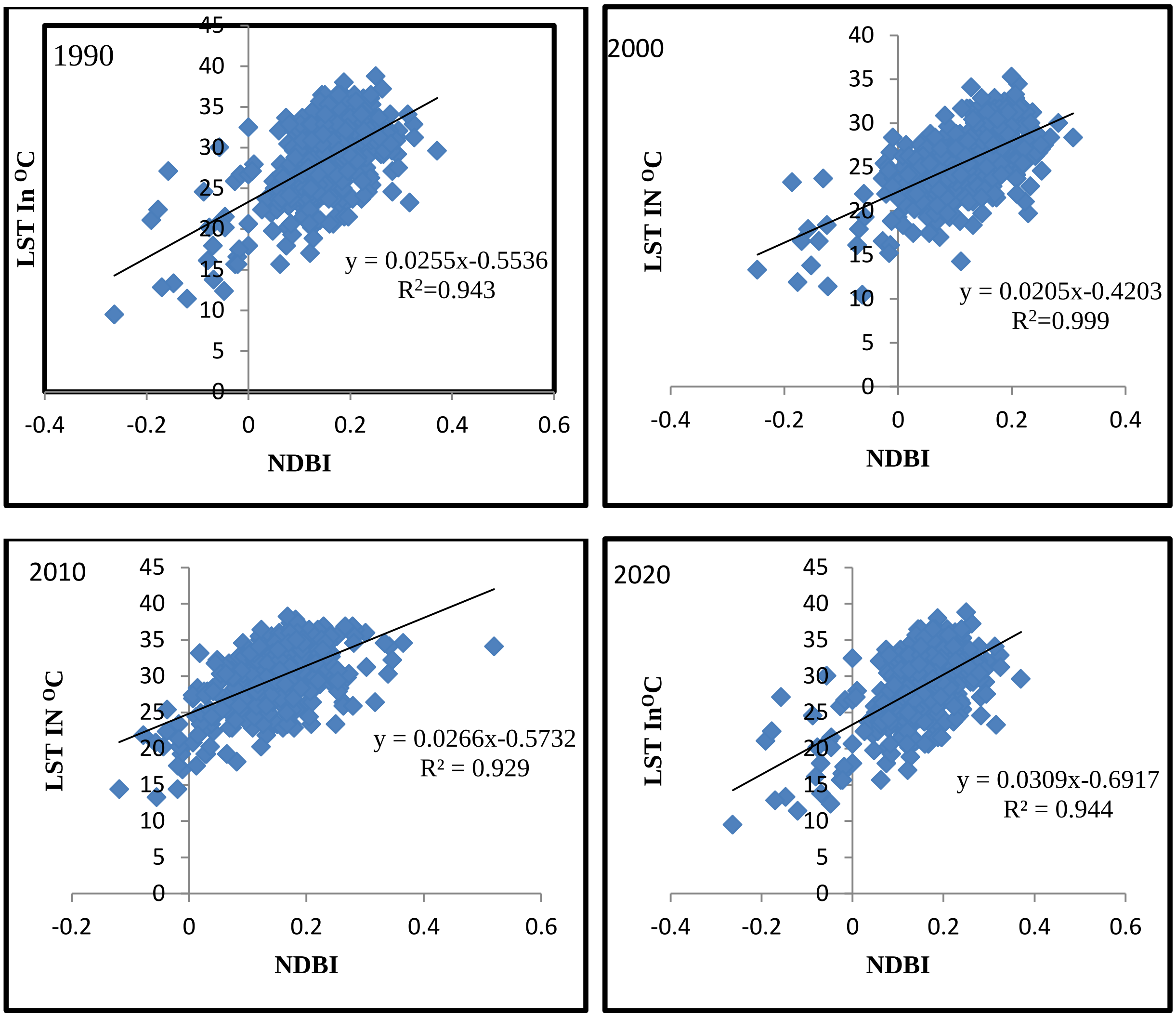

Figure 4.14: correlation of LST with NDBI for the year 1990, 2000, 2010 and 2020

Table 4.12: Pearson Correlations of LST with NDBI in 1990, 2000, 2010 and 2020

LST	Year	R^2	R	Linear equation
	1990	0.94	0.97	y = 0.0255 NDBI - 0.5536
	2000	0.99	0.98	y = 0.0205 NDBI - 0.4203
	2010	0.93	0.96	y = 0.0266 NDBI - 0.5732
	2020	0.94	0.97	y = 0.0309 NDBI - 0.6917

4.10 The Land Surface Temperature Value of Each Land Use and Land Cover

The results in this study illustrate that there was a conversion of vegetation cover to built-up or urban areas, agricultural land, and bare land (Figure 4.1). Mainly, the expansion of built-up in the north, North West, west, southwest, and central part of the town made the area warmer from 1990 - 2020. Such LULC conversion caused the increase in LST in study area.

As presented in table 4.13, 4.14, 4.15 and 4.16 agricultural land and bare land recorded higher LST than other land use and land cover. The LST of agricultural land was 37.22℃, 38.78℃, 39.11℃ and 38.00℃ and the LST of bare land was 33.26℃, 37.80℃, 38.21℃ and 41.07℃ in 1990, 2000, 2010 and 2020 respectively. In addition to this, built-up or urban areas also record maximum surface temperatures of 35.26℃, 38.04℃ 38.66 and 35.65℃, in 1990, 2000, 2010 and 2020 respectively. On the other hand, vegetation cover had 30.42℃, 32.74℃, 36.38℃ and 33.26℃ in 1990, 2000, 2010 and 2020 respectively. The LST of each LULC class is tabulated below.

Table 4.13: The LST of study area for each LULC from 1990 in ^{0}C

LULC Classes 1990	MIN	MAX	RANGE	MEAN	STD
Built up	10.44	35.26	24.81	26.49	3.00
Vegetation	7.12	30.42	22.42	18.80	3.45
Agriculture	11.41	37.22	25.82	26.61	3.14
Bare land	15.18	33.26	18.08	25.61	2.19

Table 4.14: LST of study area for each LULC for the year 2000 in ^{0}C

LULC Classes 2000	MIN	MAX	RANGE	MEAN	STD
Built up	12.90	38.04	25.14	29.38	2.83
Vegetation	10.17	32.74	22.56	18.88	3.23
Agriculture	13.69	38.00	24.31	29.23	2.73
Bare land	13.08	37.80	24.71	27.32	3.29

Table 4.15: The land surface temperature of study area for each LULC for year 2010 in ^{0}C

LULC Classes 2010	MIN	MAX	RANGE	MEAN	STD
Built up	18.69	38.66	19.98	29.92	2.44
Vegetation	11.03	36.38	25.35	19.87	4.01
Agriculture	17.09	39.11	22.03	29.81	3.23
Bare land	21.30	38.21	16.91	29.66	2.43

Table 4.16: The land surface temperature of study area for each LULC for year 2020 in ^{0}C

LULC Classes 2020	MIN	MAX	RANGE	MEAN	STD
Built up	23.25	35.65	12.40	30.55	1.63
Vegetation	7.00	33.26	25.26	23.53	3.91
Agriculture	11.89	38.78	26.89	31.15	3.39
Bare land	11.41	41.07	29.67	30.95	3.85

4.11 The association of land use land cover with mean land surface temperature change

The map of LULC and LST of study area shows how LULC and LST have changed from 1990 - 2020. This change was mainly due to the high percentage of land transformation. The LST increased from 1990 to 2020 and varied with the variation of LULC. Among the LULC classes, vegetated land regions of the study area had a low LST change and high radiation was emitted by built-up and bare land.

Table 4.17: The mean LST changes for each land use and land cover from 1990-2020

LULC class	Mean				LST Change ^{o}C			
	1990	2000	2010	2020	1990-2000	2000-2010	2010-2020	1990-2020
Built up	26.49	29.38	29.92	31.00	2.90	0.54	0.63	4.51
Vegetation	18.80	18.88	19.87	22.53	0.07	0.99	3.66	3.72
Agriculture	26.78	29.23	29.81	30.98	2.62	0.59	1.34	4.20
Bare land	25.61	27.32	29.66	30.95	1.71	2.34	1.29	5.34

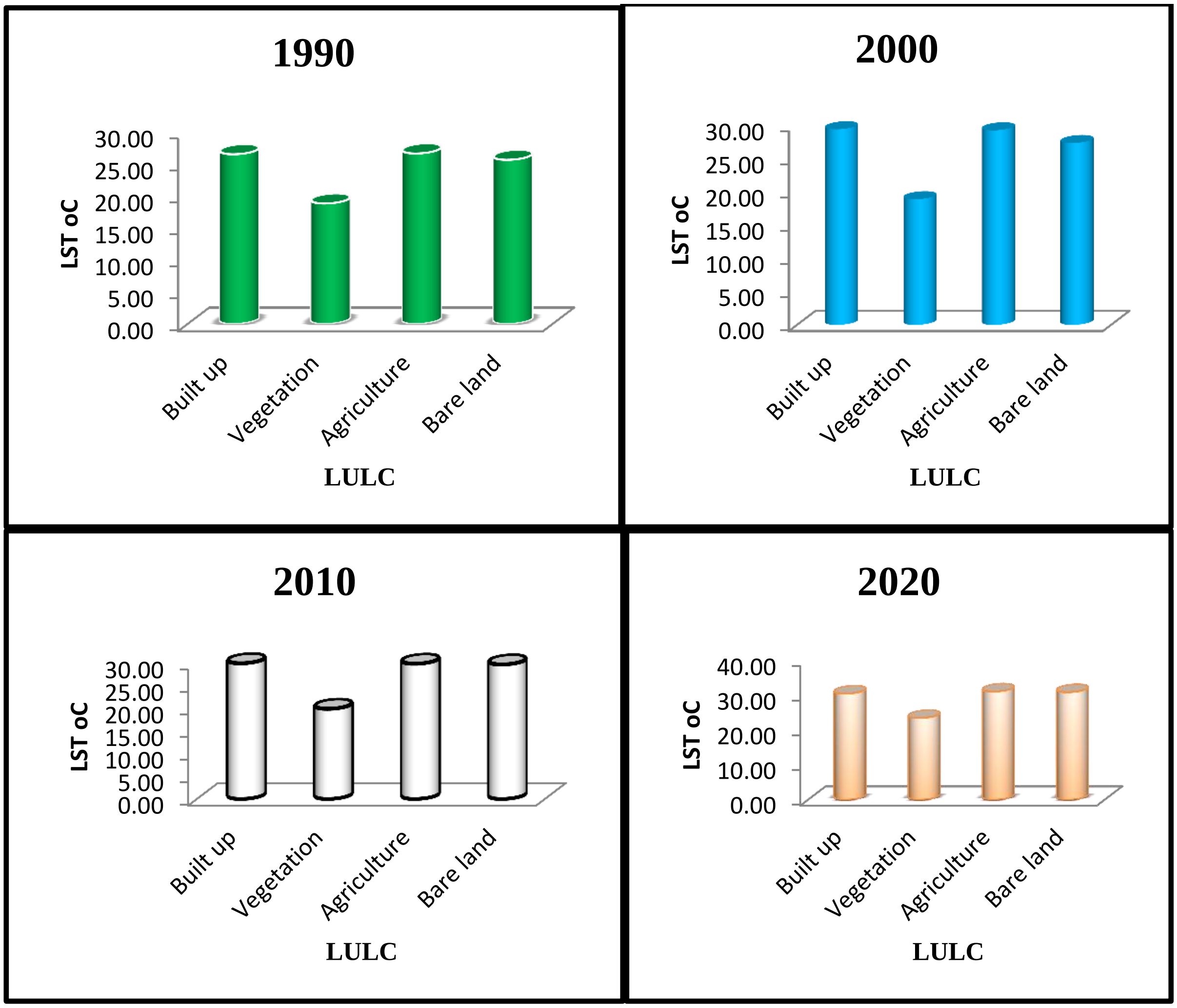

Figure 4.15: The relationship between mean land surface temperatures and each LULC

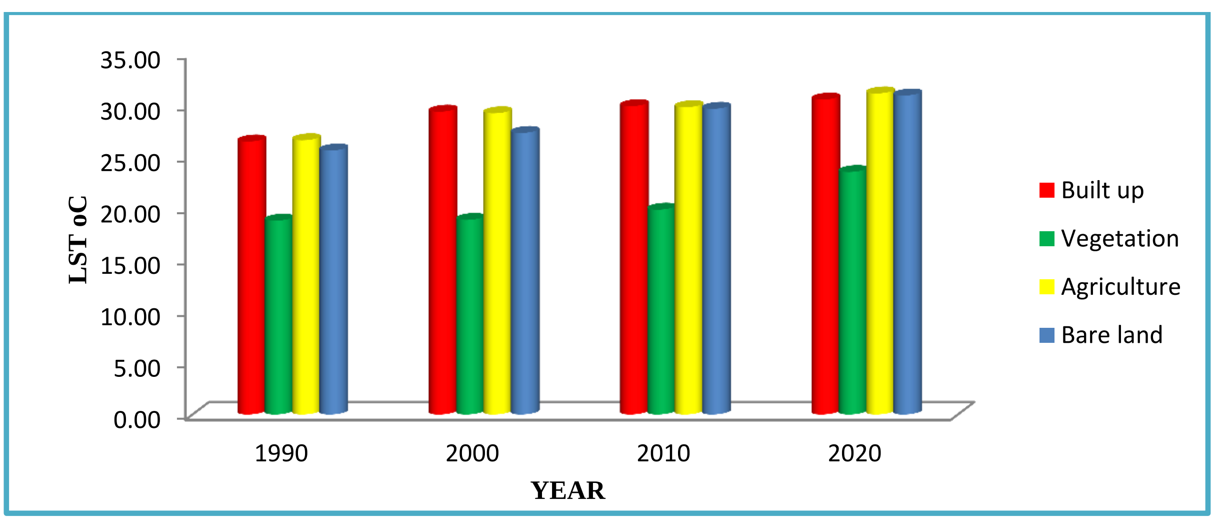

Figure 4.16: The relationship between mean land surface temperatures and each LULC

CHAPTER V CONCLUSION AND RECOMMENDATION

5.1 Conclusion

The study used geospatial techniques to detect land use and land cover change in and around Chiro town over a 30-year period. Multi-temporal satellite data and GIS techniques were employed land use/land cover pattern using the land cover maps of 1990, 2000, 2010 and 2020. In this study, the land cover maps were classified into four major Land use land cover classes (built-up area, agriculture, vegetation and bare land). This was to comprehensively understand the study area Land use land cover changes. The result of this study presented noticeable changes in the spatial and quantitative distribution of land use/land cover. It revealed that the city‘s built-up area have to grow continuously between 1990 and 2020, while other land class decreased during the study period. The result shows that the proportion of built up area was 4.4% in 1990, 5.3% in 2000, 9.9% in 2010, and 15% in 2020, with annual growth of 0.9%(582.39ha) from1990 to 2000, 4.6%(3,037.14ha) from 2000 to 2010 and 5.1 %(3354.3ha) from 2010-2020., indicates an expansion in built-up area was 10.6%(6973.83ha) for the entire period from 1990 to 2020, resulting in agriculture, barren land and vegetation -3137.8ha, -3860.15 ha and 24.03 ha respectively from 1990 to 2020.The outcome of the LULC change It was expressed that Landsat images are very useful in quantifying and mapping LULC change, NDVI, NDBI, and LST in Chiro town and its surrounding. The result of land surface temperature presented 37^0C - 7 ^{0}C, in the year 1990, 38^0C - 10 ^{0}C in the year 2000, 39 ^{0}C to 11 ^{0}C in the year 2010 and in the year 2020 it ranged from 41^0C - 7 ^{0}C. The study successfully demonstrated using remotely sensed data and GIS techniques to monitor spatio temporal Land use land cover changes. Such data are vital for informed decision-making, providing the potential information required monitoring growth and improving environmental sustainability. High temperature change is found in agricultural and bare land areas in a in this study. Therefore, tree plantation should be expanded alongside the agricultural land and bare land to refresh thermal accumulation effects in the area. Places in the city core of the town and peripheral built-up areas have higher urban heat islands. As a result, the concerned bodies are considering how to enhance tree planting, green parks, and green roofs in those locations that are particularly vulnerable.

5.2 Recommendation

On the basis of this research following future prospects and recommendation can be made:

- From the research, LULC change impact causing variation on land surface temperature, environmental aspects and other land covers. Furthermore, implementation of building bylaws and land use plans is highly recommended.
- The use of high resolution imageries such as IKONOS and Quick Bird are important in generating good quality of land cover maps. Because LULC map generating has complex and heterogonous features, high resolution imagery provides better information by mapping these areas. Moreover, the use of ancillary data as ground truth helps for better accuracy of an image classification.
- Consistent multi-temporal Landsat data for each year provides detail comparison of images, change analysis.
- Future researcher predicts land surface temperature warming, environmental experts and natural resources managers to manage natural land resource recommended.

REFERENCES

Abate, S. 2011. Evaluating the land use and land cover dynamics in Borena Woreda of South Wollo Highlands, Ethiopia. Journal of Sustainable Development in Africa, 13, 87-107.

Abbas, I., Muazu, K. & Ukoje, J. 2010. Mapping land use-land cover and change detection in Kafur local government, Katsina, Nigeria (1995-2008) using remote sensing and GIS. Research journal of environmental and Earth Sciences, 2, 6-12.

Abel, B. 2018. Impacts of land use and land cover changes on land surface temperature distribution in Bahir Dar town and its surrounding using remote sensing. MSc. Thesis Addis Ababa University, Ethiopia.

Agarwal, C., Green, G., Grove, M., Evans, T. & Schweik, C. 2000. A Review and Assessment of Land-Use Change Models Dynamics of Space, Time, and Human Choice. Alhawiti, R. H. & Mitsova, D. 2016. Using Landsat-8 data to explore the correlation between urban heat island and urban land uses. IJRET: International Journal of Research in Engineering Technology, 5, 457-466.

Aires, F., Prigent, C., Rossow, W. B., and Rothstein, M. (2001). A new neural network approach including first guess for retrieval of atmospheric water vapor, cloud liquid water path, surface temperature, and emissivities over land from satellite microwave observations. Journal of Geophysical Research: Atmospheres, 106(D14), 14887–14907.

Alhawiti, R.H. and Mitsova, D. (2016) Using Landsat-8 Data to Explore the Correlation between Urban Heat Island and Urban Land Uses. International Journal of Research in Engineering and Technology, 5, 457-466.

Ali, H. (2009). Land use and land cover change, drivers and its impact: A comparative study from Kuhar Michael and Lenche Dima of Blue Nile and Awash Basins of Ethiopia (Doctoral dissertation, Cornell University).

Amare, S. (2015). Land use/cover change at Infraz Watershed, Northwestern Ethiopia. Journal of Landscape Ecology, 8(1):69-83.

Anderson, J., Hardy, E., Roach, J. & Witmer, R. 1976. Land use and land cover classification system for use with remote sensor data [USA]. Professional Papers-US Geological Survey(USA). no. 964.

Becker, F. & Li, Z. L. 1995. Surface temperature and emissivity at various scales: Definition, measurement, and related problems. Remote Sensing Reviews, 12, 225-253.

Becker, F. & Li, Z.-L. 1990. Towards a local split-window method over land surfaces. Remote Sensing, 11, 369-393.

Bekele, H. 2005. Urbanization and Urban Sprawl Master of Science Thesis No. 294 Department of Infrastructure Section of Building and Real Estate Economics.

Belay, S., Amsalu, A. & Abebe, E. 2014. Land use and land cover changes in Awash National Park, Ethiopia: impact of decentralization on the use and management of resources. Open Journal of Ecology, 4, 950.

Birhan Asmame Miheretu and Assefa Abegaz Yimer. (2017).Land use/land cover changes and their environmental implications in the Gelanasub-watershed of Northern highlands of Ethiopia. Environmental System Research 6:7 DOI 10.1186/s40068-017-0084-7.

Brink, A. B., Bodart, C., Brodsky, L., Defourney, P., Ernst, C., Donney, F., Lupi, A. & Tuckova, K. 2014. Anthropogenic pressure in East Africa—Monitoring 20 years of land cover changes using medium resolution satellite data. International Journal of Applied Earth Observation and Geoinformation, 28, 60-69.

Brockerhoff, M. (2000). An urbanizing world. Population Reference Bureau.

Bulti DT and Assefa T (2019). Analyzing ecological footprint of residential building construction in Adama City, Ethiopia. Journal of Environmental Systems Research 8:2.

Burrough, P.A., (1990). Principles of Geographic information systems.Pp.333.Oxford University press, UK.

Central Statistical Agency (CSA). (1994). The 1984 population and housing census of Ethiopia: Analytical report at the national level (Census report). The transitional government of Ethiopia, Office of the population and housing census commission, Addis Ababa, Ethiopia.

Central Statistical Agency (CSA). (2007). The 2007 population and housing census of Ethiopia: statistical reports for the Amhara region (Census report). The Federal Democratic Republic of Ethiopia, Office of population and housing census commission, Central Statistical Agency, Addis Ababa, Ethiopia.

Central Statistical Agency (CSA). (2015). Population Projection of Ethiopia for All Regions at Wereda Level from 2014 – 2017 (Population projection). The Federal Democratic Republic of Ethiopia Central Statistical Agency, Addis Ababa, Ethiopia.

Chander, G., Markham, B. L. & Helder, D. L. 2009. Summary of current radiometric calibration coefficients for Landsat MSS, TM, ETM+, and EO-1 ALI sensors. Remote sensing of environment, 113, 893-903.

Congalton, R. & Green, K. 2009. Thematic accuracy. Assessing the Accuracy of Remotely Sensed Data: Principles and Practices, 55-61.

Congalton, R. G. 1991. A review of assessing the accuracy of classifications of remotely sensed data. Remote sensing of environment, 37, 35-46.

Coppin, P. R., and Bauer, M. E. (1996). Digital change detection in forest ecosystems with remote sensing imagery. Remote sensing reviews, 13(3-4), 207–234.

Dash, J., Mathur, A., Foody, G. M., Curran, P., Chipman, J. & Lillesand, T. 2007. Land cover classification using multi- temporal MERIS vegetation indices. International Journal of Remote Sensing, 28, 1137-1159.

Dash, P., Gottsche, F.-M., Olesen, F.-S. & Fischer, H. 2002. Land surface temperature and emissivity estimation from passive sensor data: Theory and practice-current trends. International Journal of Remote sensing, 23, 2563-2594.

Defries, R. S., Foley, J. A. & Asner, G. P. 2004. Land- use choices: Balancing human needs and ecosystem function. Frontiers in Ecology and the Environment, 2, 249-257.

Di Gregorio, A. & Jansen, L. J. 2000. Land cover classification system (LCCS): classification concepts and user manual for software version 1.0.

Di Gregorio, A., and Jansen L.J., (2000). Land-cover classification: classification concepts and user manual, Food and Agriculture Organization (FAO) of the United Nations Rome.

Dong, F., Chen, J. & Yang, F. A Study of Land Surface Temperature Retrieval and Thermal Environment Distribution Based on Landsat-8 in Jinan City. IOP Conference Series: Earth and Environmental Science, 2018. IOP Publishing, 042008.

Du, C., Ren, H., Qin, Q., Meng, J. & Li, J. Split-window algorithm for estimating land surface temperature from Landsat 8 TIRS data. 2014 IEEE Geoscience and Remote Sensing Symposium, 2014. IEEE, 3578-3581.

Eckert, S., Kiteme, B., Njuguna, E. & Zaehringer, J. G. 2017. Agricultural expansion and intensification in the foothills of Mount Kenya: a landscape perspective. Remote Sensing of Environment, 9, 784.

Emilio, C. (2008). The role of satellite RS in monitoring global environment “department of Geography University of Alkala Spain, PP. 1–2.

Fao, U. 1999. Terminology for integrated resources planning and management. Food and Agriculture Organization/United Nations Environmental Programme, Rome, Italy/Nairobi, Kenia.

Foody, G. M. 2002. Status of land cover classification accuracy assessment. Remote sensing of environment, 80, 185-201.

Galeon, F. 2009. Estimation of the population in informal settlement communities using a highresolution satellite image.

Gao, J. 2009. Digital Analysis of Remotely Sensed Imagery: Multi-Temporal Image Analysis, The McGraw-Hill Companies.

Gashaw, T., Bantider, A. & Mahari, A. 2014. Evaluations of land use/land cover changes and land degradation in Dera District, Ethiopia: GIS and remote sensing-based analysis. International Journal of Scientific Research in Environmental Sciences, 2, 199.

Gebrekidan, W. Modeling land surface temperature from satellite data, the case of Addis Ababa. Proceedings of the United Nations Conference Centre Addis Ababa, 2016. 23-24.

Gumindoga, W. (2010). Hydrologic Impact of Land-Use Change in The Upper Gilgel Abay River Basin, Ethiopia; TOPMODEL Application (Doctoral dissertation, M. Sc. Thesis, ITC Netherlands).

Guo, W., Ni. X., Jin, D., and Shuheng, L. 2014. Spatial-temporal patterns of vegetation dynamics and their relationships to climate variations in Qinghai Lake Basin using MODIS time-series data. Journal of Geographical Sciences, 2014, 24(6):1009-1021.

Hansen, M. C., Potapov, P. V., Moore, R., Hancher, M., Turubanova, S. A., Tyukavina, A., Thau, D., Stehman, S., Goetz, S. J. & Loveland, T. R. 2013. High-resolution global maps of 21st-century forest cover change. science, 342, 850-853.

Hardegree, L. C. (2006). Spatial Characteristics Of The Remotely-sensed Surface Urban Heat Island in Baton Rouge, LA: 1988-2003 (Doctoral dissertation).

Houghton, R.A., 1994. The worldwide extent of land-use change. BioScience, 44(5), pp.305-313.

Hurni, H., Tato, K. & Zeleke, G. 2005. The implications of changes in population, land use, and land management for surface runoff in the upper Nile basin area of Ethiopia. Mountain Research Development, 25, 147-154.

Jensen, J. R. 1996. Introductory digital image processing: a remote sensing perspective, Prentice-Hall Inc.

Jensen, J. R. 2015. Introductory Digital Image Processing: A Remote Sensing Perspective.

Jiménez-Muñoz, J. C., Sobrino, J. A., Skoković, D., Mattar, C. & Cristóbal, J. 2014. Land surface temperature retrieval methods from Landsat-8 thermal infrared sensor data. IEEE Geoscience and remote sensing letters, 11, 1840-1843.

Jin, M., Li, J., Wang, C. & Shang, R. 2015. A practical split-window algorithm for retrieving land surface temperature from Landsat-8 data and a case study of an urban area in China. Remote sensing 7, 4371-4390.

Kalma, J. D., Mcvicar, T. R. & Mccabe, M. F. 2008. Estimating land surface evaporation: A review of methods using remotely sensed surface temperature data. Surveys in Geophysics, 29, 421-469.

Kayet, N., Pathak, K., Chakrabarty, A. & Sahoo, S. 2016. Spatial impact of land use/land cover change on surface temperature distribution in Saranda Forest, Jharkhand. Modeling Earth Systems Environment, 2, 127.

Kern, A. (2011). Deriving Normalized Difference Vegetation Index based on remotely sensed AVHRR and MODIS data (Doctoral dissertation, Eötvös Loránd University).

Kustas, W. & Anderson, M. 2009. Advances in thermal infrared remote sensing for land surface modeling. 149, 2071-2081.

Lakshmi Kumar, T., Koteswara Rao, K., Barbosa, H. & Prabha Jothi, E. 2013. Studies on the spatial pattern of NDVI over India and its relationship with rainfall, air temperature, soil moisture adequacy, and ENSO. Geofizika, 30, 1-18.

Lambin, E. F. & Meyfroidt, P. 2011. Global land-use change, economic globalization, and the looming land scarcity. Proceedings of the National Academy of Sciences, 108, 3465-3472.

Lambin, E. F., Geist, H. J. & Lepers, E. 2003. Dynamics of land-use and land-cover change in tropical regions. Annual review of environment resources, 28, 205-241.

Lambin, E. F., Turner, B. L., Geist, H. J., Agbola, S. B., Angelsen, A., Bruce, J. W., Coomes, O. T., DiRzo, R., Fischer, G. & Folke, C. 2001. The causes of land-use and land-cover change: moving beyond the myths. Global environmental change, 11, 261-269.

Lamchin, M., Park, T., Lee, J.-Y. & Lee, W.-K. 2015. Monitoring of vegetation dynamics in Mongolia using MODIS NDVIs and their relationship to rainfall by natural zone. Journal of the Indian Society of Remote Sensing, 43, 325-337.

Lamson-Hall, P., Degroot, D., Martin, R., Tafesse, T. & ANGEL, S. 2015. A New Plan for African Cities: The Ethiopia Urban Expansion Initiative.

Lazzarini, M., Marpu, P. R. & Ghedira, H. 2013. Temperature-land cover interactions: The inversion of urban heat island phenomenon in desert city areas. Remote Sensing of Environment, 130, 136-152.

Lemlem, A. 2007. Assessing the impact of land use and land cover change on groundwater recharge using Rs and Gis; a case of Awassa catchment, Southern Ethiopia. M. Sc. Thesis. Addis Ababa University, Ethiopia.

LI, J., Lewis, J., Rowland, J., Tappan, G. & Tieszen, L. 2004. Evaluation of land performance in Senegal using multi-temporal NDVI and rainfall series. Journal of Arid Environments, 59, 463-480.

Li, Z.-L., Tang, B.-H., Wu, H., Ren, H., Yan, G., Wan, Z., Trigo, I. F. & Sobrino, J. A. 2013. Satellite-derived land surface temperature: Current status and perspectives. Remote Sensing of Environment, 14-37.

Lillesand, T., Kiefer, R. & Chipman, J. 2004. Remote sensing and image interpretation. Remote sensing and image interpretation.

Lillesand, T., Kiefer, R. & Chipman, J. J. R. S. 2008. Digital image interpretation and analysis. Remote sensing and image interpretation, 6, 545-81.

Lilly Rose A, Devadas MD (2009). Analyssis of land surface temproture and land use/ land cover type using remote sensing imagery-a case in chennai city India.

Lu, D. & Weng, Q. 2007. A survey of image classification methods and techniques for improving classification performance. International Journal of Remote sensing, 28, 823- 870.

Macleod, R. D., and Congalton, R. G. (1998). A quantitative comparison of change-detection algorithms for monitoring eelgrass from remotely sensed data. Photogrammetric engineering and remote sensing, 64(3), 207–216.

Maguire, D.J., (1991). An overview and definition of Geographic information system. In geography information systems: principles and applications. London Longman, Vol.1,9–20.

Mahmood R, Pielke Sr RA, Hubbark KG, Niogi D, et al (2010). Impact of land use/ land cover change on climate and future research priorities .Bulletin the American Meteorological society 91 37-46.

Maitima, J. M., Mugatha, S. M., Reid, R. S., Gachimbi, L. N., Majule, A., Lyaruu, H., Pomery, D., Mathai, S. & Mugisha, S. 2009. The linkages between land-use change, land degradation, and biodiversity across East Africa. African Journal of Environmental Science Technology, 3.

Malik, M.S., Shukla, J.P., and Mishra, S., 2019. Relationship of LST, NDBI, and NDVI using Landsat-8 data in Kandaihimmat Watershed, Hoshangabad, India. Indian Journal of GeoMarine Sciences, 48(01), pp.25-31.

Markham, B. & Barker 1986. Landsat MSS and TM post-calibration dynamic ranges, exoatmospheric reflectances, and at-satellite temperatures. EOSAT Landsat Tech. Notes, 1.

Mather, A. & Needle, C. 2000. The relationships between population and forest trends. Geographical Journal, 166, 2-13.

Mengistu, A. 2008. Climate variability and change. Ethiopian journal of Animal production, 8, 94-98.

Meyer, W. B. & Turner, B. L. 1992. Human population growth and global land-use/cover change. Annual review of ecology and systematics, 23, 39-61.

Miheretu Birhan and Assefa Abegaz (2017). Land use/land cover changes and their environmental implications in the Gelana sub-watershed of Northern highlands of Ethiopia. Environmental Systems Research, 6(1), 7.

Naissan, O.W., and Lily,T.(2016). Aesthetc Dermatology,effects of climate change on skin,Dermatology news USA, May 16, 2016.

Niamir-Fuller, M., Kerven, C., Reid, R. & Milner-Gulland, E. 2012. Co-existence of wildlife and pastoralism on extensive rangelands: competition or compatibility? : SpringerOpen.

Pomeroy, D., Tukahirwa, J., Mugisha, S., Nanyunja, R., Namaganda, M. & Chelimo, N. 2003. Linkages between changes in land use, land degradation, and biodiversity in SW Uganda, LUCID Project, International Livestock Research Institute.

Prata, A., Caselles, V., Coll, C., Sobrino, J. & Ottle, C. 1995. Thermal remote sensing of land surface temperature from satellites: Current status and prospects. Remote Sensing Reviews, 12, 175-224.

Price, J. C. 1984. Land surface temperature measurements from the split window channels of the NOAA 7 Advanced Very High-Resolution Radiometer. Journal of Geophysical Research: Atmospheres, 89, 7231-7237.

Qijiao, X. and Zhixiang, Z. (2015). Impact of urbanization on urban heat island effect based on TM imagery in Wuhan, China. Environ. Eng. Manag. J. 14: 647–655.

Qin, Z., Dall'olmo, G., KarnielI, A. & Berliner, P. 2001. Derivation of the split-window algorithm and its sensitivity analysis for retrieving land surface temperature from NOAA- advanced very high-resolution radiometer data. Journal of Geophysical Research: Atmospheres, 106, 22655-22670.

Rinner, C. & Hussain, M. 2011. Toronto‘s urban heat island—Exploring the relationship between land use and surface temperature. Remote Sensing, 3, 1251-1265.

Rosenstein, O., Qin, Z., Derimian, Y. & Karnieli, A. 2014. Derivation of land surface temperature for Landsat-8 TIRS using a split window algorithm. Sensors, 14, 5768-5780.

Santa, P. (2011). Forest cover and land-use changes: a study of Laljihadi forest (corridor), far western development region, Nepal.MSc Thesis Tribhuvan University.

Schmugge, T., Hook, S. & Coll, C. 1998. Recovering surface temperature and emissivity from thermal infrared multispectral data. Remote Sensing of Environment, 65, 121-131.

Sisay, H., Teshome, S., and Demel, T. 2016. Land use and land cover change in the Bale Mountain Eco-Region of Ethiopia from 1985 to 2015. Land, 5(4):41.

Small, C. 2004. Global population distribution and urban land use in geophysical parameter space. Earth Interactions, 8, 1-18.

Sobrino, J., Jimenez-Munoz, J., El-Kharraz, J., Gómez, M., Romaguera, M. & Soria, G. 2004. Single-channel and two-channel methods for land surface temperature retrieval from DAIS data and its application to the Barrax site. International Journal of Remote Sensing, 25, 215-230.

Sobrino, J., Jiménez-Muñoz, J., Zarco-Tejada, P., Sepulcre-Cantó, G., Miguel, E. D., Sòria, G., Romaguera, M., Julien, Y., Cuenca, J. & Hidalgo, V. 2009. Thermal remote sensing from Airborne Hyperspectral Scanner data in the framework of the SPARC and SEN2FLEX projects: an overview. Hydrology Earth System Sciences, 13, 2031-2037.

Sobrino, J., Raissouni, N. & LI, Z.-L. 2001. A comparative study of land surface emissivity retrieval from NOAA data. Remote Sensing of Environment, 75, 256-266.

Sun, Q., Wu, Z. & Tan, J. 2012. The relationship between land surface temperature and land use/land cover in Guangzhou, China. Environmental Earth Sciences, 65, 1687-1694.

Tempfli, K., Huurneman, G., Bakker, W., Janssen, L., Feringa, W., Gieske, A., Grabmaier, K., Hecker, C., Horn, J. & Kerle, N. 2009. Principles of remote sensing: an introductory textbook, International Institute for Geo-Information Science and Earth Observation.

Tran, T. V. & Ha, D. X. B. 2010. Study of the impact of urban development on surface temperature using remote sensing in Ho Chi Minh City, Northern Vietnam. Geographical Research, 48, 86-96.

Turner, W., Spector, S., Gardiner, N., Fladeland, M., Sterling, E., and Steininger, M. (2003). Remote sensing for biodiversity science and conservation. Trends in ecology and evolution, 18(6), 306–314.

United Nations (UN) 2014. World Urbanization Prospects: The 2014 Revision-Highlights, UN.

United States Geological Survey (USGS) in 2016. Landsat 8 (L8) data users handbook. Department of the Interior US Geological Survey, LSDS.

United States Geological Survey (USGS), 2013. Using the USGS Landsat 8 product. http://landsat.usgs.gov/Landsat8_Using_Product.php (29 Jun. 2015).

USAPA, (2004). A Summary of Models for assessing the effects of Community Growth and change on land-use patterns.EPA.600.R-00.098.U.S.Environmental protection Agency office of research and development , pp. 260.

Voogt, J. A. & Oke, T. R. 2003. Thermal remote sensing of urban climates. Remote sensing of environment, 86, 370-384.

Wan, Z. 2013. Collection-6 MODIS Land Surface Temperature Products Users' Guide.

Wang, F., Qin, Z., Song, C., Tu, L., Karnieli, A. & Zhao, S. 2015. An improved mono-window algorithm for land surface temperature retrieval from Landsat 8 thermal infrared sensor data. Remote sensing, 7, 4268-4289.

Wei, H., Yongnian, Z. and Songnian, L. (2015). An analysis of urban expansion and its associated thermal characteristics using Landsat imagery. Geocarto Int. 30: 93–103.

Weng, Q. & Larson, R. C. 2005. Satellite remote sensing of urban heat islands: current practice and prospects. Geo-spatial technologies in urban environments. Springer.

Weng, Q. 2009. Thermal infrared remote sensing for urban climate and environmental studies: Methods, applications, and trends. ISPRS Journal of Photogrammetry and Remote Sensing, 64, 335-344.

Weng, Q., Lu, D. & Schubring, J. 2004. Estimation of land surface temperature–vegetation abundance relationship for urban heat island studies. Remote sensing of Environment, 89, 467-483.

Work, N. 2018. The impacts of vegetation cover change on rainfall and land surface temperature using remote sensing: a case study of the North Gondar zone. M.Sc. Thesis Addis Ababa University, Ethiopia.

Xiong, Y., Huang, S., Chen, F., Ye, H., Wang, C. & Zhu, C. 2012. The impacts of rapid urbanization on the thermal environment: A remote sensing study of Guangzhou, South China. Remote sensing, 4, 2033-2056.

Xiuwan, C. 2002. Using remote sensing and GIS to analyze land cover change and its impacts on regional sustainable development. International journal of remote sensing, 23, 107-124.

Yang, L., Xian, G., Klaver, J. M. & Deal, B. 2003. Urban land-cover change detection through sub-pixel imperviousness mapping using remotely sensed data. Photogrammetric Engineering and Remote Sensing, 69, 1003-1010.

Yuan, F. & Bauer, M. E. 2007. Comparison of impervious surface area and normalized difference vegetation index as indicators of surface urban heat island effects in Landsat imagery. Remote Sensing Of Environment, 106, 375-386.

YUE, W., Xu, J., Tan, W. & Xu, L. 2007. The relationship between land surface temperature and NDVI with remote sensing: application to Shanghai Landsat 7 ETM+ data. International Journal of Remote Sensing, 28, 3205-3226.

Zha, Y., Gao, J. & Ni, S. 2003. Use of normalized difference built-up index in automatically mapping urban areas from TM imagery. International journal of remote sensing, 24, 583- 594.

Zha, Y., Gao, J., Jiang, J., Lu, H., and Huang, J. (2012). Normalized difference haze index: a new spectral index for monitoring urban air pollution. International journal of remote sensing, 33(1), 309–321.

ZIENA, L. 2017. Mapping land use and land cover change and their effects on urban_ pre-urban agriculture in Debre Markos town. MSc. Thesis.Addis Ababa University, Ethiopia.

Zubair, A.O. (2006). Change detection in LU/LC using RS data and GIS a case study of Ilorin and its environments in Kwara State. Department of geography, University of Ibadan.

ANNEX 1: 2020 Google earth image visualized that were used during image classification.

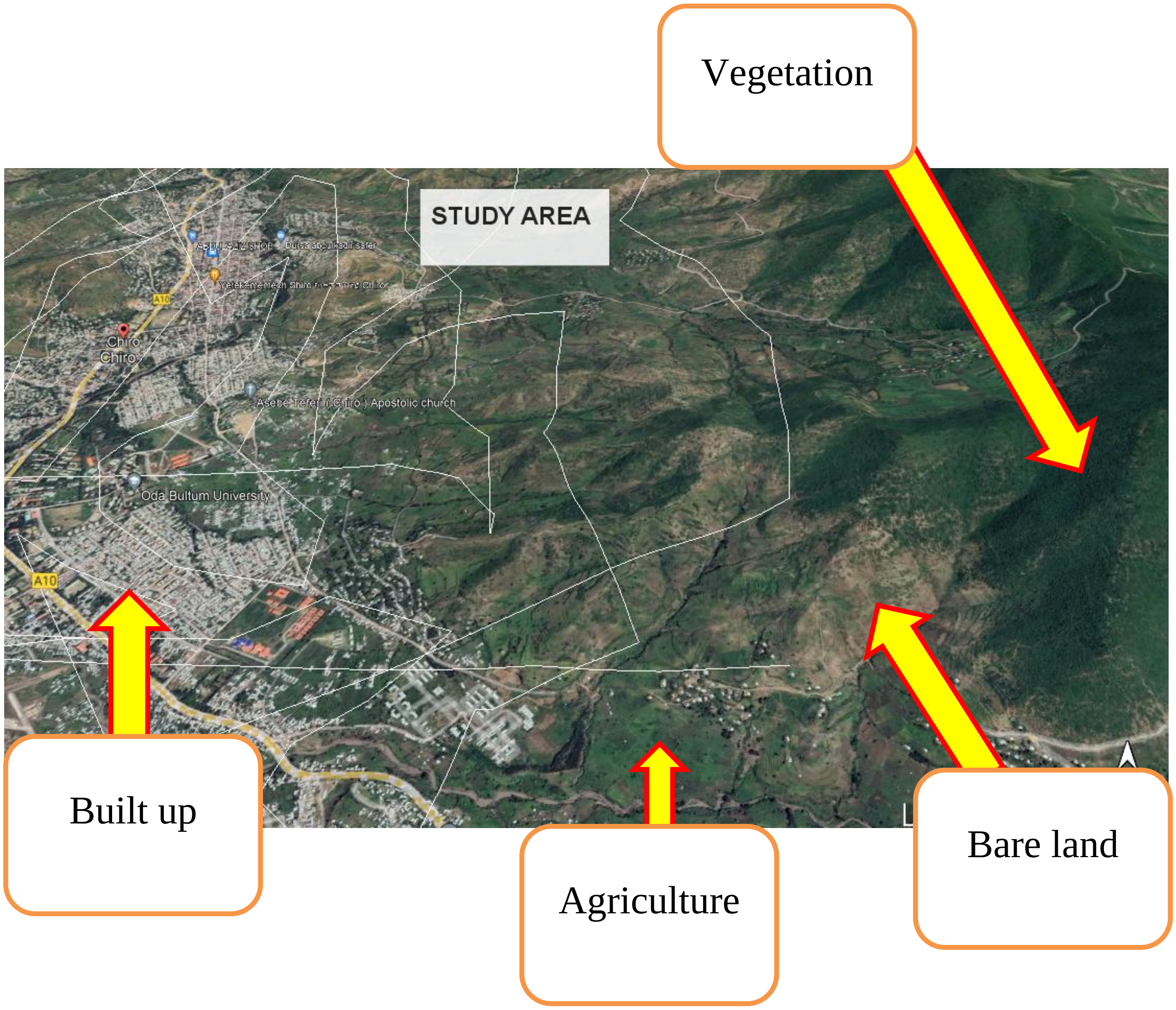

ANNEX 2: Ground points were used for accuracy assessment of LULC classification.

BUILT UP

EASTING	NORTHING
705121.63 m E	1005739.47 m N
705806.01 m E	1002590.22 m N
706016.60 m E	1002389.39 m N
706362.74 m E	1002371.39 m N
706672.24 m E	1002173.53 m N
705415.87 m E	1003958.11 m N
705732.42 m E	1004859.15 m N
704865.39 m E	1006253.64 m N
692450.30 m E	1009638.00 m N
692212.01 m E	1009465.24 m N
692093.83 m E	1007888.70 m N
679624.66 m E	9985472.93 m N
691263.91 m E	9900453.58 m N
712483.95 m E	1015200.94 m N
705966.90 m E	1004999.03 m N
704611.11 m E	1005390.73 m N
702714.60 m E	1008199.94 m N
691951.57 m E	1006489.23 m N

VEGITATION

EASTING	**NORTHING**
685745.81 m E	991176.06 m N
691678.91 m E	992099.32 m N
693741.07 m E	992772.01 m N
700551.29 m E	993674.24 m N
699537.91 m E	995959.12 m N
700235.43 m E	993495.55 m N
703485.46 m E	995692.63 m N
703947.69 m E	997942.82 m N
704418.18 m E	999736.84 m N
709392.79 m E	1003289.76 m N
708723.97 m E	1012983.76 m N
707705.89 m E	1016061.36 m N
709989.54 m E	1017591.66 m N
711224.65 m E	1017992.61 m N
708956.08 m E	1003481.06 m N
692293.79 m E	1005648.76 m N
687160.42 m E	1003622.70 m N
683174.25 m E	998918.86 m N
708966.08 m E	1003981.06 m N

AGRICULTURE

EASTING	NORTHIN
711078.96 m E	1003859.89 m N
711918.52 m E	1005623.53 m N
706300.52 m E	1003907.20 m N
705025.63 m E	1001700.72 m N
704023.71 m E	1003649.49 m N
703620.47 m E	1007627.04 m N
705839.49 m E	1012048.05 m N
708620.43 m E	1011478.85 m N
712113.12 m E	1015642.94 m N
714028.63 m E	1011601.35 m N
711463.77 m E	1000979.17 m N
707323.01 m E	998850.84 m N
696346.13 m E	999989.52 m N
688357.00 m E	998979.93 m N
679251.96 m E	1000359.00 m N
687005.67 m E	993186.69 m N
690824.94 m E	989709.94 m N
687015.68 m E	993286.62 m N
712146.29 m E	1014994.49 m N

BARE LAND

EASTING	NORTHIN
709968.35 m E	1009363.39 m N
706800.74 m E	1012081.71 m N
712280.26 m E	1010179.49 m N
706787.36 m E	1013143.01 m N
698752.44 m E	1007684.68 m N
691224.03 m E	1007673.88 m N
690191.14 m E	1005995.95 m N
688975.45 m E	1004042.29 m N
684569.70 m E	1002255.08 m N
682340.97 m E	997670.24 m N
686698.42 m E	993111.33 m N
689393.22 m E	988299.75 m N
697770.12 m E	991812.36 m N
706816.10 m E	998653.01 m N
712928.56 m E	1002911.03 m N
718158.66 m E	1008006.16 m N
714565.61 m E	1012105.59 m N
686698.42 m E	993111.33 m N
708599.75 m E	1017679.55 m N

ANNEX 3: The association of each Land Use and Land Cover with Mean Land Surface Temperature change.

1990

LULC Classes	MIN	MAX	RANGE	MEAN	STD
Built up	23.25	35.65	12.40	26.49	1.63
Vegetation	8.00	33.26	25.26	18.80	3.91
Agriculture	11.89	38.78	26.89	26.61	3.39
Bare land	11.41	41.07	29.67	25.61	3.85
2000					
LULC Classes	MIN	MAX	RANGE	MEAN	STD
Built up	10.44	35.26	24.81	29.38	3.00
Vegetation	8.00	30.42	22.42	18.88	3.45
Agriculture	11.41	37.22	25.82	29.23	3.14
Bare land	15.18	33.26	18.08	27.32	2.19
2010					
LULC Classes	MIN	MAX	RANGE	MEAN	STD
Built up	18.69	38.66	19.98	29.92	2.44
Vegetation	11.03	36.38	25.35	19.87	4.01
Agriculture	17.09	39.11	22.03	29.81	3.23
Bare land	21.30	38.21	16.91	29.66	2.43
2020					
LULC Classes	MIN	MAX	RANGE	MEAN	STD
Built up	12.90	38.04	25.14	30.55	2.83
Vegetation	10.17	32.74	22.56	23.53	3.23
Agriculture	13.69	38.00	24.31	31.15	2.73
Bare land	13.08	37.80	24.71	30.95	3.29